Sustainability in Environment
ISSN 2470-637X (Print) ISSN 2470-6388 (Online)
Vol. 11, No. 4, 2026
www.scholink.org/ojs/index.php/se

Original Paper

Upcycling Waste Plastics into Conductive Materials: Conversion Methods, Applications, and Pathways to Circularity

Ziyu Wang[1]

[1] Basis International School Shenzhen, Guangdong, Shenzhen, 518067, China

Received: October 07, 2026 Accepted: November 9, 2026 Online Published: November 24, 2026

doi:10.22158/se.v12n4p92 URL: http://dx.doi.org/10.22158/se.v12n4p92

Abstract

The escalating global production of plastics, coupled with persistently low recycling rates, demands innovative valorization strategies. Upcycling waste plastics into conductive materials offers a dual-strategy solution that addresses both environmental pollution and the growing demand for energy-storage and electronic applications. By examining four feedstock classes (hydrocarbon, oxygen-containing, nitrogen-containing, and halogenated polymers) and three conversion pathways (pyrolytic, non-pyrolytic, and hybrid), the review traces how waste plastics are transformed into advanced functional materials and how polymer structure governs carbon yield, porosity, and heteroatom retention. Plastic-derived hard carbons reach reversible capacities of roughly 300 to 450 mAh/g in sodium-ion and potassium-ion anodes, while several activated and heteroatom-doped porous carbons exceed 400 F/g in supercapacitors, and carbon nanotube and graphene additives together with conductive polymer composites further broaden the application range. These upcycled materials also enable high-performance sensors, electromagnetic interference shielding, and energy-harvesting devices. However, critical gaps including the absence of standardized testing protocols, the difficulty of scaling complex multi-step routes, and limited techno-economic and life-cycle validation for advanced chemical recycling continue to hinder commercialization. Addressing these challenges is essential to transitioning plastic upcycling from laboratory research to viable real-world deployment and to establish it as a core component of the circular economy.

Keywords

plastic waste upcycling, chemical recycling, conductive carbon materials, energy storage, circular economy, techno-economic analysis, waste valorization

1. Introduction

Plastics, known for their durability, flexibility, and ease of production, have been widely utilized across numerous industries, including packaging, construction, automotive, medical, and electronics. With sustained global demand, the annual production of plastics is projected to increase from 464 Mt in 2020 to 884 Mt in 2050, resulting in an accumulated stock of up to 4725 Mt of plastics from the year 2000 by mid-century.[1] This immense production trajectory, coupled with persistently low recycling rates and the inherent constraints of existing recycling infrastructures, facilitates the environmental degradation of plastic materials. Such degradation releases toxic monomers and additives that can bioaccumulate in food chains, disrupt ecosystems, and exacerbate global pollution.[2]

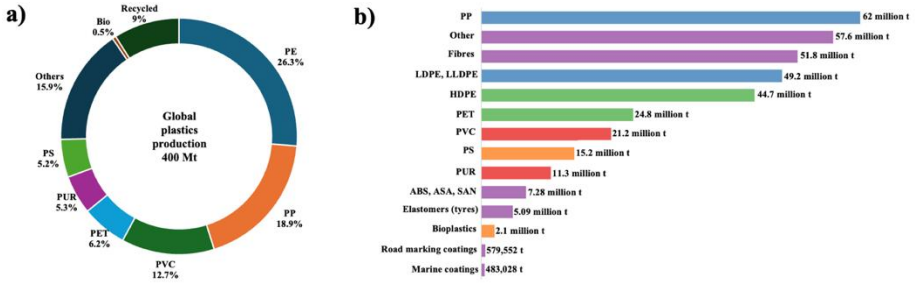


Figure 1. Distribution of plastic wastes: a) Global plastic production breakdown per polymer type. Adapted from ref [3]. b) Global primary waste generation by polymer, 2019 data. Adapted from ref [4]. Abbreviations: PE–Polyethylene; PP–Polypropylene; PVC–Polyvinyl Chloride; PET–Polyethylene Terephthalate; PUR–Polyurethane; PS–Polystyrene; LDPE–Low-Density Polyethylene; LLDPE–Linear Low-Density Polyethylene; HDPE–High-Density Polyethylene; ABS–Acrylonitrile Butadiene Styrene; ASA–Acrylonitrile Styrene Acrylate; SAN–Styrene Acrylonitrile

Critical evaluations of current plastics management strategies reveal profound systemic deficiencies. Dominant disposal practices, namely landfilling and environmental dumping, lack effective mechanisms for polymer decomposition at end of life.[5] While incineration offers energy recovery, it imposes a uniformly high carbon burden, emitting approximately 2.73 kg CO_2 equivalent per kilogram of plastic incinerated. Conversely, mechanical recycling yields substantially lower emissions ranging from 0.35 to 0.51 kg CO_2 equivalent per kilogram. However, this approach remains constrained by significant impediments, including feedstock contamination, inherent polymer incompatibility, structural degradation of macromolecular chains, and necessity for highly segregated waste streams achieved through intensive sorting and reprocessing.[6–8] These enduring constraints underscore a critical oversight in current paradigms as plastics are not merely recalcitrant waste, but highly concentrated carbon and energy reserves. With a calorific value ranging from 42 to 46 MJ/kg,[9] waste plastics represent a substantial embedded energy stock that is overwhelmingly squandered through combustion or long-term environmental accumulation.

These parallel global challenges, mounting plastic pollution and the accelerating demand for energy infrastructure, are inherently connected through a shared elemental foundation: carbon. Concurrently, the global demand for electrochemical energy storage systems, such as batteries and supercapacitors, is undergoing unprecedented growth. The global lithium-battery market exceeded USD 150 billion in 2025, an increase of over 20% from 2024.[10] Within the supercapacitor sector, the data-center segment alone is projected to grow to over USD 950 million by 2037, representing a CAGR of 40.9% from 2026.[11] Because supercapacitor electrodes are predominantly carbon-based and lithium-ion batteries require conductive carbon additives, this expansion represents a direct, carbon-intensive demand channel. At the same time, the same market growth creates demand for other upcycled material streams—including polymer-derived binders and separators, recycled metals, and biomass-derived carbons—positioning upcycled materials, carbon-based and otherwise, as increasingly strategic inputs to the energy transition. The molecular architecture of synthetic polymers, predominantly composed of hydrocarbon backbones, renders them uniquely suited as carbon precursors. Broadly, three principal conversion pathways have emerged. The first relies on thermochemical conversion, including pyrolysis and controlled carbonization, to transform hydrocarbon backbone into porous carbons, carbon nanosheets, and graphene-like architectures that exhibit high specific surface areas, tunable porosity, and excellent electrical conductivity.[12–14] The second pathway focuses on non-pyrolytic techniques such as sulfonation, solvolysis, depolymerization, solution or melt blending to convert specific plastic precursors directly into intrinsically conductive polymers or conductive polymer composites, thereby preserving the macromolecular backbone while imparting electronic functionality.[15–17] In addition to these two chemical modification techniques, hybrid techniques that employ both pyrolytic and non-pyrolytic processes have emerged, integrating chemical activation or templating with thermal decomposition to achieve enhanced porosity, graphitization, and electrochemical performance.[18–20] Such findings confirm that plastic waste can evolve from an environmental liability into a valuable resource for next-generation energy and electronic technologies through diverse upcycling strategies.

The convergence of these two pressing concerns, the mismanagement of plastic waste and the surging requirement for sustainable energy storage materials, positions upcycling as a compelling dual-strategy solution. This approach simultaneously alleviates the ecological burden of plastic pollution while furnishing cost-effective, scalable precursors for high-value conductive materials. A paradigm shift from conventional recycling toward upcycling is therefore essential, wherein waste plastics are transformed not into lower-grade products but into functional materials with enhanced economic and technical value. However, realizing this potential requires a systematic understanding of feedstock characteristics, conversion mechanisms, and the resulting material properties that govern performance in target applications.

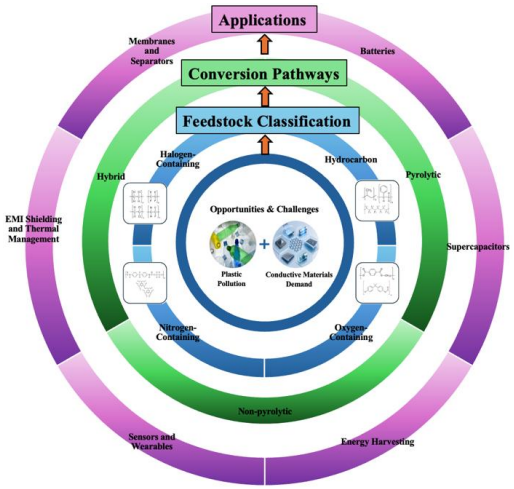


Figure 2. Conceptual overview of the paper's scope, illustrating the transformation of plastic waste into valuable carbon materials via a concentric, outward-flowing structure. At the core, the research is driven by the dual opportunities and challenges of balancing global plastic pollution with the growing demand for conductive materials. Moving outward, the inner ring categorizes the precursors based on their chemical structure into halogen-containing, nitrogen-containing, oxygen-containing, and hydrocarbon plastics. These feedstocks are subsequently processed through various conversion pathways in the middle ring, highlighting pyrolytic, non-pyrolytic, and hybrid processes as key pathways. Finally, the outer ring displays the value-added applications of the derived materials, spanning membranes and separators, batteries, supercapacitors, energy harvesting, sensors and wearables, and EMI shielding and thermal management.

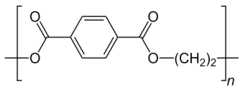
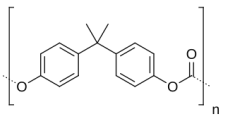
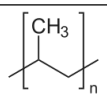
This review provides a comprehensive examination of the emerging field of plastic waste upcycling into conductive materials. The first section establishes the foundational relationship between feedstock chemistry and upcycling potential by classifying waste plastics according to their structural chemistry into hydrocarbon polymers, oxygen-containing polymers, nitrogen-containing polymers, and halogen-containing polymers, and examining how molecular architecture determines thermal degradation behavior, carbonization yield, and susceptibility to chemical modification. The second section systematically evaluates three principal conversion pathways: pyrolytic routes, which destroy and reassemble the polymer backbone into carbon frameworks through direct thermal, catalytic, autogenic, template-assisted, volatile-mediated, and non-conventional pyrolysis; non-pyrolytic routes, which preserve the polymer backbone through depolymerization, solvolysis, direct functionalization, blending, and surface assembly; and hybrid routes, which integrate multiple mechanisms to overcome the inherent trade-offs of single methods and enable precise tuning of surface area, porosity, and heteroatom doping. The third section provides a structured benchmarking framework for evaluating upcycled materials across application domains, assessing key performance metrics including

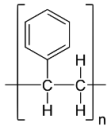
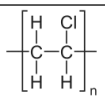
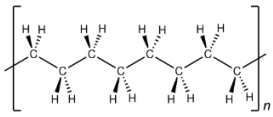
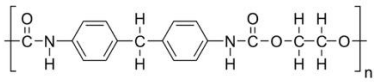
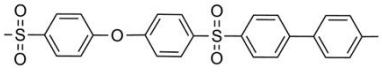
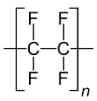
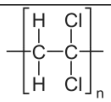
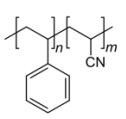
capacitance, cycling stability, rate capability, and mechanical properties to compare devices derived from waste plastics against each other and against commercially available benchmarks, thereby identifying current research gaps. The fourth section examines the critical challenges and future research directions, including the importance of life-cycle assessment and techno-economic analysis in evaluating the viability of emerging pathways such as depolymerization and solvolysis. Finally, the review concludes by discussing technology readiness levels, climate performance, and integrated assessment frameworks necessary for scaling promising technologies from laboratory demonstration to commercial implementation. Through this structured analysis, the review aims to establish upcycling as a viable pathway towards a circular economy that simultaneously addresses plastic pollution and the growing demand for sustainable energy materials.

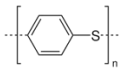
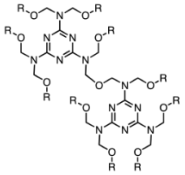
2. Feedstock Classification and Suitability for Upcycling

The chemical structure of a plastic fundamentally determines its thermal degradation behavior, carbonization yield, and susceptibility to chemical modification, all of which govern its suitability for upcycling into conductive materials. Plastics exhibit diverse structural units, including aromatic carbon rings, conjugated double bonds, saturated aliphatic chains, ester linkages, and heteroatom-containing backbones. These features dictate not only the intrinsic properties of the polymer, such as thermal stability, rigidity, and chemical reactivity, but also the pathways available for converting waste plastics into value-added conductive products. Table 1 lists common plastic feedstocks, their molecular structures, and their applications in daily life.

Table 1. Common Plastic Feedstocks, Their Molecular Structure, and Applications

Feedstock Name	Molecular Structure	Applications
Polyethylene Terephthalate (PET)		Beverage bottles, food containers, textile fibers, electronic components.
Polycarbonate (PC)		Safety glasses, optical lenses, CDs/DVDs, automotive parts, electronic device housings, baby bottles.
Polypropylene (PP)		Food containers, bottle caps, drinking straws, automotive parts, medical devices, carpet fibers.

Polystyrene (PS)		Disposable cutlery, food trays, CD jewel cases, insulation packaging, laboratory ware.
Polyvinyl Chloride (PVC)		Pipes and fittings, window profiles, cable insulation, flooring, blood bags, and IV tubing.
Polyethylene (PE)		Packaging films, plastics bags, food containers, shampoo bottles, toys, insulation materials.
Polyurethane (PU)		Furniture foam, shoe soles, coatings & adhesives, synthetic leather, automotive seats, medical catheters & dressings.
Polyethersulfone (PES)		Medical devices, food-contact components, electronic parts, water treatment membranes, wastewater, aerospace components.
Polytetrafluoroethylene (PTFE)		Non-stick cookware coatings, chemical pipes and valves, bearings and seals, electrical insulation materials.
Polyvinylidene Chloride (PVDC)		Cling films, barrier layers in food packaging, sausage casings, pharmaceutical and cosmetic packaging.
Polyvinylidene Fluoride (PVDF)		Lithium-ion battery binders, supercapacitor electrode binders, aerospace and aviation applications, chemical pipes and valves, 3D printing filaments.
Styrene-Acrylonitrile Copolymer (SAN)		Automotive parts, battery housings, transparent kitchenware, food containers,

		household appliances, medical supplies.
Polyphenylene Sulfide (PPS)		Automotive engine components, electrical connectors, relays, fuel cell components, pump and valve seals.
Melamine-Formaldehyde Resin (MF)		Tableware, decorative laminates, adhesives, electrical insulation components.

Current waste plastics can be broadly categorized based on their structural chemistry into four groups: i) hydrocarbon polymers (e.g., aliphatic polyolefins and aromatic vinyl polymers), ii) oxygen-containing polymers, iii) nitrogen-containing polymers, and iv) halogen-containing polymers. Figure 3 illustrates the specific chemical mechanisms and structural evolution pathways for upcycling these different classes of feedstocks into carbon materials. This structural chemistry is a key determinant in their functionality and behavior after upcycling.[21] However, the role a polymer plays in the upcycling process can also significantly influence the final carbon product: primary carbon feedstock, nitrogen-doping additive, structural scaffold, or template. Most of the polymers discussed in this review are thermoplastics, which can be repeatedly melted and reshaped, but MF resin is a notable exception: it is a thermoset that cannot be remelted once cured, making carbonization an especially attractive valorization route for it.[22] This section examines each group in turn, focusing on how structural chemistry and process role together determine the yield, morphology, and properties of the resulting carbon materials.

2.1 Hydrocarbon Polymers

Hydrocarbon polymers contain only carbon and hydrogen in their backbones. This group includes two structurally distinct subclasses: aliphatic polyolefins with saturated linear chains and aromatic vinyl polymers with pendant phenyl rings. Despite their shared hydrocarbon composition, the presence or absence of aromatic rings leads to fundamentally different degradation behavior and chemical reactivity, which in turn dictates different upcycling strategies.

2.1.1 Aliphatic Polyolefins

Aliphatic polyolefins such as polyethylene (PE) and polypropylene (PP) undergo thermal chain scission during pyrolysis, producing volatile hydrocarbons. For PP, the gas products include H_2, CH_4, and a C_2–C_4 fraction (ethane, ethylene, propane, propylene, and i-butene). The proposed degradation mechanism of PP under OMMT catalysis is illustrated in Figure 3a.[23] For PE, chain scission produces mainly ethylene, ethane, propylene, and propane,[24] while at high temperature PE-derived species can

shift toward C_1–C_3 fragments.[25] In the case of PP, non-catalytic pyrolysis liquids are dominated by olefins and diolefins, with aromatics being scarce.[23] In the absence of an effective combined catalyst/template, this behavior often leads to low solid-carbon yields and amorphous or poorly graphitized carbon.[23,26,27] However, under combined catalytic/template conditions, polyolefin waste can be converted into more graphitic/functional carbons, including CS-CNTs, carbon nanosheets, graphene/mesoporous carbon, and MWCNTs.[24–26,28]

2.1.2 Aromatic Vinyl Polymers

Aromatic vinyl polymers, represented primarily by polystyrene (PS), possess a vinyl backbone with pendant phenyl rings. This structure creates a fundamental challenge for pyrolytic upcycling: PS depolymerizes extensively into styrene and other aromatic volatiles during conventional thermal treatment, yielding negligible solid carbon. To overcome this, hybrid strategies have been developed. Friedel–Crafts crosslinking of PS using carbon tetrachloride and $AlCl_3$ (Figure 3c) creates carbonyl-crosslinked polystyrene with a high crosslinking density and abundant oxygen atoms, which enables carbonization to yield a 3D hierarchical porous carbon with a specific surface area of 620 m^2/g and a specific capacitance of 208 F/g at 1 A/g.[29] When cyanuric chloride is used as the crosslinker instead, nitrogen is incorporated directly into the polymer framework, and subsequent KOH activation produces an N-doped porous carbon with a specific capacitance of 327 F/g at 1 A/g.[30] Beyond pyrolytic and hybrid routes, PS can also be upcycled through non-pyrolytic pathways that preserve the polymer backbone. The aromatic phenyl ring enables sulfonation via electrophilic aromatic substitution, converting PS into poly(styrene sulfonate) (PSS), which serves as a scaffold for PEDOT:PSS conductive polymers used in organic electrochemical transistors and hybrid solar cells.[31] Additionally, PS can be melt-blended with conductive fillers such as graphene to create conductive composites, where the aromatic rings promote favorable π–π interactions that improve filler dispersion and reduce the percolation threshold.[32]

2.2 Oxygen-Containing Polymers

Oxygen-containing polymers such as polyethylene terephthalate (PET) and polycarbonate (PC) possess aromatic rings in their backbones together with ester or carbonate linkages. During pyrolysis, these linkages undergo decarboxylation and crosslinking. In PET, the ester carbonyl group releases CO/CO_2, and the remaining terephthalate units form benzenoid compounds and crosslinked structures.[12] More generally, in both PET and PC, part of the oxygen is released as volatile CO_2 and H_2O, while the residual oxygen remains in the carbon to construct a crosslinking network.[13] The proposed carbonization schemes for PC and PET are shown in Figure 3b. The presence of oxygen functional groups plays a particularly important role in suppressing carbon rearrangement, leading to highly turbostratic microstructures during conventional pyrolysis. Consequently, PET and PC typically yield hard or turbostratic carbons with limited graphitization and moderate solid-carbon yields (e.g., 15.0 wt% for PET at 391 °C and 24.3 wt% for PC at 455 °C),[13] or highly porous but still largely amorphous carbons after activation.[33] However, increasing the carbonization temperature promotes oxygen release

and allows adjacent carbon atoms to diffuse into more ordered layered domains, thereby enhancing graphitization; PET is more easily graphitized than PC under comparable conditions.[13] Moreover, under combined catalytic/templating conditions such as molten salts or laser-assisted carbonization, PET can be converted into more graphitic carbons, including graphene-like nanosheets and conductive carbon composites or nitrogen-doped graphene when urea is used as a nitrogen source.[14,34,35]

2.3 Nitrogen-Containing Polymers

Nitrogen-containing polymers offer a distinct advantage over the other feedstock classes discussed in this section: nitrogen can be retained in the carbon matrix, producing nitrogen-doped carbons without an external dopant. Nitrogen can be introduced through two routes: intrinsic doping, where nitrogen is part of the polymer backbone, or extrinsic doping, where a nitrogen-rich additive is mixed with a carbon precursor during carbonization. Polyurethane (PU) is a representative intrinsic nitrogen-containing waste polymer. When pre-carbonized at 500 °C and then activated with KOH at 750 °C, PU yields a nitrogen- and sulfur-codoped microporous carbon with a high specific surface area of 2216 m^2/g and a specific capacitance of 395 F/g at 1 A/g.[19] XPS confirms that nitrogen is incorporated as pyridinic-N, pyrrolic-N, and graphitic-N, while sulfur is bound in cyclic carbon structures and C-S-N motifs. MF resin, a thermosetting plastic with a triazine ring and three amino groups, provides a different intrinsic nitrogen source. One-step carbonization of waste MF at 400-700 °C yields N-doped carbons with nitrogen contents decreasing from 47.4 to 24.9 wt% as temperature increases.[36] Charge density diagrams of *OOH adsorption on these defects and the resulting ORR pathways are modeled in Figures 3e and 3f. In contrast, extrinsic doping uses a nitrogen-rich additive such as urea. For example, waste polystyrene mixed with urea and treated by thermal plasma yields nitrogen-doped porous carbon with a specific capacitance of 482 F/g at 1 A/g.[37] Beyond these feedstock routes, nitrogen-rich polymers such as polyaniline (PANI) are widely used as conductive additives rather than sole carbon precursors. PANI composited with an Fe-terephthalate MOF derived from waste PET improves the electrical conductivity and power density of microbial fuel cell electrodes,[17] while PANI grown in situ on a waste PU foam scaffold provides pseudocapacitance in flexible all-solid-state supercapacitors.[38] In the latter case, the PU foam is not carbonized but serves as a flexible 3D scaffold, illustrating that nitrogen-containing polymers can function in multiple roles beyond mere carbon precursors.[17,38]

2.4 Halogen-Containing Polymers

Halogen-containing polymers such as polyvinyl chloride (PVC), polyvinylidene chloride (PVDC), and polytetrafluoroethylene (PTFE) undergo dehalogenation during thermal treatment, which can proceed via two distinct routes depending on the process conditions. In thermal dehalogenation, heating PVC or PVDC releases HCl and generates unsaturated carbon structures that promote crosslinking and aromatization, yielding hard carbons with tunable porosity.[39] For example, direct carbonization of PVC at 800 °C produces hard carbon with an interlayer spacing of ~0.36 nm and a reversible capacity of 477 mAh/g as a potassium-ion battery anode.[40] The conversion of PTFE, polyvinylidene fluoride (PVDF),

and PVC into nanoporous carbon via zinc-assisted carbonization is depicted in Figure 3d. However, the corrosive HCl byproduct requires careful management. In chemical dehalogenation, alkaline agents such as KOH enable dehalogenation at room temperature, producing benign byproducts of KCl and H_2O instead of HCl, while creating reactive carbon sites that can be doped with heteroatoms.[41,42] This room-temperature route has been used to convert PVC and PVDC into N,S-codoped porous carbons with specific capacitances up to 427 F/g.[41,42] Beyond carbonization, halogen-containing polymers can also be upcycled through non-pyrolytic routes that preserve the polymer backbone, such as electrospinning PVC into nanofibers for triboelectric nanogenerators.[43] This dual reactivity makes halogen-containing polymers versatile feedstocks for pyrolytic, non-pyrolytic, and hybrid upcycling routes.

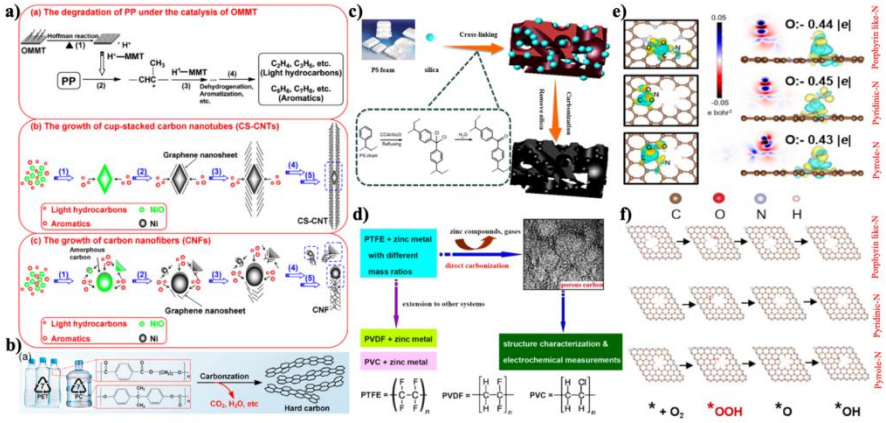


Figure 3. Chemical mechanisms and structural evolution for upcycling various plastic feedstocks into carbon materials. a) Degradation mechanisms of aliphatic polyolefins (specifically polypropylene, PP) and the effects of varying amounts of OMMT catalysts. Adapted from ref [23]. b) Carbonization scheme of oxygen-containing polymers (PC and PET). Adapted from ref [13]. c) Friedel–Crafts crosslinking of aromatic vinyl polymer (PS) to obtain porous carbon. Adapted from ref [29]. d) Conversion of halogen-containing polymers (PTFE, PVDF, PVC) into nanoporous carbon via zinc-assisted carbonization. Adapted from ref [39]. e) Charge density difference and cross-section diagrams of *OOH adsorbed on porphyrin-like, pyridinic, and pyrrolic carbon defects. f) Modeling of the oxygen reduction reaction (ORR) process from O_2 adsorption to $2e^-$ and $4e^-$ pathways. Panels e) and f) are adapted from ref [36], which explores the carbonization of MF resin for nitrogen-containing polymers

3. Conversion Technologies

The conversion of plastic waste into functional carbon materials is achieved through a diverse array of technologies that can be broadly categorized into pyrolytic, non-pyrolytic, and hybrid routes. These pathways offer distinct strategies for valorization, ranging from the high-temperature decomposition of polymers into carbonaceous solids to the milder, structure-preserving chemical modification of intact polymer chains. Pyrolytic routes, including direct thermal, catalytic, and template-assisted methods, are

defined by the destruction and reassembly of the polymer backbone into a carbon framework, where the yield, microstructure, and heteroatom content are governed by the intricate interplay of feedstock chemistry, process environment, and the degree of process control. In contrast, non-pyrolytic routes, such as depolymerization and direct functionalization, preserve the polymer's core structure to produce high-value monomers, polymers, and composites. Bridging these approaches, hybrid routes integrate multiple mechanisms to overcome the inherent trade-offs of single methods, enabling the precise tuning of properties like surface area, porosity, and heteroatom doping. Across this spectrum of technologies, a central theme emerges: the transformation of plastic waste is not merely a destructive process but a sophisticated opportunity to design advanced materials for applications in energy storage, environmental remediation, and beyond.

3.1 Pyrolytic Routes

Pyrolytic routes encompass all thermal conversion technologies in which plastic waste is decomposed at elevated temperatures, typically 500 to 1400 °C, under an inert or controlled atmosphere to yield carbonaceous materials. The defining feature of this family is that the polymer backbone is destroyed and reassembled into a carbon framework, so the carbon yield, microstructure, and heteroatom content depend on the interplay between feedstock chemistry, heating method, and process environment. As established in Section 2, aromatic polymers such as PET, PC, and PS retain carbon through stable ring structures and yield 15 to 25 wt% residue under direct pyrolysis, whereas aliphatic polyolefins such as PE and PP decompose almost completely into volatile hydrocarbons under atmospheric pressure. The six subsections that follow are organized by the degree of process control rather than by feedstock. Direct thermal pyrolysis is the baseline route without additives. Catalytic pyrolysis introduces metal or acid catalysts to direct decomposition and provide nucleation sites for ordered carbon growth. Autogenic carbonization uses a sealed reactor to retain volatiles and force secondary carbonization reactions. Template- and activation-assisted carbonization adds sacrificial scaffolds and chemical activation to control pore architecture. Volatile-mediated pyrolysis decouples polymer decomposition from carbon growth by first generating a hydrocarbon gas that is then decomposed over a catalyst or deposited onto a substrate. Finally, non-conventional and medium-assisted pyrolysis changes the heating mechanism or reaction environment through microwaves, molten salts, plasma, hydrothermal water, or reactive reagents such as sulfur. Figure 4 and Figure 5 provide a schematic overview of these representative pathways. Across these routes, three trade-offs recur: carbon yield versus porosity, graphitic order versus surface area, and process simplicity versus control over microstructure and heteroatom doping.

3.1.1 Direct Thermal Pyrolysis and Carbonization

Direct thermal pyrolysis is the simplest pyrolytic route, heating plastic waste in an inert atmosphere without catalysis, templates, or chemical pretreatment. However, its utility depends on the plastic's structure and heating protocol. Aromatic polymers such as PET and PC yield hard carbons with expanded interlayer spacing and 15–25 wt% residue,[12,13] whereas aliphatic polyolefins produce

negligible char under atmospheric pressure. Beyond feedstock selection, heating method and carbonization temperature provide additional control over the balance between defects, interlayer spacing, and closed porosity, which determines whether the carbon stores ions through adsorption, intercalation, or pore filling. Zhang et al. demonstrated this by carbonizing PET via conventional tube-furnace pyrolysis versus microwave-assisted pyrolysis. In the first cycle at 20 mA/g, the MW-900 sample exhibited a charging capacity of 344 mAh/g with a 70.1% initial coulombic efficiency (ICE), compared with 260 mAh/g and 58.0% for TF-900; the corresponding discharge capacities were 491 and 448 mAh/g, respectively. In situ Raman revealed that MW-900 stored sodium through adsorption and closed-pore filling rather than intercalation, with closed pore volume increasing from 0.089 to 0.139 cm^3/g.[44] He et al. showed that for PVC-derived soft carbon (Figure 4a), moderate temperatures (~800 °C) maximize defect density and adsorption capacity, while higher temperatures favor intercalation (208 mAh/g for SC-1200) due to graphitization.[45] Together, these studies establish that direct pyrolysis can be tuned—through heating mode and temperature—to favor adsorption, intercalation, or pore filling without catalysts or pretreatment, though aliphatic feedstocks remain poorly suited and pore architecture remains difficult to control compared with catalytic or template-assisted routes.

3.1.2 Catalytic Pyrolysis and Catalytic Graphitization

Catalytic pyrolysis adds a catalyst to direct polymer decomposition toward light hydrocarbons and aromatics and to provide nucleation sites for ordered carbon growth. This route is especially important for aliphatic polyolefins, which otherwise produce little solid carbon. Gong et al. established a combined acid and metal catalyst for polypropylene using organically modified montmorillonite (OMMT) and NiO. NiO alone gave only 7.0 wt% carbon, but adding 1.0 g OMMT per 100 g PP raised the yield to 41.0 wt%, and 5.0 g OMMT per 100 g PP raised it to 63.1%.[23] The catalyst ratio also controlled morphology. Low OMMT produced long, straight, smooth-surface, cup-stacked carbon nanotubes with narrow length and diameter distributions, whereas high OMMT produced short, winding, rugged-surface carbon nanofibers. The proposed mechanism is that proton acid sites on OMMT degrade PP into light hydrocarbons and aromatics. A low aromatics content promotes coalescence and reconstruction of NiO into rhombic shapes, which then catalyze carbon nanotube growth, while a high aromatics content leads to amorphous carbon and nanofibers.

The same group extended this concept to graphene flakes. With waste PP bumper and panel as feedstock, OMMT at 700 °C gave graphene yields from 14.6 to 83.8 wt% for bumper and 15.2 and 86.6 wt% for panel as the OMMT to waste PP ratio increased from 0.5 to 8.[46] OMMT acted as both degradation catalyst and template, promoting formation of light hydrocarbons and aromatics and supporting in situ graphene growth. Karakoti et al. similarly used MMT nanoclay as a degradation catalyst in a two-stage pyrolysis process (400 °C followed by 900 °C) to convert mixed waste plastics into graphene nanosheets at 18-20% yield; the resulting material delivered 38.78 F/g as a supercapacitor electrode with an aluminum sheet current collector.[47] In parallel, Wen et al. developed a universal catalyst of nanosized carbon black (CB) and Ni_2O_3 for PP, PE, PS, and their blends (Figure

4c). Carbon yields reached 42.1 wt% for PP, 36.4 wt% for PE, 25.6 wt% for PS, and 31.6 wt% for a real-world polyolefin mixture.[48] CB catalyzed degradation to aromatic compounds, and CB together with Ni catalyzed dehydrogenation and reassembly into carbon nanotubes. Importantly, the presence of PS did not suppress carbonization of PP and PE in the blends. Cheng et al. later used waste PVDF and $Ni(NO_3)_2 \cdot 6H_2O$ for synchronous carbonization and graphitization. Increasing temperature from 800 to 1200 °C increased graphitization but decreased BET surface area from 1048.9 to 817.1 m^2/g, which illustrates the tradeoff between graphitic order and porosity.[49]

More recent work has moved toward designed precatalysts and post treatment. Liu et al. designed 3D rose like $Co_xMn_{3-x}O_4$ spinel precatalysts that self-convert into Co/MnO. At a precatalyst to plastic ratio of 1:14, carbon and H_2 yields reached 41 wt% and 36 $mmol \cdot g^{-1}_{pla.}$, with specific yields of 7.48 $g^{-1}_{cat.}$ and 634 $mmol \cdot g^{-1}_{pla.} \cdot g^{-1}_{cat.}$, more than one order of magnitude above previous reports.[50] Urgunde et al. used a Ni-butanethiolate ink at 800 °C followed by hydrogen annealing at 1000 °C to convert waste polystyrene and sugar into graphitic carbon, reaching 158 F/g at 1 A/g and two orders higher conductivity than without hydrogen annealing.[51] The most recent advance connects catalytic graphitization to ion storage mechanism. Kim et al. grew turbostratic graphite from waste polystyrene and nylon 6 on a Ni mesh at 1000 °C. Potassium intercalation in this turbostratic carbon proceeded without long range ordering and delivered about 92% of the theoretical KC_8 plateau capacity.[52] This result shows that catalyst design can tune not only yield and graphitization degree but also the local stacking order that governs intercalation thermodynamics. The historical arc is therefore clear. Early combined catalysts established how acid sites and metal nanoparticles cooperate to convert polyolefins into carbon nanotubes and graphene.[23,48,46] Subsequent studies refined catalyst composition, precatalyst architecture, and post treatment.[49–51] The newest work uses catalytic graphitization to create turbostratic carbon with distinct potassium storage behavior.[36]

3.1.3 Autogenic or Pressurized Carbonization

Autogenic carbonization uses a sealed reactor. Volatile products from polymer decomposition cannot escape, so internal pressure rises, secondary cyclization, aromatization, and condensation are forced, and carbonization can occur even for aliphatic plastics that normally yield little or no char. The earliest studies in this group, both from 2009, established the basic approach. Pol and Thiyagarajan heated waste HDPE with 20 wt% cobalt acetate (CoAc) in 5 cc autoclave at 700 °C. Pressure rose from about 50 psi at 680 °C to 1000 psi at 700 °C and then to 1200 psi during catalytic cracking, producing multiwalled carbon nanotubes (MWCNTs) with a yield of 0.4 g from 1 g of mixture, a room temperature conductivity of 43 S/m, and paramagnetic behavior.[25] Zhang et al. pyrolyzed polypropylene and maleated polypropylene with ferrocene in a 20 mL autoclave at 600 and 700 °C for 12h. At 600 °C, carbon nanotubes assembled into microspheres with diameters of 5.5 to 7.5 micrometers and individual tube diameters of 35 to 55 nm, giving a BET surface area of 140.6 m^2/g. At 700 °C, the product became dispersed carbon nanotubes with a lower BET surface area of 74.5 m^2/g. Temperature therefore controlled both assembly and porosity.[53]

Pol then showed that autogenic carbonization can proceed without a catalyst. Mixed waste LDPE, HDPE, PET, and PS were heated in a closed reactor under about 1000 psi, producing solid carbon microsphere with 30 to 55% conversion and 40% as a typical value. The product contained more than 99% elemental carbon, had a single sphere conductivity of 45 S/m, and showed room temperature paramagnetism.[54] The same study noted that adding 20 wt% cobalt acetate instead produced cobalt encapsulated carbon nanotubes, which directly connects catalyst free microsphere formation to the earlier catalytic work.[25,54] Zhang et al. extended the method to magnetic composites at a lower temperature of 500 °C. Waste PE, ferrocene, and ammonium acid carbonate in a 20 mL autoclave gave one-dimensional Fe_3O_4@C core shell structures about 800 nm in diameter and tens of micrometers in length, with a carbon shell of about 300 nm and Fe_3O_4 cores of 80 to 200 nm. The structures were acid resistant and ferromagnetic at room temperature, with saturation magnetization of 22.5 emu/g and coercivity of 152.9 Oe.[24] Finally, Fonesca et al. applied autogenic carbonization to saturation magnetization waste polystyrene cups (Figure 4b), which cannot be carbonized under conventional conditions because PS decomposes at about 450 °C. Heating 400 mg of PS in a sealed 4 mL Swagelok reactor at 600 or 700 °C for 3h produced disordered carbon. The 700 °C sample delivered 271.3 in the first discharge and retained about 116.1 mAh/g after 80 cycles, with an initial Coulombic efficiency of 52.8% and a BET surface area of 88 m^2/g. [55] This historical arc is therefore clear. The earliest studies used catalysts and ferrocene to grow carbon nanotubes and microsphere under autogenic pressure.[25,53] Pol demonstrated that pressure alone can retain carbon and yield pure conducting microsphere.[54] Later work expanded the route to magnetic core shell composites and sodium ion battery anodes, showing that autogenic carbonization is a versatile platform for converting mixed and otherwise non-carbonizable plastics into functional carbons.[24,55]

3.1.4 Template and Activation-Assisted Carbonization

Template and activation-assisted carbonization uses a sacrificial scaffold to control pore architecture, sometimes combined with chemical activation to further develop porosity. The hard template provides a rigid skeleton that the carbon replicates, and the template is later removed by acid washing. MgO is widely used because it can be removed by dilute non-corrosive acid, unlike silica templates that require hazardous HF. Within this family, four studies illustrate how template choice and activation conditions determine the final carbon architecture and its electrochemical performance.

Liang et al. developed a pyrolysis-deposition method that converts waste polystyrene into ordered mesoporous carbon using SBA-15 as hard template and $Fe(NO_3)_3$ catalyst. The method avoids complex CVD equipment by accomplishing pyrolysis and deposition in a single tube furnace. PS is pyrolyzed into small organic gases that are adsorbed into the mesochannels of Fe-SBA-15 by capillary actions and deposited as carbon under Fe catalysis. After etching the silica and Fe, the ordered mesoporous carbon replicates, the SBA-15 morphology with a 2D hexagonal *p6mm* structure. The optimal sample had a BET surface area of 1156 m^2/g and a pore volume of 1.23 cm^3/g. Without Fe catalyst, no carbon was

obtained, demonstrating the essential role of the catalyst. The ordered mesoporous carbon delivered 118 F/g at 0.2 A/g in 6 M KOH and retained 87.2% after 5000 cycles at 2 A/g.[56]

Ma et al. used MgO as template for pressurized carbonization of mixed plastics at 500 °C. The feedstock composition reflected real-world thermoplastic waste: PP 24%, LDPE 30%, HDPE 26%, PS 13%, PET 4%, and PVC 3%. The autoclave reactor prevented volatile products from escaping, forcing secondary reactions that increased carbon yield. MgO served two functions: as template for shape-controlled growth of carbon sheets and as HCl absorbent for PVC decomposition. The maximum BET surface area was 713 m^2/g at a MgO to polymer ratio of 4, and the maximum pore volume was 5.27 cm^3/g at a ratio of 6. Model experiments with aromatic compounds showed that anthracene produced the highest carbon yield (44.1 wt%), while benzene produced only 0.4 wt%, establishing that polycyclic aromatic hydrocarbons, especially acenes, are the main carbon sources.[57]

Min et al. addressed the critical limitation of halogen-containing polymers in catalytic carbonization by developing a universal MgO/$Fe(acac)_3$ combined template (Figure 4d). HCl released from PVC decomposition erodes equipment and poisons metal catalysts, but the basic MgO neutralizes the acid. The $Fe(acac)_3$ converts to Fe_3O_4 nanoparticles (15 to 20 nm) during carbonization, catalyzing growth of hollow carbon spheres on porous carbon flakes. The resulting 3D hollow carbon sphere/porous carbon flake hybrid was successfully produced from PS, PP, PE, PVC, and their mixtures with yields exceeding 70 wt%. The hollow carbon spheres had diameters of 15 to 20 nm matching the Fe_3O_4 nanoparticle size. BET surface areas ranged from 1245 to 1382 m^2/g with pore volumes of 4.45 to 4.68 cm^3/g. As a lithium-ion battery anode, the material delivered 802 mAh/g after 50 cycles at 0.5 A/g.[58]

Kumar et al. applied carbonization followed by physical activation to styrene-acrylonitrile (SAN) plastics from end-of-life printers. The SAN plastics were carbonized at 700 to 900 °C under nitrogen, then activated with CO_2 for 3 hours at the same temperature. The resulting activated carbons had disordered non-graphitic structures with interlayer spacing of 0.38 nm, larger than the critical value of 0.37 nm for sodium insertion. The S700 sample, carbonized and activated at 700 °C, delivered 180 mAh/g after 25 cycles at 3 mA/g and retained 100% of its second discharge capacity after 100 cycles at 20 mA/g. Higher activation temperature increased surface area from 497 to 1358 m^2/g but decreased capacity, because excessive surface area caused irreversible sodium uptake and thicker SEI formation. Solid-state 23 Na NMR revealed four distinct sodium environments at approximately -2, -10, -12, and -14 ppm, attributed to Na_2CO_3, $NaPF_6$-derived SEI species, graphitic intercalation, and nanopore filling, respectively. An additional site at 10 ppm present in S700 and S800 was electrochemically active and completely cycled out during charge, while the other sites were only partially reversible.[59]

Together, these studies demonstrate that template and activation-assisted carbonization can produce carbons with precisely controlled pore architecture from a wide range of plastic feedstocks, including halogen-containing polymers that poison conventional catalysts. The choice of template determines morphology: SBA-15 yields ordered mesoporous carbon,[56] MgO yields porous carbon sheets,[57] and

$MgO/Fe(acac)_3$ yields hollow carbon sphere/porous carbon flake hybrids.[58] Post-synthesis activation with CO_2 further tunes porosity and surface chemistry for specific applications.[59]

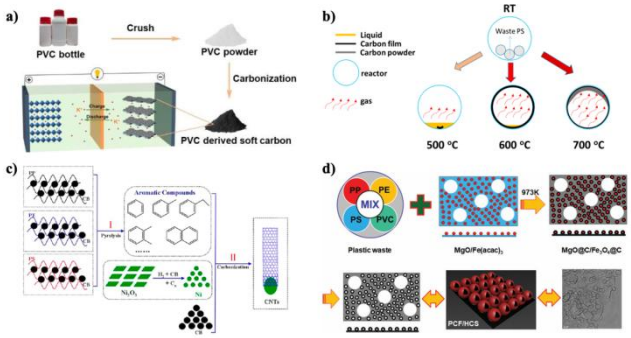


Figure 4. Overview of representative carbonization pathways for plastic waste upcycling. a) Direct carbonization of PVC into soft carbon for potassium-ion battery anodes. Adapted from ref [45]. b) Autogenic carbonization of waste polystyrene within a sealed reactor at different temperatures (500–700°C). Adapted from ref [55]. c) Catalytic carbonization showing the synergistic effect of combined catalysts on PP, PE, and PS to form carbon nanotubes (CNTs). Adapted from ref [48]. d) Template-assisted carbonization forming 3D porous hollow carbon sphere/porous carbon flake (HCS/PCF) nanomaterials. Adapted from ref [58]

3.1.5 Volatile-mediated Pyrolysis: CVD, Gasification, Deposition

Volatile-mediated routes decouple polymer decomposition from carbon growth. The plastic is first pyrolyzed into hydrocarbon-rich gas, and this gas is then decomposed over a catalyst or deposited onto a substrate. This separation allows the growth step to be tuned independently of the feedstock. The earliest work in this group used a single-stage configuration in which plastic and catalyst were heated together in one reactor. Mishra et al. pyrolyzed waste polypropylene with Ni catalyst at 600, 700, and 800 °C under Ar and H_2 for one hour (Figure 5a). The Raman I_G/I_D ratio rose to 1.74 at 800 °C, indicating improved purity and fewer defects relative to the lower-temperature products. XRD of the 800 °C sample showed 88.3% graphite and 11.7% Ni, whereas the 600 °C product contained iron-nickel oxide, magnetite, and NiFe impurities. The MWCNTs had diameters of 10 to 25 nm with about 20 graphene layers and reached 85% transmittance at 550 nm.[60] The same group later used these MWCNTs as binder-free supercapacitor electrodes.[61] The 800 °C sample delivered 59 F/g at 5 mV/s in 1 N KOH, compared with 44 and 37 F/g for the 600 and 700 °C samples, and also had the lowest resistance (0.73 Ω versus 2.72 and 2.78 Ω). Notably, the 600 °C sample had the highest surface area, so surface area alone did not determine capacitance. Residual Ni in the 700 °C sample produced faradaic reactions that raised capacitance at high scan rates, showing that metal residues can confound the surface-area-to-capacitance relationship.

Yang et al. scaled the concept to a pilot fluidized-bed system. Waste PP pellets packed in a PE bag were gasified at 600 °C, and the product gas passed through three parallel fixed-bed reactors containing Ni/Al_2O_3. The catalysts were calcined in air, N_2, or 5% H_2/He, labelled A, N, and H. Only the H_2-calcined catalyst contained NiO, and it also had the smallest NiO crystallite size at 6.4 nm. At 680 °C, H-Ni/Al_2O_3 gave 24.3% CNT yield and a H_2 production rate of 325.4 mmol/(h·g) of catalyst, with a H_2 promotion ratio of 48.9% relative to the uncatalyzed gas. The fluidized bed itself produced 23.9 mmol H_2 per gram of plastic without downstream catalysis, higher than fixed-bed reports, because of better heat and mass transfer. Increasing the catalysis temperature to 750 °C raised CNT yield to 30.5% but lowered graphitization, so 680 °C was optimal.[62]

Later work separated the process into three or more stages and tuned the catalyst for specific CNT morphologies. Abbas et al. treated flexible plastic packaging waste (PET 11.8%, PE 53%, PP 28.2%, plus Al, inks, and adhesives) in a three-stage train: pyrolysis at 550 °C, catalytic cracking of volatiles over Fe-ZSM at 400 °C, and CCVD over Ni-Ca at 700 °C. HNO_3 functionalization introduced oxygen and nitrogen groups (pyridinic N, pyrrolic N, nitro) at the expense of surface area, which fell from 189 to 144 m^2/g, yet specific capacitance rose from 23.9 to 33.5 F/g at 0.5 A/g and remained higher at every current density up to 5 A/g. Commercial MWCNTs delivered only 16.5 F/g. The authors concluded that surface functional groups, not surface area, controlled capacitive performance.[63] Nam et al. extended the approach to waste face masks and solid recovered fuel (SRF) via pyrolysis at 800 °C followed by CVD at 900 °C. CoMo/MgO favored few-walled CNTs (average diameter 3.46 nm for mask feedstock), while FeMo/MgO favored multiwalled CNTs (6.36 nm). Mask pyrolysis gas, rich in C_1–C_3 hydrocarbons and H_2, gave far higher yields than SRF gas, which contained more CO_2 and N_2. The combination of mask gas with FeMo/MgO reached 516.7 wt% carbon yield per catalyst and 97.9 wt% CNT purity. SRF gas produced bamboo-like CNTs because CO_2 drove dry reforming. When used as a cathode conductive additive at a low loading (NCM811/carbon/PVDF = 94:2:4), FeMo-CNT outperformed both Super P and commercial CNTs at high C-rates and gave 93.6% initial Coulombic efficiency versus 45.6% for Super P.[64]

A different variant of the volatile-mediated route deposits the carbon onto a solid substrate rather than growing free CNTs. Zhang et al. placed waste polystyrene foam and glass fibers side by side in a tube furnace and heated them under N_2 at 700 to 1000 °C (Fig. 5b). Polystyrene decomposed into alkylbenzenes, which carbonized and deposited as a graphene-like layer on the SiO_2 surface. The 900 °C, 2 h sample reached 614.7 S/m for the composite and 4.3×10^4 for the carbon layer, with a layer thickness of 200 nm. The sp^2/sp^3 ratio rose from 1.88 at 700 °C to 3.16 at 1000 °C, and C–Si bonds formed at 800 °C and above (19% at 900 °C, 26% at 1000 °C), anchoring the carbon to the glass. Tensile strength decreased only slightly, from 554 to 524 MPa. The carbon layer conductivity continued to rise to 5.5×10^4 S/m at 1000 °C, but composite conductivity peaked at 900 °C because of an optimal balance between carbon content and graphitization.[65]

Together these studies show that volatile-mediated routes give independent control over gas generation and carbon growth, and that this separation lets catalyst and substrate selection dictate product morphology, purity, and function. The earliest single-stage work established that temperature controls graphitization and purity,[60,61] the pilot-scale fluidized-bed work showed that catalyst calcination atmosphere controls the active Ni species and that gasification can co-produce H_2 and CNTs at scale,[62] and the more recent multistage studies demonstrated that catalyst composition and feedstock gas chemistry determine whether few-walled, multiwalled, or bamboo-like CNTs form and how they perform as battery additives or conductive coatings.[63–65]

3.1.6 Non-conventional and Medium-assisted Pyrolysis

Non-conventional and medium-assisted pyrolysis routes change the heating mechanism or the reaction environment rather than the feedstock chemistry. Microwave irradiation delivers volumetric heating through susceptors, molten salts provide a liquid medium that protects carbon and promotes graphitization, plasma supplies rapid thermal enthalpy, and hydrothermal water acts as both solvent and reactant. Palanisamy et al. used graphene nanoplatelets as microwave absorbers to convert polyethylene Ziploc bags and polystyrene packing foam into graphitic shell encapsulated cobalt nanoparticles in 2 minutes. The graphitic shell protected the cobalt from electrolyte contact, and the materials delivered 377 mAh/g for the polyethylene derived sample and 509 mAh/g for the polystyrene derived sample at the 250th cycle, compared with less than 1 mAh/g for the pristine cobalt graphene nanoplatelet mixture.[66] Cao et al. used MAX phase Ti_3AlC_2 as both microwave susceptor and catalyst for low density polyethylene (LDPE), high density polyethylene (HDPE), and polypropylene (PP) (Figure 5d).[67] Hydrogen selectivity reached 75, 78, and 78 vol% respectively, among the highest reported, and the resulting graphitic carbon nanofibers served as sodium ion battery anodes with stable cycling over 2000 cycles. Thermal plasma, mentioned earlier for waste polystyrene, converts polystyrene and urea into nitrogen doped porous carbon in 10 minutes with 482 F/g at 1 A/g (Figure 5e).[37] In the molten salt category, Kamali et al. showed that heating PET in molten NaCl at 1300 °C under an air atmosphere produces graphene nanostructures with 1150 S/m electrical conductivity and 522 m^2/g surface area,[34] while Ren and Kamali later demonstrated that NaCl-KCl molten salt at 800 °C increases PET carbonization yield from 44.8% to 50.8% and that subsequent ball milling raises reversible sodium capacity to 217.8 mAh/g after 100 cycles with 91.44% retention.[68] Kong et al. used a one-step hydrothermal route at 700 °C with polyethylene (PE) and metallic magnesium to form sandwich like porous carbon nanosheet-supported hexagonal carbon micro-flakes (WPWMC). The material delivered 528.7 mAh/g at 0.2 A/g, retained 373.4 mAh/g after 200 cycles, and still delivered 112.1 mAh/g after 10,000 cycles at 5 A/g, while a hybrid capacitor with CMK-3 achieved 222.7 Wh/kg at 446.2 W/kg.[69]

Chemically reactive media alter the pyrolysis pathway through a reagent that reacts with the polymer or its volatiles. Padha et al. used a reactive carbothermal route in which PET, TiO_2, and Li_2CO_3 were heated together at 800 °C to form a TiC-$Ti_3C_2O_2$ MXene carbide composite, which served as the electrode in a self-powered wearable supercapacitor with 556 F/g, 111.11 Wh/kg, and up to 700 mV

self-charging voltage.[70] Tang et al. introduced elemental sulfur at a 1:4 mass ratio with PE, PP, PS, and PVC at 700 °C. Sulfur underwent ring opening polymerization into linear polysulfanes that attacked carbon hydrogen bonds and crosslinked the polymer chains, inhibiting decomposition into volatile hydrocarbons. Carbon atom recovery reached 85% for PE, 80% for PP, 67% for PVC, and 56% for PS, far above conventional pyrolysis. The sulfur rich carbons had enlarged interlayer spacing and delivered 662 mAh/g initially and 289 mAh/g at 10 A/gfor PE, while the polystyrene derived carbon retained 256 mAh/g after 4000 cycles at 10 A/g.[71] Qiu et al. demonstrated co-pyrolysis of spent NCM battery cathodes with PET and other plastics at 550 °C (Figure 5c). The NCM was reduced to $NiCoMnO_x$ and Li_2CO_3, and the NiCo alloy catalyzed growth of carbon nanotubes with a carbon conversion rate of 33%. The product achieved a microwave absorption bandwidth of 7.01 GHz at 2.41 mm, and life-cycle analysis showed global warming potential at only 47.5% of the pyrometallurgical route, with an estimated profit of $1500 per kilogram.[72] Thus, these routes show that non-conventional heating and reactive media can overcome the limitations of conventional pyrolysis, including low carbon yield from polyolefins, high energy input, and poor control over graphitization and heteroatom doping.

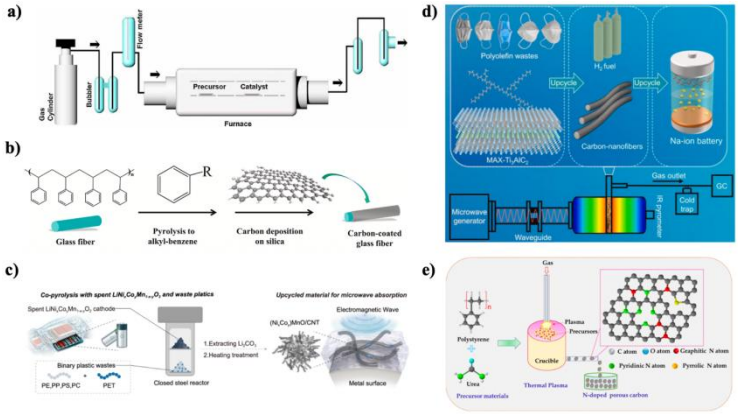


Figure 5. Representative volatile-mediated and medium-assisted pyrolysis routes for plastic upcycling. a) Volatile-mediated pyrolysis CVD: Schematic of the single-stage CVD setup for synthesizing CNTs from waste polypropylene. Label denotes: a) gas cylinder, b) bubbler, c) flow meter, d) stainless steel tube, e) furnace, f) precursor boat, and g) catalyst boat. Adapted from ref [60]. b) Volatile-mediated pyrolysis deposition: Schematic preparation of carbon-coated glass fibers (CGFs) from waste polystyrene foam. Adapted from ref [65]. c) Co-pyrolysis of spent NCM cathodes and binary plastic waste to produce (Ni_xCo_y)MnO/CNT composites for microwave absorption. Adapted from ref [72]. d) Microwave-initiated MAX (Ti_3AlC_2)-catalytic upcycling of polyolefin wastes into hydrogen fuel and carbon nanofibers for sodium-ion batteries. Adapted from ref [67]. e) Thermal plasma-assisted pyrolysis converting polystyrene and urea into nitrogen-doped porous carbon. Adapted from ref [37]

3.2 Non-pyrolytic Routes

Non-pyrolytic routes convert waste plastics into functional materials without destroying the polymer backbone through high-temperature carbonization. These approaches preserve the intrinsic chemical structure and often the morphology of the original plastic, enabling precise control over the final product's composition and properties. They encompass chemical depolymerization to recover monomers for repolymerization, direct functionalization of intact polymer chains, blending and composite fabrication with fillers, surface and interface assembly to add functionality while retaining flexibility, and the synthesis of metal-organic frameworks from plastic-derived ligands. Compared with pyrolysis, these routes offer milder processing conditions, lower energy consumption, and the ability to produce high-value materials such as polyurethanes, polymer electrolytes, conductive composites, and porous frameworks for energy storage and environmental applications. The following subsections detail these strategies, highlighting their mechanisms, products, and performance metrics.

3.2.1 Depolymerization, Solvolysis, and Downstream Polymerization

Chemical depolymerization cleaves the ester or amide bonds of condensation polymers to recover monomers or oligomers that can be repolymerized into high-value materials. Unlike pyrolysis, which destroys the polymer backbone entirely, depolymerization preserves the aromatic and functional groups of the original monomer, enabling products with defined structure and functionality. This section covers hydrolysis, glycolysis, aminolysis, molten-salt depolymerization, and electrochemical routes, followed by downstream polymerization into polyurethanes, polyesters, polymer electrolytes, and ionogels.

Hydrolysis of PET yields terephthalic acid and ethylene glycol. Kamali and Li used a eutectic KCl-LiCl molten salt containing $SnCl_2$ at 500 °C for 20 minutes under atmospheric pressure. $SnCl_2$ co-melts with PET at about 250 °C, and the molten salt enhances crystallization of terephthalic acid while promoting partial oxidation of $SnCl_2$ to SnO_2 nanocrystals. The product contained 28.3 wt% SnO_2 with crystallites below 5 nm embedded in terephthalic acid. As a lithium-ion battery anode, it delivered 498 mAh/g after 500 cycles at 200 mA/g, corresponding to 1657 mAh/g of SnO_2.The terephthalic acid matrix formed hydrogen bonds with SnO_2, accommodating volume changes during cycling. The lithium-ion diffusion coefficient increased from 2.80×10^{-11} cm^2/s in the fresh electrode to 8.51×10^{-10} cm^2/s after 300 cycles. The production yield reached 82.4% with respect to the initial PET.[15] Wang et al. used hydrolysis followed by solvothermal synthesis to convert PET into CoNi-MOF. PET was hydrolyzed in ethylene glycol and water at 210 °C for 8 hours, yielding terephthalic acid with nearly 100% conversion. The recovered BDC was combined with $CoCl_2 \cdot 6H_2O$ and $NiCl_2 \cdot 6H_2O$ in DMF, ethanol, and water and heated at 150 °C for 24 hours. The optimal $Co_{0.8}$Ni-MOF had a dandelion-like morphology and a BET surface area of 13.69 m^2/g. As a lithium-ion battery anode, it delivered initial discharge and charge capacities of 2496 and 1729 mAh/g, with Coulombic efficiency over 99% after 200 cycles.[16] The low surface area was advantageous because ultrahigh surface area MOFs can cause excessive side reactions with the electrolyte at low potentials. Kaur et al. depolymerized PET via alkaline hydrolysis using NaOH and ethylene glycol at 200 °C for 30 minutes.

The resulting terephthalic acid was used as an organic linker for MIL-53(Fe) synthesis via hydrothermal treatment at 150 °C for 12 hours. The Fe-MOF was then coated with polyaniline via in-situ oxidative polymerization at 0 °C. The composite was hot-pressed onto stainless steel mesh and used in a microbial fuel cell. The device achieved 680 mW/m^2 power density, 0.67 V open-circuit potential, and 3500 mA/m^2 limiting current density. It maintained stable voltage output over 370 hours across three cycles with fresh anolyte.[17] Zhang et al. introduced paired electrolysis to simultaneously recover cathode metals from spent lithium-ion batteries and depolymerize PET. The strategy couples electrochemical reduction of $LiCoO_2$ at the cathode with oxidative degradation of PET hydrolysate at the anode. Protons generated from PET oxidation replace the oxygen evolution reaction, reducing cell voltage from 1.86 V to 1.35 V, a 35% energy saving. After 12 hours of electrolysis at 1.5 V vs RHE, lithium leaching reached nearly 100%, and cobalt was recovered as $Co/Co(OH)_2$. Ethylene glycol was selectively oxidized to formate with 86% yield and over 80% Faradaic efficiency, while terephthalic acid remained unreacted and was recovered by pH adjustment. Net profit reached $813.20 per ton of spent batteries, exceeding pyrometallurgy and hydrometallurgy, with CO_2 emissions reduced by 1.10 to 2.80 tons per ton (Figure 6a).[73]

Glycolysis uses diols such as ethylene glycol to cleave ester bonds, producing bis(2-hydroxyethyl) terephthalate (BHET). Guo used polycaprolactone diol to alcoholize PET at 180 to 185 °C for 3 hours, yielding a PCL-PET oligomer. This was chain-extended with hexamethylene diisocyanate and 1,4-butanediol to form a polyurethane elastomer. Lithium bistrifluoromethanesulphonylimide (LiTFSI) was added during prepolymerization to confer ionic conductivity. The optimal sample with 10 wt% LiTFSI achieved 7.05 S/cm^2 conductivity, 0.112 mm^2/s thermal diffusivity, and thermal stability up to 260 °C. XPS confirmed that LiTFSI was chemically bonded rather than merely dissolved, so the product was a copolymer rather than a composite.[74] Hao et al. developed a one pot glycolysis and polymerization route to produce a eutectogel (E-GEL) for flexible ionic conductors. Waste PET was glycolyzed using a ternary deep eutectic solvent of choline chloride, ethylene glycol, and zinc acetate at 180 °C for 3 hours, achieving 100% PET conversion and 70.09% BHET yield. The glycolysis solution was used directly without purification to synthesize waterborne polyurethane via reaction with isophorone diisocyanate. The waterborne polyurethane (WPU) was combined with acrylamide, acrylic acid, and a binary DES and cured under UV light for 20 seconds. The optimal eutectogel had 8.87 MPa tensile strength, 680% elongation at break, and 9.65 mS/cm ionic conductivity. It withstood temperatures from -50 to 80 °C with a glass transition temperature of -53.5 °C. As a strain sensor, it detected finger bending at 30°, 60°, and 90°, wrist bending, and swallowing motions, and maintained stable resistance over 1000 cycles at 25% strain.[75] Hao et al. extended this approach to ionogels using ionic liquid catalyst [EMIM][DCA] as catalyst. PET was glycolyzed at 175 to 195 °C for 2 to 3 hours, achieving 100% conversion with 90.47% BHET and 9.53% oligomers. The glycolysis solution was used directly to synthesize polyurethane, which was then combined with acrylamide, acrylic acid, and the ionic liquid EMIES and UV-cured. Because of the high ionic liquid content, the optimal ionogel

achieved a high ionic conductivity of 0.09 S/cm (comparable to that of the neat ionic liquid), alongside a tensile strength of 4.2 MPa and a 990% elongation at break. It self-healed at room temperature within 6 hours, recovering 100% of its conductivity and 90% of its tensile strength. It served as an ionic skin sensor over 500 cycles at 25% strain.[76] Shafik used glycolysis to produce a functional additive for waste polystyrene and PVC blends. PET was glycolyzed with ethylene glycol at 180 to 190 °C using zinc acetate as catalyst, yielding GPET. This was then reacted with adipic acid and phthalic anhydride to form an unsaturated polyester. The polyester increased melt flow rate from 0.48 to 0.975 g/10 min and tensile strength from 10.6 to 21.96 MPa, while GPET increased elongation at break from 12% to 37%. The polyester reduced burning rate from about 4 mm/s to 0.5 mm/s and combustion energy from 552 cal to 404 cal. Dielectric analysis showed that polyester exhibited the strongest interfacial polarization, increasing permittivity and dielectric loss (Figure 6b).[77] Wang et al. used glycolysis to produce BHET for self-healing polyurethane electrodes. PET was glycolyzed with ethylene glycol at 200 °C for 3 hours using zinc acetate, yielding 97.1% BHET after recrystallization. The BHET was used as a chain extender for polyurethane synthesized from polytetrahydrofuran and isophorone diisocyanate. The PU elastomer had a glass transition temperature of -64.1°C, tensile strength of 8.13 MPa, and elongation at break of 1874%. The abundant hydrogen bonds in the hard segments enabled self-healing at 70°C with 90% recovery after 2 hours. The PU was combined with hybrid carbon nanofillers (CB and CNT at 1 to 3 ratio, 15 vol%) to form a conductive composite with 8.20×10^2 S/m conductivity. The composite electrode maintained 94.3% capacitance after five cutting and healing cycles and 95.1% after 1000 bending cycles. Areal capacitance reached 119.7 mF/cm^2, and energy density reached 16.5 μWh/cm^2.[78]

Aminolysis uses amines such as ethanolamine to cleave ester bonds, producing bis(2-hydroxyethyl) terephthalamide (BHETA). Tan et al. depolymerized PET with ethanolamine at 150 to 200 °C using an organocatalyst. The BHETA was reacted with polyethylene glycol and hexamethylene diisocyanate to form a polyurethane electrolyte. Polymer yields ranged from 91.2% to 96.6% depending on the PEG ratio. The solid polymer electrolyte achieved 2.5×10^{-7} S/cm at 20 °C and 3.4×10^{-6} S/cm at 60 °C. The gel polymer electrolyte with ionic liquid reached 3.9×10^{-4} S/cm at 20 °C and 1.5×10^{-3} S/cm at 60 °C. The lithium transference number was 0.48, and Coulombic efficiency exceeded 98% after 150 cycles.[79]

Molten salt and solvothermal depolymerization provide high-boiling inorganic media or controlled solvothermal conditions. Kamali and Li demonstrated molten salt for PET at 500 °C under atmospheric pressure.[15] Wang et al. used solvothermal conditions at 210 °C for hydrolysis and 150 °C for MOF synthesis. These routes avoid the high-pressure reactors required for supercritical water or ethanol.[16]

Downstream polymerization and polycondensation convert recovered monomers and oligomers into polyurethanes, polyesters, polymer electrolytes, and ionogels. A common theme is that one pot approaches, in which the glycolysis or aminolysis product is used directly without monomer purification, simplify the process and improve economics. Hao et al. demonstrated this for both eutectogels and ionogels.[75,76] Wang et al. achieved 97.1% BHET yield but still required recrystallization

to obtain high-purity monomer. The trade-off between purity and process simplicity depends on the application.[78] For polymer electrolytes and ionogels, oligomers may be acceptable or even beneficial as plasticizers or crosslinkers. The integration of depolymerization with downstream polymerization also enables incorporation of functional fillers and additives, as shown by Wang et al. with carbon nanofillers,[78] Hao et al. with deep eutectic solvents and ionic liquids,[75,76] and Guo with LiTFSI.[74]

3.2.2 Direct Functionalization of Intact Polymers

Direct functionalization modifies the chemistry of an intact polymer chain without cleaving the backbone. Because the molecular weight and often the morphology of the original material are retained, this route is attractive for converting commodity plastics into membranes, separators, dielectric films, and electronic materials. The main chemistries in this group are grafting or copolymerization, sulfonation, and nitration. Early work focused on membranes and model catalysts, while later studies have moved toward waste feedstocks, precise control over functional group density, and electronic applications.

Grafting, click chemistry, and copolymerization allow functional groups or organometallic units to be attached to an intact polymer backbone. Wang et al. functionalized commercial PVC with diiron carbonyl units through two routes. One route used direct reaction between reduced diiron hexacarbonyl and the C–Cl bonds of PVC, while the other first converted PVC to PVC azide and then used copper catalyzed click chemistry with alkynyl diiron complexes. The functionalized polymers were blended with multiwalled carbon nanotubes (MWCNT) and Nafion and assembled into film electrodes. The electrodes showed catalytic proton reduction with a positive shift in reduction potential of more than 400 mV compared with the monomeric diiron complexes. However, repetitive scanning caused about 80% loss of the reduction current after the first scan, indicating reductive bleaching of the active units.[80] Zhang et al. used metallocene mediated copolymerization to prepare polyethylene-based anion exchange membranes. Ethylene was copolymerized with a silane protected amino-olefin and a styrene diene crosslinker, and the resulting films were thermally crosslinked and converted into quaternary ammonium chloride groups. The optimized membrane contained 28.1 mol% ammonium chloride groups and 0.2 mol% crosslinker. It reached an ionic conductivity of 119.6 mS/cm in 2 N HCl and 78.8 mS/cm in 2 N HCl-0.2 N CuCl, which is one order of magnitude higher than commercial anion exchange membranes. The crosslinked film also had a tensile strength of about 20 MPa and an elongation at break of 181%.[81] Both studies date from 2011, but they illustrate different goals for direct functionalization. Wang et al. approach anchors molecular catalysts for electrocatalysis[80] while Zhang et al. builds ion conducting membranes for electrochemical devices.[81] Later studies extend the same principle to waste polystyrene and to dielectric energy storage, showing that direct functionalization remains a versatile route for upgrading plastics without depolymerization.[31,82]

Sulfonation introduces sulfonic acid groups onto aromatic rings or polymer backbones. Allan et al. sulfonated porous PVC membranes through a two-step reaction with ethylenediamine followed by sulfuric acid. The reaction preserved the original porous morphology, and the ion exchange capacity

reached 0.78 meq/g after one day. The sulfonated PVC showed proton conductivity 2.5 to 4 times higher than Nafion 115 at similar relative humidity, and even at 45% relative humidity it outperformed unmodified PVC measured at 95% relative humidity. The improvement came from both proton hopping through the sulfonic acid groups and increased water retention.[83] Kim et al. applied sulfonation to waste respirator masks. The middle polypropylene filter layer was treated with fuming sulfuric acid for 4 minutes, which converted the hydrophobic surface into a hydrophilic one with hydroxyl and sulfonic acid groups. The contact angle decreased from 144.2° ± 1 for the pristine mask to 74.2° ± 1 for the optimized sample. In a Zn//Zn symmetric cell, the sulfonated mask separator reduced the overpotential from about 80 mV for glass fiber to 24 mV, and a Zn-MnO_2 full cell retained 93.5% of its capacity after 200 cycles. The separator also showed an anodic stability of 4.75 V versus Li/Li+ and stable cycling for 1000 hours at 2 mA/cm^2.[84] As discussed earlier, Lo et al. used an imidazolium based sulfonating agent to sulfonate polystyrene with controlled degrees of sulfonation. Expanded polystyrene waste reached 92 to 94% sulfonation, and the resulting PEDOT:PSS showed a conductivity of 8.5 S/cm, an OECT mobility capacitance product of 113.6 F/(cm·V·s), and a hybrid solar cell efficiency of 6.9%, close to the 8.4% of commercial Clevios PH1000.[31] Compared with the earlier PVC and mask studies, this work shows a shift from morphology retention and separator engineering toward precise control of functional group density and electronic device integration (Figure 6c).

Nitration adds nitro groups to aromatic rings and is another way to tune dielectric properties without breaking the polymer chain. Tang et al. nitrated polystyrene in one step using nitric acid and sulfuric acid in 3-nitrotoluene. The nitro group has a dipole moment of 3.6 D, and its incorporation increased both the glass transition temperature and the permittivity. The glass transition temperature rose linearly from 105 °C to 165 °C as the substitution degree increased from 5% to 66%, while the permittivity at 1 kHz increased non-linearly from 2.6 to 4.27. The sample with 15% substitution achieved a discharge energy density of 6.32 J/cm^3 at 640 MV/m, which is 2.38 times that of neat polystyrene. The sample with 66% substitution produced 1.1 J/cm^3 at 200 MV/m and 100 °C with 88% efficiency, benefiting from its high glass transition temperature. Density functional theory showed that the nitrobenzene units act as charge traps and disrupt the $\pi-\pi$ accumulation pathways that would otherwise allow high field conduction.[82] This study demonstrates that direct nitration can simultaneously raise permittivity and breakdown strength, which are usually difficult to improve together (Figure 6d).

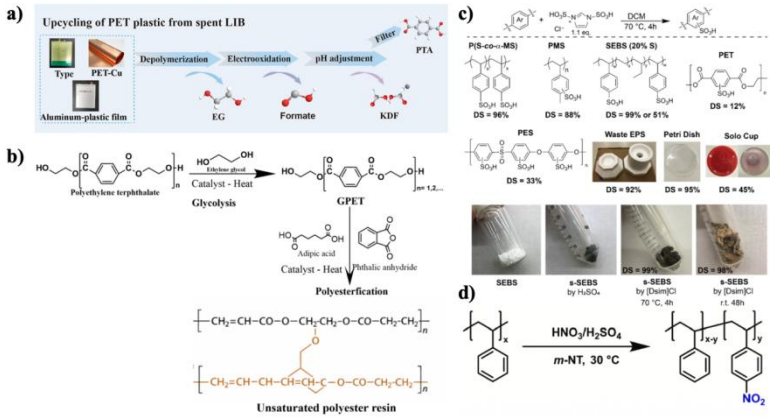


Figure 6. Representative non-pyrolytic routes for upcycling waste plastics into functional materials. a) Paired electrolysis of spent $LiCoO_2$ cathodes and PET hydrolysate, integrating cathode metal recovery with PET oxidation to formate, terephthalic acid (PTA), and potassium diformate (KDF). Adapted from ref [73]. b) Glycolysis of PET to glycolyzed PET (GPET) and subsequent synthesis of an unsaturated polyester resin used as an additive for waste polystyrene/PVC blends. Adapted from ref [77]. c) Sulfonation of polystyrene (PS) using the imidazolium-based sulfonating agent [Dsim]Cl. Top: previous strategies can produce defects such as chain scission, incomplete sulfonation, ortho-substitution, and sulfone crosslinking. Bottom: this work uses a stoichiometric, regenerable [Dsim]Cl to achieve controlled degrees of sulfonation and high para-selectivity. Adapted from ref [85]. d) One-step nitration of polystyrene with HNO_3/H_2SO_4 in 3-nitrotoluene to produce nitrated polystyrene with tunable nitro substitution. Adapted from ref [82]

3.2.3 Blending and Composite Fabrication

Blending and composite fabrication incorporate fillers or a second polymer phase into a plastic matrix without chemically converting the backbone. Solution blending disperses fillers in a polymer solution, melt blending mixes components in the molten state, sulfur crosslinking stabilizes the interface through covalent bonds, and thermal welding preserves molecular orientation while building layered architectures.

Solution blending was first established with virgin polymers. Chang et al. dispersed single wall carbon nanotubes in polystyrene using o-dichlorobenzene (DCB) and ultrasonication, reaching a percolation threshold below 0.3 wt% after thermal annealing of the nanotubes and a linear Raman D*-band shift of approximately 0.43 cm^{-1} per MPa, indicating good load transfer.[86] Qi et al. later compared graphene and carbon nanotubes in polystyrene and found that graphene reached 3.49 S/m at 1.1 vol%, two to four orders of magnitude higher than carbon nanotubes, while the addition of polylactic acid forced graphene into the polystyrene rich regions and reduced the percolation threshold from 0.33 to 0.075 vol%.[32] These early studies used virgin polystyrene but established the principles of filler dispersion and selective localization that later work applied to waste feedstocks. Ighalo and Adeniyi dissolved

waste polystyrene into a resin and mixed in 150 μm aluminum particles at 10 to 40 wt%, reducing the resistivity from 1.32×10^7 to 1.38×10^6 ohm·cm while density increased from 0.81 to 1.20 g/cm^3 and voidage decreased from 5.26% to 1.41%.[87] Vijaya and Kennedy mixed waste expanded polystyrene (EPS) with reduced graphene oxide (rGO) in a 1 to 1 ratio and observed a sharp infrared band at 694 cm^{-1} and an increased intensity ratio I_G/I_D from 0.418 to 0.539, both attributed to π–π stacking between the phenyl rings and the graphene basal plane. The composite electrode delivered 11.9 mF/cm^2 at 0.1 mA/cm^2 in 6 M KOH and retained 99.5% of its capacitance after 10,000 cycles in 1 M Na_2SO_4.[88]

Melt blending avoids solvents and is more scalable. Ahmadian Hoseini et al. used a non-recyclable waste consisting of 60 wt% vulcanized rubber and 35 wt% PVC as an excluded volume filler in a polystyrene and carbon nanotube system. Because the waste did not melt at 180 °C, carbon nanotubes were confined to the polystyrene phase, reducing the percolation threshold by 30% and increasing conductivity by four orders of magnitude at 1.0 wt% carbon nanotubes compared with the composite without waste. The composite with 50 wt% waste and 3.0 wt% carbon nanotubes reached an EMI shielding effectiveness of 9.55 dB with absorption dominating.[89] Hu et al. blended recycled high-density polyethylene (HDPE) with virgin high-density polyethylene and carbon black for positive temperature coefficient thermistors. Increasing the recycled content from 0 to 25% raised the room temperature resistivity from 0.401 to 0.568 ohm·cm and the PTC intensity from 3.253 to 4.922 but also strengthened the negative temperature coefficient effect. Adding 0.2 wt% dicumyl peroxide (DCP) eliminated this effect, increased the PTC intensity by 64.5% over the virgin system, and reduced the resistivity increase after three thermal cycles to 24.91%.[90] Slobodian et al. took a different route and used unsorted postconsumer plastic waste directly as triboelectric layers without any filler or chemical treatment. A blend containing 60 wt% polyethylene terephthalate (PET) and 40 wt% of an equal mixture of polystyrene (PS), high density polyethylene (HDPE), and polypropylene (PP), paired with a polyethylene terephthalate (PET) bottle film, produced a peak output voltage of 130 V, a short circuit current density of 50 μA/cm^2, and a power density of 2604 μW/cm^2.[91] The authors attributed this to the immiscibility of the mixed plastics, which created heterogeneous hardness and stress concentration regions that promoted contact electrification. Even the rejected recyclable plastic waste fraction, which is largely landfilled, generated over 60 V when paired with polyethylene terephthalate (PET).

Sulfur crosslinking introduces covalent bonds that reduce interfacial thermal resistance. Wang et al. combined waste polystyrene and pyrrhotite tailings with a styrene butadiene styrene copolymer and sulfur. Crosslinking formed C–S bonds between the copolymer and the pyrrhotite surface, as confirmed by infrared peaks at 751 and 983 cm^{-1} and a sulfur 2p X-ray photoelectron spectroscopy peak at 162.7 eV. The composite with 95 wt% pyrrhotite achieved a thermal conductivity of 1.36 W/(m·K), an electrical resistivity above 10^8 Ω·m, and an EMI shielding effectiveness of 33.1 dB with absorption dominating. An LED attached to this composite reached only 26.8 °C after extended operation, compared with 47.6 °C for an LED on neat polystyrene.[92] Wang et al. extended this approach with approximately 5 nm carbon dots as a dual interface coupling enhancer. The carbon dots formed C–S

and C=S bonds with both the pyrrhotite (Pyr) and the waste poly(acrylonitrile-co-butadiene-co-styrene) (ABS) matrix, and the optimal composite with 88 wt% pyrrhotite reached a thermal conductivity of 1.68 W/(m·K), an improvement of 1988% over the neat polymer. The tensile strength reached 41.7 MPa, exceeding commercial acrylonitrile butadiene styrene, while the electrical resistivity remained above 10^{11} Ω·m and the EMI shielding effectiveness reached 43.1 dB with reflection accounting for only 2.64% of the total shielding.[93]

Thermal welding preserves molecular orientation while building layered architectures. Jiang et al. used discarded biaxially oriented polypropylene films as insulating layers and polypropylene random copolymer sheets containing multiwalled carbon nanotubes and graphene nanoplatelets as conductive layers. The layers were alternately stacked and welded at 160 °C, above the melting point of the random copolymer at 140 °C but near the onset of biaxially oriented polypropylene melting at 168 °C. At this temperature the biaxially oriented polypropylene (BOPP) entered a partially molten state that allowed interfacial chain diffusion without fully relaxing the oriented structure, as confirmed by the elliptical small angle X-ray scattering pattern with equatorial intensity maxima. The resulting composite had an in-plane conductivity of 11.4 S/m and a through thickness resistivity above 10^8 Ω·m, an anisotropy spanning nine orders of magnitude. The tensile strength reached 52.08 MPa and the impact toughness reached 46.75 kJ/m^2, improvements of 224% and 360% over the isotropic control. In an LED circuit test, the composite illuminated the LED brightly in the in-plane directions but not through the thickness, and the surface temperature rose by only 3.4 °C after 180 seconds, compared with 25.1 °C for the isotropic control.[94]

3.2.4 Surface and Interface Assembly

Surface and interface assembly modifies the surface of waste plastics or builds functional layers on their surfaces without changing the bulk polymer. These routes are especially useful for textiles, foams, masks, and films because they preserve flexibility and porosity while adding conductivity, sensing, or energy harvesting functions. The main approaches are layer-by-layer assembly, dip coating and related solution coating, electropolymerization and in situ polymerization, electrostatic assembly and sputtering, and electrospinning with surface modification.

Layer-by-layer assembly builds alternating cationic and anionic layers through electrostatic and hydrogen bonding interactions. Chang et al. used upcycled thermoplastic polyester elastomer (TPEE) films from PET waste as substrates and alternately deposited poly(ionic liquid-co-acrylic acid) (PIL-co-PAA) and MXene nanosheets. The films elongated more than 700%, healed at room temperature in 3 seconds with 33% tensile strength recovery and over 75% after 3 hours, and showed gauge factors of about 270 at 0 to 10% strain and 2800 at 30 to 40% strain. Alkaline vapor increased conductivity by 2.9 to 13.1% depending on bilayer number.[95] In a related study, Chang et al. replaced the cationic layer with chitosan or PDAC. The PDAC-based films had higher conductivity because PDAC has more charged sites, and they retained about 91% of ultimate tensile strength after 100 cycles, with gauge factors of 7.4 at 40 to 60% strain and 33.5 at 80 to 100% strain.[96] These studies show that

layer-by-layer assembly can combine self-healing, stretchability, and strain sensing on a waste-derived elastomer.

Dip coating and related solution coating are the simplest surface assembly methods. Hu et al. established the approach by dipping cotton and polyester textiles into single-walled carbon nanotube ink, reaching a sheet resistance below 1 Ω/sq and a conductivity of 125 S/cm. The porous textile enabled an areal capacitance of 0.48 F/cm^2 and a specific capacitance of 140 F/g, and the device retained performance over 130,000 cycles.[97] This early work did not use waste plastics but provided the template for later waste-based electrodes. Xie et al. coated polyester textile with carbon nanotubes for microbial fuel cell anodes. The open three-dimensional structure gave a tenfold larger interfacial area than carbon cloth, a maximum current density of 7.2 A/m^2, a power density of 1098 mW/m^2, and a charge transfer resistance of about 30 Ω compared with 300 Ω for carbon cloth.[98] Xie et al. then replaced textile with polyurethane (PU) sponge. The continuous three-dimensional carbon nanotube coating gave a conductance of about 1 S/cm, a current density of 2.13 mA/cm^2 in glucose, and power densities of 1.24 W/m^2 and 182 W/m^3 with domestic wastewater, the highest values reported at the time.[99] Wang et al. applied a similar dip coating and freeze-drying route to waste polyurethane foam, using carbon nanotubes and cellulose nanofibers followed by in situ polymerization of aniline. The all-solid-state supercapacitor delivered 284.6 F/g at 0.25 A/g and retained 97.8% of capacitance after 1000 cycles, and a wristband device powered an electronic watch.[38] Mendoza et al. used solution coating and doctor-blade deposition on waste face masks. Graphene ink was dropped onto mask disks, and $Ca_3Co_4O_{9-\delta}$ (CaCo) oxide was deposited from a slurry. The device with oxide reached 1706.2 F/g and 208.4 Wh/kg, maintained a stable output for 10 hours, and retained 82.1% of capacitance after 1500 cycles. Pressing with 0.1 to 0.5 kg weights reduced capacitance by only 0.7 to 1.5%.[100]

Electropolymerization and in situ polymerization form conductive polymer coatings directly on the waste substrate. Zuo et al. fully utilized all three layers of waste surgical masks to fabricate a quasi-solid-state flexible supercapacitor. The two outer polypropylene spunbonded layers were sputtered with gold to serve as conductive current collectors, then polypyrrole microcones were grown on them by electropolymerization at 2 V for 80 minutes. The interlayer was soaked in PVA/H_2SO_4 hydrogel electrolyte and used as the separator. The PPy/WSM-80 electrode achieved an areal capacitance of 1039.1 mF/cm^2 (37.2 F/cm^3) at 1 mA/cm^2, and the assembled device delivered 219.1 mF/cm^2 (8.0 F/cm^3) at 1 mA/cm^2. The device exhibited a maximum energy density of 19.48 μWh/cm^2 at a power density of 219.2 μW/cm^2, and a maximum power density of 3.3 mW/cm^2 at an energy density of 15.2 μWh/cm^2. The device retained 92.1% of capacitance after 10,000 charge/discharge cycles and 88.3% after 100,000 bending cycles. The electrode could be cut into designable shapes such as Chinese characters or aircraft while maintaining performance.[101] This study demonstrates that electropolymerization on gold-sputtered waste masks can produce high-performance, flexible, and shape-designable supercapacitors without additional binders or current collectors. In a related approach, Wang et al. used in situ polymerization of aniline on a carbon nanotube and cellulose nanofiber coated

waste polyurethane foam. The composite electrode reached 372.6 F/g in liquid electrolyte and 284.6 F/g in all-solid-state form.[38] This method avoids separate binder and ensures conformal coating on complex foam surfaces.

Electrostatic assembly, sputtering, and lamination build functional layers through charge interactions or physical transfer. Das et al. laminated waste plastic bags with aluminum foil and paired them with layered VS_2, SnS_2, or hBN. The plastic-hBN triboelectric nanogenerator produced 68 V, 6.1 μA, and 460 mW/m^2, and remained stable over 10,000 cycles.[102] The output scaled with the product of resistivity and dielectric constant, linking material selection to device performance. Feng et al. sputtered gold onto recycled polyamide (PA), PVC, and PE plastic bags and assembled triboelectric pairs. The PA-PVC device gave 35.7 V, 5.85 μA, and 152.6 mW/m^2, and after rectification it charged a supercapacitor to drive LEDs and serve as an antitheft alarm.[103] Zhang et al. used electrostatic self-assembly to coat tannic acid onto polypropylene fibers from waste masks and then assemble graphene nanoplatelets through cation-π interactions and hot pressing. The resulting composite reached a thermal conductivity of 87 W/(m·K), an EMI shielding effectiveness of 88 dB (1100 dB/cm), an electrical conductivity of 893 S/m, and a peeling force of 970 N.[104] Jiang et al. used thermal welding and alternating layer assembly of discarded biaxially oriented polypropylene films and conductive polypropylene random copolymer layers. The in-plane conductivity was 11.4 S/m, through-thickness insulation exceeded 10^8 Ω, tensile strength reached 52.08 MPa, and toughness reached 46.75 kJ/m^2, with a temperature rise of only 3.4 °C under electrical heating compared with 25.1 °C for the isotropic control.[94]

Electrospinning and surface modification convert waste polymers into nanofibers and then modify their surfaces for added function. Yavari et al. dissolved waste PVC pipes and electrospun PVC/ZnO nanofibers. The optimal 0.5 wt% ZnO sample reached 196 V, 8.1 μA, and a power density of 726.3 μW/cm^2, maintained 90% stability after 172,800 cycles, and lit 192 green and 50 red LEDs. The piezoelectric ZnO coupled with the triboelectric PVC enhanced charge generation.[43] Roy et al. electrospun waste PET bottles into a three-dimensional aerogel, then coated it with polydopamine and polyethyleneimine. The aerogel (PPP) removed 98.3% of Pb(II), 95.3% of Hg(II), and 92.7% of Zn(II) from water, and as a triboelectric layer with PVDF it produced 67.7 V, 9.4 μA, and a power density of 5.47 W/m^2. It lit 36 LEDs, remained stable over 10,000 cycles, and retained performance after 65 days.[105] These studies show that electrospinning can create high-surface-area architectures for both environmental remediation and energy harvesting.

3.2.5 MOF and Coordination Polymer Synthesis from Plastic-derived Ligands

Metal-organic frameworks built from waste plastic linkers offer a high-value route to porous materials. PET is especially suitable because hydrolysis yields terephthalic acid, a rigid aromatic dicarboxylate that is a common MOF linker. Wang et al. hydrolyzed waste PET at 210 °C for 8 hours with nearly 100% conversion to terephthalic acid, then combined it with $CoCl_2$ and $NiCl_2$ in DMF, ethanol, and water at 150 °C for 24 hours to form CoNi-MOF. The optimal $Co_{0.8}$Ni-MOF delivered 2496 mAh/g

initial discharge and 1729 mAh/g initial charge as a lithium-ion battery anode, with Coulombic efficiency over 99% after 200 cycles.[16] Kaur et al. used alkaline hydrolysis of PET to obtain terephthalic acid, then synthesized MIL-53(Fe) by hydrothermal treatment at 150 °C for 12 hours. The Fe-MOF was coated with polyaniline by in-situ oxidative polymerization and hot-pressed onto stainless steel mesh for a microbial fuel cell. The device achieved 680 mW/m^2 power density, 0.67 V open-circuit potential, and 3500 mA/m^2 limiting current density, with stable voltage over 370 hours across three cycles.[17] Both studies show that PET-derived terephthalic acid is a versatile linker for energy storage and bioenergy devices, with the main challenge being the low electrical conductivity of pristine MOFs.

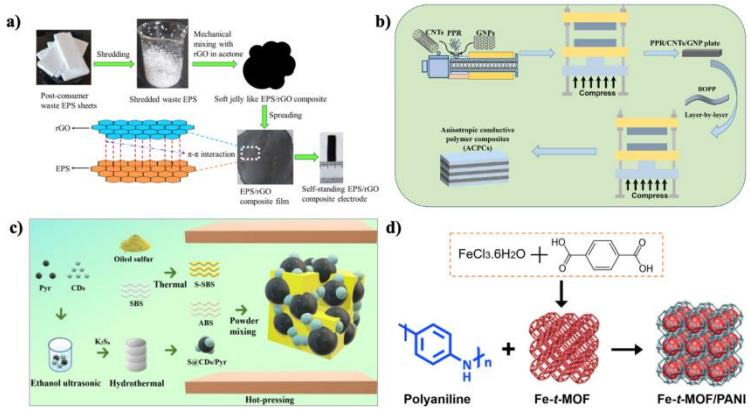


Figure 7. Selected non-pyrolytic upcycling routes for waste plastics. a) Solution blending of waste EPS with rGO to form a self-standing electrode. Adapted from ref [88]. b) Layer-by-layer assembly and thermal welding of waste BOPP films with conductive PPR layers to form an anisotropic conductive composite. Adapted from ref [94]. c) Sulfur-crosslinked, hot-pressed composite from waste ABS, pyrrhotite, and S-CDs. Adapted from ref [93]. d) Fe-t-MOF/PANI synthesized from PET-derived terephthalic acid for microbial fuel cell electrodes. Adapted from ref [17].

3.3 Hybrid Routes

Hybrid routes integrate multiple synthesis steps or mechanisms to overcome the limitations of single-route approaches, producing carbons with properties that cannot be achieved by any one method alone. A single method often imposes a trade-off: KOH activation generates high surface area but may collapse mesopores, sulfonation enables carbonization of polyolefins but introduces sulfur that can be lost at high temperatures, and template carbonization controls morphology but requires additional doping for pseudocapacitance. By combining processes such as pre-carbonization with activation, sulfonation with KOH etching, dehalogenation with annealing, Friedel–Crafts crosslinking with carbonization, template carbonization with post-synthetic oxide deposition, MOF-mediated or depolymerization-based carbonization, and pyrolytic residue valorization, researchers can independently tune surface area, pore architecture, heteroatom content, and oxide loading. This section

covers a range of hybrid strategies that illustrate how the choice of intermediate and the sequence of treatments determine whether the final carbon is optimized for supercapacitors, lithium-ion batteries, lithium-sulfur batteries, sodium-ion batteries, or electrocatalysis. The unifying theme is that plastic waste is not merely a carbon source but a precursor whose chemistry, additives, and degradation products can be exploited to direct the structure and function of the resulting material.

3.3.1 Pyrolysis and Carbonization with Chemical Treatment

Pyrolysis and carbonization with chemical treatment convert plastic waste into porous carbons through thermal decomposition followed by activation or doping. Unlike depolymerization, which recovers monomers, this route destroys the polymer backbone entirely to produce carbon materials with tunable porosity, surface chemistry, and electronic properties. The resulting carbons serve as electrodes for supercapacitors, lithium-ion batteries, and electrocatalysts. This section covers pre-carbonization followed by KOH activation, one-pot reactive chemical activation, microwave-assisted pyrolysis, carbonization with ammonia or urea doping, ionothermal synthesis using deep eutectic solvents, and oxidative stabilization followed by catalytic graphitization.

Pre-carbonization followed by KOH activation is the most widely used route for converting plastic waste into porous carbons. The plastic is first pyrolyzed at moderate temperatures to form a char, which is then mixed with KOH and heated to 700–900 °C. During activation, KOH reacts with carbon according to $6KOH + 2C \rightarrow 2K + 3H_2 + 2K_2CO_3$, followed by decomposition of K_2CO_3 and reaction of $K/K_2CO_3K/CO_2$ with carbon to etch the matrix and create micropores and mesopores.[26,33] Hu et al. employed waste PET bottles as both separator and carbon precursor, using $Ca(OH)_2$-assisted pyrolysis at 700 °C followed by KOH activation at 800 °C. The $Ca(OH)_2$ facilitated ester bond cleavage and acted as a mild template, while KOH activation increased the surface area from 672 to 1845 m^2/g. The resulting carbon delivered 190.3 F/g at 0.5 A/g and retained 81% at 10 A/g.[18] Surface area governs capacitance at low current densities, whereas meso/macropores improve ion diffusion and enhance high-rate performance. This trade-off between surface area and mesoporosity became a recurring theme. Zhang et al. developed autogenic pressure carbonization for LDPE, where the closed reactor generated high pressure from decomposed gases, increasing carbon yield to 45% compared to near-zero yield under normal pressure. The KOH activation produced hierarchical porous carbon spheres with surface areas up to 3059 m^2/g. The optimal sample delivered 355 F/g at 0.2 A/g and 274 F/g at 10 A/g, with 89.3% retention.[20] Macropores shorten the electrolyte transfer distance, mesopores accelerate electrolyte transport, and micropores offer abundant formation sites for the electrochemical double layer. Ma et al. used a MgO template combined with KOH activation to produce hierarchical porous carbon nanosheets from polystyrene. The optimal sample achieved 323 F/g at 0.5 A/g and retained 73.2% at 20 A/g.[106] Micropores mainly accommodate large amounts of charge and meso and macropores are beneficial for the diffusion of electrolyte ions. Wen et al. applied a similar strategy to real-world mixed waste plastics containing PP, PE, PS, PET, and PVC. The mixed plastics were carbonized on organically-modified montmorillonite (OMMT) at 700 °C, followed by KOH activation

at 850 °C. The resulting porous carbon nanosheets had a surface area of 2198 m^2/g and delivered 207 F/g at 0.2 A/g in aqueous electrolyte and 120 F/g in organic electrolyte (Figure 8a).[107] The interconnected large mesopores serve as ion-buffering reservoirs and rapid ion-transport pathways. Liu et al. introduced a co-etching concept for PET-derived carbons, finding that low-temperature carbonization at 500 °C produced a carbon with both sp^2 and sp^3 hybridized domains. During KOH activation, the unstable sp^3 carbon was etched preferentially to form mesopores and macropores, while the stable sp^2 carbon was etched more slowly to form micropores. The optimal sample achieved 413 F/g at 0.5 A/g and 290 F/g at 20 A/g.[108] The co-etching effect of $sp^2$and sp^3 hybridized carbon produces micropores and meso-/macropores, respectively. Liu et al. extended this work to polypropylene using a combined catalyst of ferrocene and sulfur, yielding carbon nanosheets with a thickness of 4–4.5 nm and a carbon yield of 62.8%, much higher than the 18.1% obtained with ferrocene alone. After KOH activation, the surface area reached 3200 m^2/g and the capacitance reached 349 F/g at 0.5 A/g.[26] The meso-/macropores in the carbon nanosheets acted as shortcuts and minimized the ion transfer resistance. Wen et al. used MgO templating coupled with KOH activation to produce porous carbon sheets from polystyrene, achieving 135 F/g at 1 mV/s and 97 F/g at 1 A/g with 82.9% retention at 20 A/g.[109] Ma et al. developed a three-dimensional hierarchically porous carbon from polystyrene using Fe_2O_3 particles as both catalyst and template, achieving 284.1 F/g at 0.5 A/g and 198 F/g at 20 A/g. [110] Macropores with open spaces can serve as ion-buffering reservoirs to decrease the ion diffusion distance while micropores mainly accommodate large amounts of charges and improve the specific capacitance. Chen et al. used polyurethane as a precursor, which contains heteroatoms that promote crosslinking during pyrolysis. The optimal sample with a KOH/carbon ratio of 2:1 achieved 395 F/g at 1 A/g and retained 95.3% after 4000 cycles.[19] The nitrogen and sulfur co-doping from the PU backbone introduced pseudocapacitance, demonstrating that heteroatom-containing plastics offer advantages over pure polyolefins.

One-pot reactive chemical activation combines carbonization and activation in a single step, reducing processing time and energy consumption. Dědek et al. compared eight different plastics including PE, PP, PS, PA, polyethersulfone (PES), PET, PU, and acrylonitrile butadiene styrene (ABS) using K_2CO_3 as the activating agent at 800 °C for 2 hours. The polyamide-derived carbon achieved the highest capacitance of 521 F/g at 1 A/g in three-electrode configuration and 220 F/g in two-electrode symmetric cell. Polymer glass transition temperature, polymer-activating agent miscibility, activating agent K_2CO_3:AC ratio, and AC water dispersion stability also play a crucial role in determining performance. This systematic comparison revealed that the glass transition temperature affects grinding and mixing, while dispersion stability influences electrode fabrication. The C-PA sample with a 1:1 K_2CO_3 ratio exhibited the best combination of surface area (1974 m^2/g) and micropore volume (0.59 cm^3/g), as shown in Figure 8c.[111] Lian et al. developed a graphene/mesoporous carbon composite from waste polyethylene using basic magnesium carbonate as a flame retardant and template. The PE was ball-milled with basic magnesium carbonate and graphene oxide, then carbonized at 700 °C. The

magnesium carbonate decomposed to MgO, which served as a template, while CO_2 and H_2O etched the carbon to create micropores. The optimal sample achieved 360 F/g at 0.5 A/g in three-electrode configuration and 239 F/g at 2 A/g in two-electrode symmetric cell. The mesoporous carbon particles act as spacers to prevent agglomeration of graphene, leading to the ultra-high specific surface area of graphene to be fully exploited. In ionic liquid electrolyte, the symmetric supercapacitor operated at 4 V and delivered 63.3 Wh/kg.[28]

Microwave-assisted pyrolysis offers faster heating and lower energy consumption compared to conventional furnace heating. Mohd Abdah et al. converted polypropylene from used centrifuge tubes into activated carbon using microwave-assisted pyrolysis followed by KOH activation. The process was optimized using response surface methodology with a central composite design. The optimal conditions were 3.5 M HNO_3, 230 °C microwave temperature, and 25 minutes holding time, yielding a carbon with an I_D/I_G ratio of 0.681. After KOH activation at 800 °C, the sample achieved a surface area of 3200 m^2/g and delivered 381 mAh/g as a lithium-ion battery anode with 85.1% initial Coulombic efficiency (Figure 8b).[112] The presence of both macropores and mesopores in electrochemical systems provides several advantages including increased electroactive surface sites and efficient penetration of the electrolyte. This was one of the few studies to use microwave heating for plastic-derived carbons, demonstrating a potential route for faster and more energy-efficient processing.

Carbonization with ammonia or urea doping introduces nitrogen functional groups that enhance capacitance through pseudocapacitance and improve wettability. Lian et al. used NH_3 activation to produce nitrogen-doped porous carbon from waste polyethylene bags. The PE was ball-milled with basic magnesium carbonate and carbonized at 900 °C, followed by NH_3 activation at 900°C. The NH_3 etched the carbon and introduced nitrogen, resulting in a surface area of 1219 m^2/g and a nitrogen content of 4.22 at%. The optimal sample achieved 244 F/g at 0.2 A/g in three-electrode configuration and 110 F/g at 0.05 A/g in two-electrode symmetric cell, with 97.1% retention after 10,000 cycles. The high content of graphitic N in carbon skeleton can improve the electronic conductivity while pyridinic- and pyrrolic-N can contribute to the electrochemical capacitance by introducing Faradic reactions. In ionic liquid electrolyte, the symmetric supercapacitor delivered 43 Wh/kg at 4 V.[27] Wang et al. produced Fe, N, S codoped honeycomb-like porous carbon from polyphenylene sulfide fibers using KOH activation and NH_3 pyrolysis. The resulting carbon had a surface area of 2223 m^2/g and contained Fe_2N and FeO nanoparticles with a core-shell structure. As a bifunctional oxygen electrocatalyst, it exhibited an ORR half-wave potential of 0.85 V and an OER overpotential of 339 mV at 10 mA/cm^2. The ultrahigh SSA of Fe-N/S-HPC greatly increases the electrode/electrolyte contact area, while the introduction of heteroatoms (Fe, N, and S) as highly efficient active centers enables the efficient catalytic activity. The Zn-air battery constructed with this catalyst achieved a power density of 188.4 mW/cm^2 and stable cycling for over 240 hours.[113] Huang et al. used urea as a nitrogen source to produce N-doped porous carbon from foam polystyrene, achieving a surface area of 508.3 m^2/g and delivering 600 mAh/g after 200 cycles at 1 A/g, as a lithium-ion battery anode.[114] N-doping increased

the defects, providing a large amount of effective surface for lithium ions storage and that N-doping improves the electrical conductivity, which also enhances the rate performance.

Ionothermal synthesis using deep eutectic solvents combines carbonization and activation in a single step while providing a nitrogen source. Ehi-Eromosele et al. used choline chloride-urea DES to convert waste PET bottles into activated carbon. The PET was mixed with the DES and annealed at 400 °C in air, then pyrolyzed at 800 °C under nitrogen. The resulting carbon had a low surface area of 23 m^2/g but a high nitrogen content of 7.3 wt% and a high degree of graphitization. As a lithium-ion battery anode, it delivered 460 mAh/g in the first cycle and retained 98% capacity from the second to the 100th cycle. The use of CU-DES as the solvent medium and nitrogen source enhanced the simplicity, reduced toxicity and resulted in low-cost ACs. The low surface area was compensated by the high graphitization and nitrogen doping, which provided efficient electron transport and lithium storage sites.[115]

Oxidative stabilization followed by catalytic graphitization produces highly crystalline graphite rather than porous carbon. Kim et al. developed a method to convert bulk polyethylene waste into graphite powder using solid additives during air processing. The PE was mixed with NaCl and heated at 310 °C in air, which oxidized the polymer and created a stabilized char. The NaCl provided a surface for the polymer melt to wet as a thin layer, enabling oxygen diffusion and oxidative stabilization. Without the solid additive, the PE decomposed completely during carbonization. The oxidized PE was then carbonized at 800 °C and catalytically graphitized with iron particles at high temperature. The resulting graphite had a degree of graphitization of 88–97%, an interlayer spacing of 0.3356–0.3365 nm, and an I_D/I_G ratio of 0.013. As a lithium-ion battery anode, it delivered 345 mAh/g at 0.05C with 87% initial Coulombic efficiency and 313 mAh/g at 0.5C after 250 cycles.[116] This method allows, for the first time, the pretreatment of bulk forms of PE waste using a simple air processing method. The solid additive approach solved the oxygen diffusion limitation that had previously prevented oxidative stabilization of bulk PE.

Across these studies, several design principles emerge. The plastic precursor determines carbon yield and heteroatom content: heteroatom-containing polymers (PET, PU, PPS) yield higher carbon residues and functional groups, while polyolefins (PE, PP, PS) require templates or catalysts to prevent complete decomposition. Activation conditions control pore architecture, with KOH activation at 700–800 °C and a KOH/carbon ratio of 2:1 to 4:1 producing hierarchical carbons with balanced micro/mesoporosity; higher temperatures increase surface area but may collapse mesopores and reduce rate capability. Heteroatom doping enhances capacitance through pseudocapacitance and improved wettability, with nitrogen from NH_3, urea, or DES introducing pyridinic and pyrrolic nitrogen for redox reactions while graphitic nitrogen improves conductivity. Carbonization temperature before activation affects graphitization degree and etchability: low-temperature carbonization (500 °C) produces sp^2/sp^3 domains that can be co-etched to form hierarchical pores, while high-temperature carbonization (700 °C) produces more graphitic carbon that resists etching. Finally, the field has shifted from simple template methods using MgO or OMMT with KOH activation toward more sophisticated approaches combining

catalytic graphitization, ionothermal synthesis, and oxidative stabilization, with recent studies emphasizing scalability and cost-effectiveness through mixed plastic waste and real-world feedstocks.

3.3.2 Sulfonation and Sulfur-assisted Carbonization

Sulfonation and sulfur-assisted carbonization use sulfuric acid or elemental sulfur to introduce sulfonic acid groups or C–S bonds into polyolefin chains, which crosslink the polymer and prevent complete decomposition during pyrolysis. This stabilization step is essential because pristine polyolefins such as PE, PP, and PS volatilize almost entirely at temperatures above 400 to 500 °C. The sulfur introduced during this step can remain in the carbon matrix as a dopant, providing active sites for polysulfide trapping in lithium-sulfur batteries and for alkali metal ion adsorption in sodium and potassium ion batteries. The choice of whether to add KOH activation after sulfonation determines whether the product is a hard carbon for battery anodes or a high surface area porous carbon for supercapacitors.

Sulfonation followed by direct carbonization without KOH activation converts polyolefin waste into hard carbons with yields that would be impossible to achieve otherwise. Villagomez-Salas et al. treated waste LDPE and HDPE bags with concentrated H_2SO_4 at 110 °C for 12 h and carbonized the sulfonated products at 900 °C. The process retained 50 and 46 wt% of the initial mass, whereas pristine PE leaves no residue under the same conditions, establishing sulfonation as the critical step that enables carbon formation. The amorphous carbon chips had surface areas of 752.3 and 673.5 m^2/g and delivered 230 and 350 mAh/g at C/5 as lithium-ion battery anodes (Figure 8d).[117] Kim et al. used microwave promoted sulfonation of LDPE for 15 min, which produced a porous carbon with a surface area of 570 m^2/g and a zeta potential of -53.7 mV. The negative surface charge enabled the carbon to serve as a lithium sulfur battery interlayer that repelled anionic polysulfides, delivering 776 mAh/g at 0.5C with 79% retention over 200 cycles.[118] This shift from anode material to interlayer demonstrates that the same sulfonated carbon can serve different functions depending on device architecture. Hong et al. compared HDPE and LDPE and found that C-HDPE had a more defective structure with a higher I_D/I_G ratio of 1.28 compared with 0.95 for C-LDPE. The more defective C-HDPE delivered higher capacities of 358 and 470 mAh/g for charge and discharge, with an initial Coulombic efficiency of 78.6%, while C-LDPE delivered 254 and 370 mAh/g with 68.6% efficiency.[119] The difference arises from the higher crystallinity and density of HDPE, which limits acid penetration during sulfonation and produces a more disordered carbon with additional lithium storage sites. Zhao et al. extended sulfonation to polystyrene foams and added phosphoric acid before carbonization to achieve simultaneous S and P codoping. The resulting carbon had a surface area of 2335 m^2/g and accommodated 72 wt% sulfur. The lithium sulfur cathode delivered 893 mAh/g at 2C with only 0.049% capacity loss per cycle over 800 cycles, demonstrating that codoping and high surface area together improve polysulfide confinement.[120] Lee et al. sulfonated polypropylene masks at 120 °C for 6 h and carbonized at temperatures up to 2400 °C. Even at 2400 °C the carbon remained non-graphitizable, confirming that sulfonated polypropylene is intrinsically hard carbon. The C16 electrode delivered about 340 mAh/g at 0.01 A g^{-1} for sodium ion storage, and a full cell achieved 352 Wh/kg.[121] Zhang et

al. varied the sulfonation temperature from 120 to 200 °C and found that higher temperatures increased the carbon yield from 23.9% to 40.1% and expanded the interlayer spacing from 0.36 to 0.40 nm. The CM-180 electrode achieved 327.4 mAh/g at 0.1C with 78.4% initial Coulombic efficiency, and a sodium ion full cell delivered 238 Wh/kg. The expanded interlayer spacing, which arises from oxygen functional groups that remain after carbonization, is critical for accommodating the larger sodium ion.[122] Yuwen et al. used microwave driven sulfonation of COVID-19 masks for 8 to 10 min and self-activated pyrolysis at 900 °C. The surface area increased from 2.0 to 830.9 m^2/g without any added activator, because the sulfur and oxygen functional groups introduced during sulfonation decomposed during pyrolysis and etched the carbon matrix. The lithium sulfur cathode delivered 1313.6 mAh/g at 0.1C.[67] In a related route, Yuwen et al. added urea to the microwave sulfonation system, achieving in situ S, N, and O codoping while maintaining 51 wt% mass at 1000 °C. The self-activated carbon delivered 1459.8 mAh/g at 0.1C and retained 52.3% after 400 cycles at 0.5C.[123] The progression from single element sulfur doping to S, N, and O codoping shows that the sulfonation step can be modified to introduce multiple heteroatoms simultaneously, which provides additional active sites for polysulfide adsorption.

Sulfonation followed by KOH activation and heteroatom doping combines the stabilizing effect of sulfonation with pore etching and additional doping, producing carbons suitable for supercapacitors. Hu and Lin sulfonated waste polypropylene face masks at 110 °C for 12 h, mixed the product with KOH, and activated at 750 °C. The optimal CMS-3 sample had a dense hollow fiber porous structure with sulfur doping. It delivered 328.9 F/g at 1 A/g in aqueous electrolyte, and a solid-state symmetric device achieved 52.1 F/g at 1 A/g, 10.4 Wh/kg at 600 W/kg, and 81.1% capacitance retention after 3000 cycles.[124] The hollow fiber morphology, which originated from the non-woven fabric structure of the mask, was preserved through sulfonation and activation, demonstrating that the precursor architecture can be retained in the final carbon. Archana et al. converted thermocol polystyrene waste by sulfuric acid sulfonation, pre-carbonization at 400 °C, and KOH activation with thiourea at 800 °C. The N and S codoped carbon NSTC-800 had a surface area of 1849 m^2/g and contained thiophene and thiol sulfur species. The aqueous symmetric supercapacitor delivered 60 Wh/kg at 75 W/kg and 27 Wh/kg at 3780 W/kg. A non-aqueous sodium ion capacitor delivered 150 Wh/kg at 520 W/kg with nearly 100% Coulombic efficiency after 10,000 cycles. As a lithium sulfur host, the NSTC-S composite with 69.8 wt% sulfur delivered 1079 mAh/g at 0.1C and maintained about 900 mAh/g over 500 cycles.[85] The dual application in supercapacitors and lithium sulfur batteries demonstrates that the same heteroatom-doped carbon can serve multiple energy storage functions, which improves the economic case for plastic upcycling (Figure 8e).

Elemental sulfur assisted pyrolysis and in-situ vulcanization use sulfur as both a reaction medium and a dopant during carbonization, which simplifies the process compared with sulfuric acid sulfonation. Chen et al. mixed polystyrene spheres with sulfur powder at a mass ratio of 1:3 and annealed at 600 °C. Molten sulfur immersed the polystyrene and reacted with the carbon skeleton to form covalent C–S

bonds, which suppressed volatilization of polystyrene and increased carbon yield. The resulting SHC-3 contained 27.05 at% sulfur, had an expanded interlayer spacing of 0.382 nm, and a surface area of 121 m^2/g. As a potassium ion battery anode, SHC-3 delivered 298.1 mAh/g at 100 mA/g after 1000 cycles with 95.2% retention and 220.2 mAh/g at 500 mA/g after 5200 cycles. Density functional theory showed that sulfur doping sites adsorbed potassium more strongly than ideal graphene or vacancy defects, with adsorption energies of -3.07 and -3.57 eV compared with -1.16 eV for graphene and -2.51 eV for a vacancy defect.[22] The theoretical calculation provides a mechanistic explanation for why sulfur doping enhances capacity, which is more difficult to obtain from experimental data alone. The in-situ vulcanization route avoids the use of concentrated sulfuric acid, which is corrosive and requires careful handling, and the sulfur serves both as a stabilizer and as a dopant in a single step.

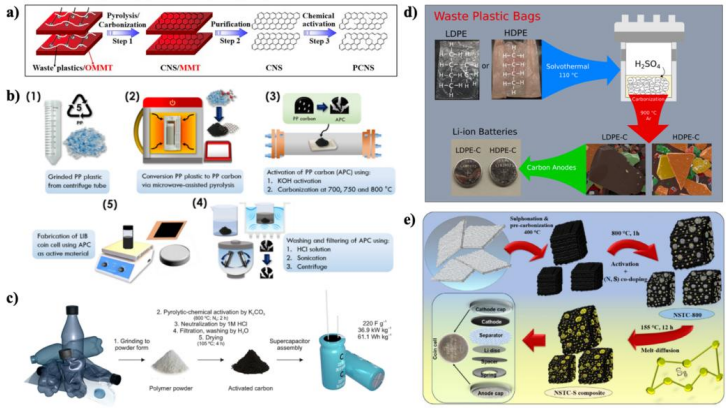


Figure 8. Selected hybrid routes for plastic-waste-derived carbons. a) OMMT-assisted carbonization and KOH activation of mixed waste plastics to PCNSs. Adapted from ref [107]. b) Microwave pyrolysis and KOH activation of PP waste to APC for Li-ion battery anodes. Adapted from ref [112]. c) K_2CO_3 activation of eight plastics to activated carbons of supercapacitors. Adapted from ref [111]. d) Solvothermal sulfonation and carbonization of LDPE/HDPE bags to carbon chips for Li-ion battery anodes. Adapted from ref [117]. e) Sulfonation and KOH/thiourea activation of polystyrene waste to N,S-codoped carbon and NSTC-S for supercapacitors and Li-S batteries. Adapted from ref [45].

3.3.3 Dehalogenation Followed by Annealing or Carbonization

Dehalogenation followed by annealing or carbonization uses alkaline reagents to strip halogen atoms from polymers such as PVC and PVDC at or near room temperature, producing a carbonaceous precursor that is then annealed to improve conductivity and porosity. This route is attractive because the dehalogenation step avoids the high temperatures and hazardous byproducts associated with direct pyrolysis of chlorinated plastics. The halogen atoms are removed as chloride salts, which are water soluble and easily separated.

Chang et al. demonstrated room temperature dehalogenation of PVC using KOH in a ball mill with DMF and DMSO as solvents. The dehalogenation reaction produced KCl as a byproduct, which was removed by water washing. After annealing at 600 °C, the resulting carbons had surface areas of 611 to 765 m^2/g and contained both N and S from the solvents. The PVC plastic wrap derived carbon achieved 399 F/g at 1.0 A/g in 6.0 M KOH and 363 F/g in 1.0 M H_2SO_4, with over 92% capacitance retention after 1000 cycles.[41] The method was effective for tablecloth, document bag, plastic wrap, and PVC tube, showing that common PVC products can be processed without sorting. Chang et al. extended the approach to PVDC and used DMF and DMSO as N and S sources during ball milling. The dehalogenation step produced a carbonaceous material with 3.0 at% N and 2.4 at% S after annealing at 600°C. The carbon delivered 427 F/g at 1.0 A/g in 1.0 M H_2SO_4 and retained about 60% of that capacitance at 100 A/g. It also achieved a desalination capacity of 32.3 mg/g in 40 mg/L NaCl for capacitive deionization, demonstrating that the same material can serve both energy storage and water treatment.[42] Hu et al. used PVC plastic bags, KOH, and thiourea as the N and S source in a ball mill at room temperature, followed by annealing at 600 °C. The resulting carbon had a surface area of 808 m^2/g and contained 6.5 at% N and 7.2 at% S. As a sulfur host for lithium sulfur batteries, it delivered 1230 mAh/g at 0.1C and retained 680 mAh/g after 200 cycles at 1C, with 83.4% capacity retention. Even at a sulfur loading of 5 mg/cm^2, it maintained 79.4% retention after 200 cycles.[125] The high heteroatom content, which is difficult to achieve by other routes, enabled strong polysulfide trapping and improved cycling stability. Therefore, these studies show that dehalogenation is a versatile platform for converting chlorinated plastic waste into doped carbons with tunable properties, and the annealing temperature and dopant choice determine whether the final material is optimized for supercapacitors, deionization, or lithium sulfur batteries.

3.3.4 Friedel–Crafts Crosslinking Followed by Carbonization or Activation

Friedel–Crafts crosslinking uses a Lewis acid catalyst to form covalent bridges between aromatic polymer chains, converting linear polystyrene into a hypercrosslinked network that can survive carbonization. Without crosslinking, polystyrene decomposes completely into volatile aromatic molecules at temperatures above 400 °C, leaving negligible carbon residue. The crosslinking chemistry determines the carbon yield, pore architecture, and heteroatom content of the final material. Zhang et al. dissolved waste polystyrene foam in carbon tetrachloride and used anhydrous $AlCl_3$ to catalyze Friedel–Crafts alkylation, forming -CCl_2 bridges that hydrolyzed to carbonyl crosslinks. Silica particles were embedded during crosslinking and removed by HF etching after carbonization at 600 °C, creating mesopores. The resulting carbon had a surface area of 620 m^2/g and a three-dimensional network structure. It delivered 208 F/g at 1 A/g in 6 M KOH and retained 94.3% after 5000 cycles.[29] Deka et al. synthesized a hypercrosslinked polymer from waste expanded polystyrene and cyanuric chloride, which introduced triazine rings as nitrogen-rich crosslinking sites. After KOH activation at 700 °C, the carbon had a surface area of 810 m^2/g and contained 5.23% nitrogen and 8.93% oxygen. It delivered 327 F/g at 1 A/g in 1 M H_2SO_4 and 100% capacitance retention after 10,000 cycles.[30] The same

material achieved 34.8 mg/g electrosorption capacity for capacitive deionization at 1.6 V. The higher capacitance and cycling stability of Deka et al. compared to Zhang et al. arise from the combination of nitrogen doping, which provides pseudocapacitance, and a hierarchical pore network that facilitates ion transport.[29,30]

Qiu et al. compared two crosslinking chemistries for polystyrene nanospheres before carbonization at 800 °C. Carbonyl crosslinking produced well-preserved nanospheres with high surface area and abundant open pores, while triazine crosslinking caused in-situ fusion into a layered carbon with low surface area and abundant closed pores. By co-carbonizing both precursors, they created a hybrid hard carbon in which the fused layered carbon served as a matrix embedding the intact nanospheres. The hybrid had a surface area of only 7 m^2/g and a closed pore volume of 0.034 cm^3/g, intermediate between the two individual carbons. As a sodium ion battery anode, it delivered 279.3 mAh/g with 70.2% initial Coulombic efficiency and retained 85% capacity after 500 cycles at 1000 mA/g.[126] The closed pores provided sites for quasi-metallic sodium storage, while the low external surface area minimized irreversible solid electrolyte interphase formation. The same strategy was applied to waste polystyrene, demonstrating that the crosslinking chemistry can be used to tailor carbon architecture for high-value battery applications. This progression from single crosslinker systems to hybrid architectures shows that Friedel–Crafts chemistry provides a versatile platform for converting polystyrene waste into carbons with properties optimized for supercapacitors, deionization, or sodium storage.

3.3.5 Template Carbonization with Post-synthetic Doping

Template carbonization produces porous carbons with controlled pore architectures, but the resulting materials often lack the pseudocapacitance or high specific capacity needed for advanced energy storage. Post-synthetic doping introduces metal oxides into the carbon framework after carbonization and template removal, combining the conductivity and stability of the carbon scaffold with the high theoretical capacity of the oxide. This section covers two approaches: redox deposition of manganese oxides on template-derived carbons for supercapacitors, and hydrothermal doping of tin dioxide into three-dimensional carbon frameworks for lithium-ion battery anodes.

Redox deposition of MnO_x uses the reducing power of carbon to drive spontaneous MnO_4^- reduction on the carbon surface. Cheng et al. converted waste PVC into nanoporous carbon using $Mg(OH)_2$ as a hard template at 700 °C. The $Mg(OH)_2$ decomposed to MgO, which served as a template, while released HCl gas acted as a soft template, creating a hierarchical pore structure with a surface area of 958.6 m^2/g and a pore volume of 3.56 cm^3/g. The carbon was then immersed in $KMnO_4$ solution at 70 °C, where the redox reaction between carbon and permanganate deposited MnO_x nanoparticles on the carbon surface. The carbon-Mn2 sample with a 1:1 mass ratio of carbon to $KMnO_4$ achieved 751.5 F/g at 1 A/g, compared with only 47.8 F/g for the undoped carbon, and retained 83.1% after 5000 cycles.[127] The increase in capacitance came from the pseudocapacitance of MnO_x, while the carbon scaffold provided conductivity and structural stability. Min et al. produced porous carbon flakes from polystyrene foam

waste using flake-structured MgO as a template, then deposited MnO_2 nanosheets by spontaneous redox deposition in neutral $KMnO_4$ solution. The carbon flakes had a surface area of 1087 m^2/g and a pore volume of 4.42 cm^3/g. After MnO_2 deposition, the surface area decreased to 911 m^2/g, but the specific capacitance in LiCl electrolyte increased to 247 F/g at 1 A/g and 308 F/g at 1 mV/s, with 93.4% retention over 10,000 cycles. The synergistic effect between the conductive carbon flakes and the pseudocapacitive MnO_2 nanosheets enabled both high capacitance and long cycle life.[128] Together, these studies show that redox deposition is a simple and effective way to introduce pseudocapacitive oxides into template-derived carbons, with the oxide loading determining the balance between double-layer and faradaic contributions.

Hydrothermal doping of SnO_2 into three-dimensional carbon frameworks creates yolk-shell structures that accommodate the large volume changes of alloying-type anodes. Min et al. used a mixed plastic waste feedstock containing PP, PE, PS, and PVC with a dual MgO/$Fe(acac)_3$ template at 800 °C to produce a three-dimensional hollow carbon sphere/porous carbon flake framework. The framework had a surface area of up to 1450 m^2/g and contained interconnected micro-, meso-, and macropores. SnO_2 nanoparticles were introduced by vacuum filling with $SnCl_2$, followed by hydrothermal treatment in $NH_3 \cdot H_2O$ and annealing at 450 °C. By varying the number of filling cycles and the synthesis conditions, the SnO_2 morphology could be tuned from nanospheres to nanocubes, nanoflakes, and blocks. The SnO_2 sphere@HCS/PCF-3 and SnO_2 cube@HCS/PCF samples, with loadings of 34.7 and 58.9 wt% respectively, delivered the best performance. The cube@HCS/PCF anode achieved 1.229 Ah/g at 0.1 A/g and retained 0.4982 Ah/g after 1000 cycles at 5 A/g, with an average capacity decay of only 0.05% per cycle. The spherical and cubic SnO_2 nanoparticles were confined within the carbon framework, which accommodated their volume expansion during lithiation and prevented pulverization. The larger flake and block SnO_2 particles, by contrast, were deposited on the external surface and showed poorer cycling stability.[129] The study demonstrates that the morphology and spatial distribution of the oxide, controlled during hydrothermal doping, are as important as the oxide loading in determining electrochemical performance.

3.3.6 MOF-mediated and Depolymerization Carbonization

MOF-mediated and depolymerization carbonization uses metal-organic frameworks or depolymerization products as intermediates to produce porous carbons with controlled heteroatom doping and pore architecture. The MOF or depolymerized monomer serves as both a carbon precursor and a template, while additional nitrogen sources can be introduced during or after synthesis. This section covers solvothermal depolymerization coupled with MOF synthesis, laser-assisted MOF carbonization, and aminolysis combined with in-situ templating and microwave carbonization.

Xu et al. demonstrated a closed-loop approach in which waste PET bottles and aluminum cans were converted into MIL-53(Al) through a one-pot solvothermal reaction. The PET was hydrolyzed to terephthalic acid, which served as the organic linker, while the aluminum cans dissolved in the acidic medium to provide the metal nodes. The resulting MIL-53(Al) was then carbonized with urea at 800 °C.

Urea served two functions: it introduced nitrogen into the carbon framework and released ammonia and carbon dioxide during decomposition, which acted as physical activators to create micropores. The optimal sample, AMUPC-1.0 with a urea to MOF ratio of 1.0, achieved a surface area of 1324 m^2/g and a nitrogen content of 4.52 at%. The hierarchical porous carbon delivered 355 F/g at 0.5 A/g in 6 M KOH and retained 88.2% capacitance after 10,000 cycles in a symmetric supercapacitor. The work is notable for using two separate waste streams, PET and aluminum, in a single process to produce a high-performance electrode material, demonstrating that waste-derived MOFs can compete with those made from virgin precursors.[130]

Kogolev et al. used a laser-assisted approach to carbonize UiO-66 grown directly on the surface of recycled PET sheets. A homogeneous UiO-66 layer was formed by solvothermal treatment, and a 405 nm laser was then used to selectively carbonize the MOF layer without significantly affecting the bulk PET substrate. The laser treatment produced a composite layer containing zirconium carbide and graphene, which was fused into the PET matrix. The resulting material had a sheet resistance of 10.4 Ω per square and exhibited a photothermal response, reaching 71 °C under 660 nm LED illumination at 0.036 kW/m^2. The carbon layer remained conductive after mechanical abrasion in sand for 24 hours, with sheet resistance increasing only to 18.7 Ω per square.[35] This study shows that MOF-mediated carbonization can be used to create functional conductive patterns on flexible polymer substrates, which is relevant for wearable sensors and flexible electronics.

Zhang et al. combined aminolysis of PET with in-situ templating and microwave carbonization to produce nitrogen-doped hard carbon for sodium-ion batteries. Waste PET was depolymerized with ethanolamine to bis(2-hydroxyethyl) terephthalamide, which was then co-dissolved with guanine and freeze-dried before microwave pyrolysis. Guanine acted as a two-dimensional self-template, forming an interconnected honeycomb-like porous structure, and also served as a nitrogen source. The optimal sample contained 12.24 at% nitrogen and had an interlayer spacing of 0.375 nm. As a sodium-ion battery anode, it delivered 452 mAh/g at 20 mA/g, 386 mAh/g at 500 mA/g, and retained 87.6% capacity after 2000 cycles. The full cell with an NVP cathode achieved 91.87% retention after 2000 cycles, and a pouch cell retained 90.78% after 100 cycles at 200 mA/g. Density functional theory showed that pyrrolic and pyridinic nitrogen expanded the interlayer spacing and enhanced sodium adsorption, providing a mechanistic explanation for the improved performance.[131] This study demonstrates that depolymerization and templating can be integrated into a single process to produce hard carbons with both high nitrogen content and well-defined porosity, avoiding the dopant loss that often occurs with post-synthetic doping.

3.3.7 Pyrolytic Residue Secondary Valorization

Pyrolytic residue secondary valorization converts the solid char remaining after waste plastic pyrolysis into functional carbon rather than discarding or incinerating it. This residue is already carbonized and often contains heteroatoms and metal oxide impurities from additives in the original plastics, which can be exploited for doping and polysulfide anchoring. Gim et al. synthesized boron and nitrogen codoped

porous hybrid carbon from pyrolytic plastic waste residue by heat treatment with $CaCO_3$ nanoparticles and boric acid. $CaCO_3$ decomposition created porosity through CO_2 activation, while boric acid introduced boron and removed impurity crystals. The resulting carbon had a surface area of 368.8 m^2/g, a pore volume of 0.55 cm^3/g, and contained TiO_2 as a polar phase. As a coating on a polypropylene separator in a lithium sulfur battery, it delivered 756 mAh/g after 200 cycles at 0.5C and a capacity decay of only 0.057% per cycle over 500 cycles at 1C. The residue was used directly as a separator modifier without a separate carbonization step, which reduces process complexity.[132] Kim et al. extended the concept by using the same type of pyrolytic residue as a sulfur host rather than a separator coating. Sequential KOH activation and ammonia thermal treatment produced N-doped carbon with hierarchical porosity, a pore volume of 1.472 cm^3/g, and 38.2% mesoporosity. Ammonia treatment also reduced TiO_2 to TiO_{2-x}, creating oxygen vacancies and Ti^{3+} sites, while introducing edge-nitrogen defects. These N defects and TiO_{2-x} acted together to anchor lithium polysulfides through chemical interactions. The cell delivered 623 mAh/g after 200 cycles at 0.5C and 512 mAh/g after 500 cycles at 1C, with a decay rate of 0.089% per cycle.[133] Compared with the separator coating by Gim et al., this study places the functional carbon inside the cathode, where the coupled defects and sub-stoichiometric oxide provide both polysulfide trapping and improved redox kinetics. Together, the two studies establish pyrolytic residue as a viable feedstock for lithium sulfur battery components, with the choice of separator versus cathode host determining the dominant performance benefit.

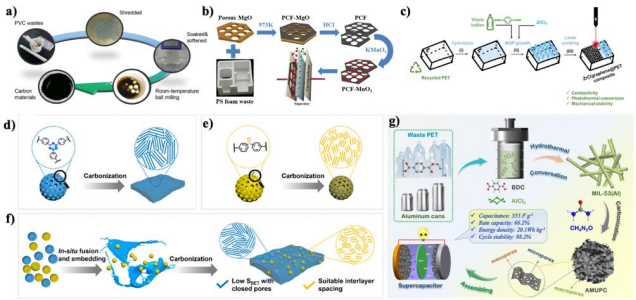


Figure 9. Selected hybrid routes for the synthesis of plastic-waste-derived carbons. a) Room-temperature dehalogenation and annealing of PVC waste. Adapted from ref [41]. b) MgO-templated carbonization of polystyrene (PS) foam to produce porous carbon foam (PCF), followed by MnO_2 deposition. Adapted from ref [128]. c) PET hydrolysis, UiO-66 metal-organic framework growth, and laser scribing to form ZrO_2/nanoporous carbon composites (PET@LB-UiO-66). Adapted from ref [35]. d-f) Schematic diagrams of the synthesis processes for HHC from different polystyrene precursors: d) Friedel–Crafts crosslinking of TZ-PS followed by carbonization; e) carbonization of CO-PS; and f) the resulting in-situ fusion and embedding process, yielding carbon with a low specific surface area (S_{BET}), closed pores, and suitable interlayer spacing. Adapted from ref [126]. g) Conversion of waste PET and aluminum cans into

MIL-53(Al), followed by urea-assisted carbonization to produce AMUPC for supercapacitor applications. Adapted from ref [130]

4. Application and Performance Benchmarking

The conversion of plastic waste into conductive materials has generated a diverse portfolio of upcycled products spanning porous carbons, carbon nanotubes and graphene derivatives, conductive polymer composites, and metal-containing composites. These materials target applications ranging from electrochemical energy storage and conversion to electromagnetic interference shielding, sensing, and water treatment. However, the proliferation of synthesis routes, feedstock choices, and device architectures has created a benchmarking challenge: how to meaningfully compare materials produced from different waste streams using different processing methods and tested under different conditions. This section provides a structured framework for evaluating upcycled conductive materials, organizing the discussion by application domain while highlighting the metrics that matter most for each.

4.1 Overview and Benchmarking Metrics

Plastic waste upcycling produces conductive materials that fall into four main categories. Porous carbon materials include hard carbon, activated carbon, hierarchical porous carbon, carbon nanosheets, and heteroatom doped carbons. They are made by pyrolysis, catalytic carbonization, template carbonization, or chemical activation and are used in supercapacitors, lithium, sodium, and potassium ion batteries, lithium sulfur batteries, capacitive deionization, and electrocatalysis.[12,13,19,20,30,33,44] Carbon nanotubes and graphene derivatives include MWCNTs, SWCNTs, graphene nanosheets, cup stacked CNTs, and CNT microspheres. They are made by catalytic pyrolysis, CVD (chemical vapor deposition), or autogenic carbonization and serve as supercapacitor electrodes, conductive additives, transparent electrodes, EMI shielding materials, and microbial fuel cell anodes.[23,32,34,46,48,60,63,86] Conductive polymer composites include solution blended and melt blended systems such as PS/CNT, PS/graphene, rHDPE/CB, and anisotropic BOPP/PPR/CNT/GNP. They are used in EMI shielding, strain sensors, thermistors, and flexible electronics.[32,86–90,94] Metal containing composites include MOF derived materials, SnO_2/carbon hybrids, Fe3O4@C core shell structures, MnO_2/carbon composites, and $NiCoMnO_x$/CNT composites. They are used in lithium-ion battery anodes, supercapacitors, microbial fuel cells, and microwave absorption.[15–17,72,92,93,127,129,130,134] Three emerging classes are polymer electrolytes and ion conducting materials,[74–76,78,79,81,83,84] integrated devices such as triboelectric nanogenerators, strain sensors, conductive textiles, and aerogels,[43,91,95–99,99,101,102,105] and chemical precursors and monomers such as BHET, BHETA, terephthalic acid, PSS, and PEDOT:PSS.[31,73,79] Table 2 links each category to representative feedstocks, key performance metrics, and application domains. The categories overlap, and the same feedstock can yield different materials depending on the conversion route.

Benchmarking uses two common levels: material characterization and electrode electrochemistry. Material characterization includes XRD for interlayer spacing and graphitization,[13,44,126] Raman for

defect density and graphitic order,[49,122,126] FTIR for surface functional groups,[31,83,125] SEM, EDS, and XPS for morphology, elemental composition, and heteroatom bonding,[22,30,42,126,135] BET for surface area and pore size distribution,[20,26,26,33,110] and TGA for carbon yield, sulfur content, and thermal stability.[79,116,119,121] These techniques explain why, for example, hard carbon with expanded interlayer spacing stores sodium by intercalation and pore filling,[44,126] while hierarchical porous carbon with high mesopore volume supports high-rate supercapacitor performance.[26] Electrode electrochemistry uses CV, GCD, and EIS. Ideal double layer capacitors show rectangular CV and triangular GCD profiles.[20,106,111,124] Redox peaks or sloping profiles indicate pseudocapacitance or battery type behavior.[19,127,136] EIS separates series resistance, charge transfer resistance, and diffusion.[26,40,126] The b value from CV separates surface controlled from diffusion-controlled storage.[122,126,131] GITT gives diffusion coefficients, and in situ or ex situ XRD and Raman track structural changes during cycling.[22,40,44] Application specific metrics are introduced in Sections 4.2 to 4.6.

Table 2. Classification of Upcycled Conductive Materials from Plastic Waste, with Representative Feedstocks, Key Performance Metrics, and Application Domains

Material Category	Examples	Representative Feedstock	Key Performance Metric	Applications
Porous carbon materials	Hard carbon, activated carbon, hierarchical porous carbon, carbon nanosheets, N/S-doped carbons	PET, PP, PS, PC, PVC, PU, mixed plastics	Supercapacitors: 118–482 F/g; SIB/PIB: 150–477 mAh/g; LIB: 498–1101 mAh/g; Li-S: 550–1459 mAh/g; SSA up to 3200 m^2/g	Supercapacitors, Lithium-ion batteries (LIB)/Sodium-ion batteries (SIB)/Potassium-ion batteries (PIB) anodes, Lithium-Sulfur (Li-S) batteries hosts, capacitive deionization (CDI), Zn-air, H_2O_2 electrosynthesis
CNTs & graphene derivatives	MWCNTs, SWCNTs, graphene nanosheets, cup-stacked CNTs, graphene/mesoporous carbon, CNT microspheres	PP, PE, PS, mixed plastics, flexible packaging	CNT yield up to 86.6 wt%; 33.5–140 F/g; conductivity 43–1150 S/m; transmittance 85%; EMI SE 88dB for PP@G	Supercapacitors, conductive additives, transparent electrodes, EMI shielding, thermal management, MFC anodes
Conductive polymer composites	PS/CNT, PS/graphene, rHDPE/CB, anisotropic BOPP, WPS/PVC, TPEE-MXene	PS, PE, BOPP, waste foam, PET	Percolation threshold 0.075–0.33 vol%; conductivity 7.05 S/cm–11.4 S/m; tensile strength 21.96–52.08	EMI shielding, sensors, thermistors, flexible electronics, thermal management

			MPa; EMI SE 9.5–43.1 dB; thermal conductivity 1.36–1.68 W/m·k	
Metal-containing composites	SnO_2@C, CoNi-MOF, Fe_3O_4@C, MnO_2/carbon, $NiCoMnO_x$/CNTs, Fe-MOF/PANI	PET, mixed plastics, PVC, spent batteries	LIB: 498–2496 mAh/g; supercapacitors: 210.5–751.5 F/g; MFC: 680 mW/m^2; microwave adsorption: 7.01 GHz	LIB anodes, supercapacitors, microbial fuel cells (MFCs), microwave absorption, catalysis
Polymer electrolytes & ion-conducting materials	PU electrolytes, eutectogels, ionogels, PE-AEM, sulfonated PVC/PP	PET via glycolysis/aminolysis, PE, PVC, PP	Ionic conductivity: 2.5 × 10^{-7}–11.6 mS/cm; elongation 680-990%; self-healing 100% in 6h; separator stability 1000 h	Batteries, sensors, ionic skins, fuel cells, separators
Devices & functional structures	TENGs, strain sensors, MFC electrodes, conductive textiles, aerogels	Waste bags, masks, PVC pipes, PET, PU foam, textiles	TENG: 35.7–196V; power 152.6–2604 μ W/cm^2; MFC: 1098–1990 mW/m^2; gauge factor: 7.4–2800; 100k bending cycles	Energy harvesting, bioenergy, wearable sensors, e-textiles
Chemical precursors & monomers	BHET, BHETA, terephthalic acid, PSS, PEDOT:PSS, Li_2CO_3/PTA/KDF	PET, EPS/PS, spent LCO	BHET: 70–97%; PSS: 74%; PTA/KDF 0.036/0.039 t per t spent batteries; profit $813.20/ton	PU, polyesters, MOFs, conductive polymers, battery recycling

4.2 Battery Technologies

Plastic waste-derived carbons and composites are versatile across battery technologies, but their performance is governed by distinct storage mechanisms and trade-offs. In LIB anodes, intercalation-type carbons offer graphite-like capacities (~345–381 mAh/g) with good stability and ICE but often require complex activation/graphitization, conversion/alloying composites deliver much higher capacities (up to ~2500 mAh/g) yet suffer low ICE and need sophisticated yolk-shell or confined architectures to manage volume expansion, and plastic-derived CNTs/graphene mainly enhance conductivity rather than capacity. SIBs rely on hard carbons whose performance balances

defect/surface adsorption, interlayer intercalation, and closed-pore filling; higher carbonization and pore engineering increase plateau capacity but can reduce rate capability, while heteroatom doping boosts capacity at the expense of ICE and SEI formation. PIBs similarly use hard or turbostratic carbons, where expanded interlayers, ink-bottle pores, and S-doping improve K^+ storage, though ICE, pore reversibility, and scalable synthesis remain challenging. For Zn-air batteries, a single PPS-derived Fe,N,S-codoped carbon demonstrates promising bifunctional ORR/OER activity and 188.4 mW/cm^2 peak power, but scalability is unproven. Overall, plastic-derived carbons offer a broad platform for battery upcycling, with the central challenge being to balance high capacity, initial efficiency, cycling stability, and scalable processing.

4.2.1 Lithium-ion Batteries

Plastic-derived carbons and composites are attractive for LIB anodes because they offer a low-cost, high-carbon-content alternative to commercial graphite. Their performance, however, is not monolithic; it is dictated by the storage mechanism, which can be broadly classified into intercalation, conversion/alloying, and conductive additive functions. This section synthesizes representative performance data to highlight the trade-offs inherent in each approach.

Intercalation-type carbons, primarily hard and soft carbons, store Li^+ by insertion between graphene layers, similar to graphite. Their capacity is often limited to near the theoretical value of graphite (372 mAh/g), but they can offer superior rate capability and cycling stability. For example, a hard carbon derived from PET via a two-step microwave-assisted pyrolysis and KOH activation delivered a high initial discharge capacity of 381.0 mAh/g with an 85.1% initial Coulombic efficiency (ICE), maintaining excellent reversibility with a capacity of 355.1 mAh/g after 100 cycles[112]. This high performance was attributed to its ordered 3D porous structure, which shortens Li^+ diffusion paths. Similarly, a highly crystalline graphite powder synthesized from bulk PE waste via a novel oxidative stabilization and catalytic graphitization process achieved a reversible capacity of 345 mAh/g at 0.05C with 87% ICE, demonstrating performance comparable to commercial battery-grade graphite.[116] The key trade-off here is that while these materials can approach the capacity of graphite, achieving this often requires complex, multi-step processes like catalytic graphitization or microwave-assisted activation.

Conversion and alloying-type anodes, typically metal oxide/carbon composites, offer much higher theoretical capacities (500–2500 mAh/g) but often suffer from poor ICE and rapid capacity fade due to massive volume changes during cycling. The carbon matrix is crucial for accommodating this expansion and maintaining electrical contact. A CoNi-MOF derived from PET, for instance, delivered a remarkable initial discharge capacity of 2496 mAh/g and a reversible capacity of ~1200 mAh/g after 200 cycles with >99% Coulombic efficiency.[16] Its low surface area (13.69 m^2/g) was actually advantageous, as it minimized parasitic side reactions and SEI formation. However, the initial ICE was only ~69%, a common limitation for conversion-type anodes.

To mitigate the volume expansion problem, researchers have engineered yolk-shell (YSS) structures. A YSS Co_3O_4@C composite from mixed plastics exhibited a high reversible capacity of 1066 mAh/g after 100 cycles at 0.1 A/g, and the void space in the YSS structure was shown to accommodate the stress from lithiation.[134] Even more impressive stability has been achieved with SnO_2-based anodes. A SnO_2 sphere@HCS/PCF composite, where SnO_2 nanoparticles were confined within a 3D hollow carbon sphere/porous carbon flake framework, delivered an ultra-stable capacity of 0.45 Ah/g after 1000 cycles at 5 A/g, with a capacity decay of only 0.048% per cycle.[129] This exceptional stability was attributed to the effective confinement of the SnO_2 nanoparticles, which prevented pulverization and loss of electrical contact. The trade-off for these high-capacity anodes remains their generally lower ICE and the need for complex, multi-step synthesis to create the sophisticated architectures required for stable cycling. Conductive additives represent a different value proposition. Plastic-derived CNTs and graphene are not used for their capacity but to improve the rate capability and efficiency of other active materials. For example, FeMo-CNTs derived from waste face masks, when used as a cathode conductive additive at a low loading (2 wt%), outperformed commercial carbon black (Super P) and CNTs at high rates, achieving a higher ICE of 93.6% versus 45.6% for Super P.[64] This demonstrates that the value of plastic waste upcycling can be realized not just in the anode, but also in enabling the performance of existing battery chemistries.

In summary, plastic waste offers a versatile platform for LIB anode materials. Intercalation-type carbons provide moderate capacity with high stability and ICE, but their performance often relies on complex processing. Conversion/alloying-type anodes offer high capacity but require sophisticated carbon architectures to overcome their inherent instability, leading to lower ICE. Finally, as conductive additives, plastic-derived nanocarbons can significantly enhance the performance of other electrode materials. The key challenge remains to develop scalable, cost-effective processes that can deliver the best-performing architectures from real-world plastic waste streams.

4.2.2 Sodium-ion Batteries

Sodium-ion batteries (SIBs) are attractive for large-scale energy storage because sodium is abundant and low cost, but graphite cannot store Na^+ effectively due to the thermodynamic instability of Na-graphite intercalation compounds. Hard carbon is the leading anode candidate, and its performance is governed by the balance between three storage mechanisms: adsorption on defects and surfaces (sloping region, >0.1 V), intercalation between expanded graphene layers, and filling of closed pores (plateau region, <0.1 V).[12,44,122,126,131] Plastic-derived hard carbons are particularly interesting because feedstock chemistry and conversion route determine which mechanism dominates.

Adsorption-dominated carbons are typically produced at lower carbonization temperatures, where defects and open pores are abundant. An activated carbon derived from e-waste SAN plastics carbonized at 700 °C delivered 190 mAh/g after 25 cycles, with ^{23}Na NMR revealing that Na^+ was stored in pores and defects rather than intercalated between layers.[59] The (002) reflection did not shift during cycling, confirming that intercalation was negligible. Similarly, PET carbonized in a

conventional tube furnace at 900 °C (TF-900) delivered 260 mAh/g with a b-value of 0.68 for the anodic peak, indicating mixed diffusion and surface control.[44] These materials offer good rate capability but limited plateau capacity, which is essential for high energy density in full cells.

Intercalation-dominated carbons require expanded interlayer spacing (typically 0.36 to 0.40 nm) and a pseudo-graphitic domain structure. PET carbonized via microwave-assisted pyrolysis at 900 °C (MW-900) delivered 344 mAh/g with 70.1% ICE, compared with 260 mAh/g and 58.0% for TF-900.[44] In situ Raman showed that MW-900 stored Na^+ through adsorption and closed-pore filling rather than intercalation, with closed pore volume increasing from 0.089 to 0.139 cm^3/g. Waste PET carbonized at 1000 °C (WPET-1000) delivered 337 mAh/g with a plateau contribution of 68%, one of the highest reported for PET-derived hard carbon.[12] The larger interlayer spacing (0.396 nm) and partially closed slit-shaped pores were responsible for the high plateau capacity. Full cells achieved 352 Wh/kg with a $Na_{0.9}[Li_{0.05}(Ni_{0.25}Fe_{0.25}Mn_{0.2})_{0.95}]O_2$ cathode, demonstrating practical viability.[121]

Pore-filling-dominated carbons are produced when closed pores are abundant and interlayer spacing is large enough for Na^+ insertion but the graphitic domains are too small for extensive intercalation. A sulfur-assisted pyrolysis strategy converted PE, PP, PS, and PVC into sulfur-rich carbons with an enlarged interlayer spacing of 0.40 nm.[71] The PE-derived carbon (SWPEC) delivered 662 mAh/g initially and 289 mAh/g at 10 A/g, with a capacitive contribution of 79.3% at 1 mV/s. The high sulfur content (24 wt%) and microporous structure enabled strong Na^+ adsorption and fast kinetics. Sulfonated PP masks carbonized at 1200 °C (CM-180) delivered 327.4 mAh/g with 78.4% ICE and a plateau contribution of 70.4%.[122] The expanded interlayer spacing (0.384 nm) and low surface area (30.0 m^2/g) minimized SEI formation while maximizing closed-pore filling. Full cells with an O_3-$NaNi_1/3Fe_1/_3Mn_1/_3O_2$ cathode achieved 238 Wh/kg and retained 75 mAh/g at 50C, demonstrating exceptional rate capability.

Hybrid carbons combine multiple mechanisms by design. A hybrid hard carbon derived from polystyrene with two distinct crosslinkers (triazine and carbonyl) achieved 279.3 mAh/g with 70.2% ICE at only 800 °C.[126] The triazine-crosslinked spheres fused into a layered carbon matrix with low surface area and abundant closed pores, while the carbonyl-crosslinked spheres were embedded as intact nanospheres with high surface area and defects. The intimate interface (PHEC = 0.97) enabled synergistic Na^+ storage. In situ Raman confirmed G-band redshift during sodiation, and phenolphthalein tests confirmed quasi-metallic Na in closed pores. Waste PET via aminolysis and guanine-assisted in situ templating achieved 452 mAh/g with 83% ICE and 12.24% nitrogen doping.[131] DFT calculations showed that pyrrolic N (N5) and pyridinic N (N6) expanded interlayer spacing and enhanced Na^+ adsorption. The optimized material retained 87.6% capacity after 2000 cycles at 500 mA/g, and full cells achieved 91.87% retention after 2000 cycles.

Several trade-offs emerge across these studies. Higher carbonization temperatures increase closed pore volume and plateau capacity but reduce rate capability because Na^+ diffusion into closed pores is sluggish.[40,44] Heteroatom doping (N, S, P) expands interlayer spacing and enhances adsorption but can

lower ICE by increasing surface defects and SEI formation.[71,131] Sulfonation enables polyolefin carbonization but introduces oxygen functional groups that increase charge transfer resistance.[122] The best-performing materials balance these trade-offs by combining moderate surface area, expanded interlayer spacing, and abundant closed pores, often through multi-step or hybrid routes that may be difficult to scale. Key gaps remain in understanding the relationship between plastic feedstock composition and the resulting closed pore structure, and in developing scalable processes that deliver high plateau capacity without compromising rate performance.

4.2.3 Potassium-ion Batteries

Potassium-ion batteries (PIBs) share the same rocking-chair principle as lithium-ion batteries and benefit from potassium's abundance and low redox potential (-2.93 V vs. SHE). Unlike sodium, K^+ can intercalate into graphite to form KC_8, but the large K^+ radius (1.38 Å) causes a 61% volume expansion, leading to rapid structural degradation of graphite. Hard carbon is therefore attractive because its disordered structure and expanded interlayer spacing accommodate K^+ without catastrophic collapse.[22,40] The storage mechanism in hard carbons follows a three-stage sequence similar to that in SIBs: adsorption on defects and surfaces (sloping region), intercalation between graphene layers, and filling of pores (plateau region).[12,40,45]

Adsorption and intercalation-dominated carbons are typically produced at moderate carbonization temperatures where defects and short-range ordered graphene domains coexist. Waste PET carbonized at 800 °C (WPET-800) delivered 305 mAh/g with a plateau contribution of 32% and 87.5% capacity retention after 50 cycles.[12] The larger interlayer spacing (0.396 nm) facilitated K^+ intercalation, while the plateau capacity originated from intercalation followed by pore filling. PVC-derived soft carbon carbonized at 800 °C (SC-800) exhibited the highest defect concentration and delivered 302 mAh/g.[45] In situ Raman revealed that the G-band blue-shifted during discharge and returned during charge, confirming reversible adsorption–intercalation behavior. The intercalation capacity increased with carbonization temperature (166 mAh/g for SC-600 to 208 mAh/g for SC-1200), while the adsorption capacity peaked at 800 °C (123 mAh/g), demonstrating the trade-off between defect density and graphitic ordering.

Pore morphology plays a critical role in determining both capacity and reversibility. PVC-derived hard carbon with ink-bottle-shaped partially closed pores (CPVC) delivered 477 mAh/g with 58% ICE, compared with 378 mAh/g and 53% ICE for wedge-shaped open pores (WPVC).[40] The narrowed pore mouth of ink-bottle pores provides high adsorption affinity while limiting electrolyte access and SEI formation. However, the open wedge-shaped pores of WPVC exhibited better capacity retention (78% vs. 64% after 500 cycles at 1C) because they facilitate reversible K^+ filling and emptying. Full cells using CPVC and WPVC anodes paired with a Prussian white cathode achieved 284 Wh/kg with 93% retention over 1000 cycles at 1C. This demonstrates that pore architecture must balance initial Coulombic efficiency against long-term cyclability.

Heteroatom doping enhances both capacity and kinetics. Sulfur-doped hard carbon derived from polystyrene (SHC-3) with 27.05 at% sulfur delivered 298.1 mAh/g after 1000 cycles at 100 mA/g with 95.2% retention, and 220.2 mAh/g after 5200 cycles at 500 mA/g.[22] The enlarged interlayer spacing (0.382 nm) and abundant C–S bonds provided additional active sites for K^+ adsorption. DFT calculations showed that sulfur doping at the S-6 site gave a K^+ adsorption energy of -3.57 eV, substantially higher than that of graphene (-1.16 eV) or vacancy defects (-2.51 eV). The capacitive contribution reached 84.28% at 0.6 mV/s, confirming that sulfur doping promotes pseudocapacitive storage.

Turbostratic carbons represent a distinct structural class for K^+ storage. Highly turbostratic graphite (HTG) synthesized from waste polystyrene via catalytic CVD at 1000 °C achieved a plateau capacity close to 92% of the theoretical KC_8 capacity.[52] Unlike lithium, which requires AA stacking of intercalated layers, potassium can form multiple KC_8 configurations with similar energies (ABCD, ADCD, ADAD), enabling turbostratic intercalation without long-range ordering. This mechanism provides a low-voltage plateau with better kinetics than two-phase staging in well-ordered graphite. Full cells with an HTG anode and PTCDA cathode delivered approximately 206 Wh/kg and 450 W/kg.

A unique strategy for high-capacity PIB anodes is the sandwich-like porous carbon nanosheet-supported hexagonal carbon micro-flakes (WPwMC) derived from PE waste via hydrothermal carbonization with Mg inducer.[69] The (002) plane orientation exposed abundant edge active sites and shortened K^+ diffusion paths. WPwMC delivered 528.7 mAh/g at 0.2 A/g, retained 373.4 mAh/g after 200 cycles, and delivered 112.1 mAh/g after 10,000 cycles at 5 A/g. A potassium-ion hybrid capacitor using WPwMC anode and CMK-3 cathode achieved 222.7 Wh/kg at 446.2 W/kg.

Several trade-offs emerge. Higher carbonization temperatures increase intercalation capacity and graphitic ordering but reduce defect-based adsorption and rate capability[5]. Ink-bottle pores improve ICE and capacity but hinder reversible K^+ extraction compared with open pores [108]. Sulfur doping enhances capacity but introduces polysulfide dissolution risk at high sulfur loadings.[22] Turbostratic carbons outperform graphite-like carbons in K^+ storage but require catalytic synthesis routes that may not be scalable. Key gaps remain in understanding the relationship between plastic feedstock composition and turbostratic domain formation, and in developing scalable processes that deliver both high plateau capacity and long-term stability.

4.2.4 Zn-air Batteries

Only one study in this review reports plastic waste-derived carbons for Zn-air batteries. Wang et al. converted sulfur-rich polyphenylene sulfide (PPS) fiber waste into Fe, N, S codoped honeycomb-like porous carbon (Fe-N/S-HPC) with an ultrahigh surface area of 2223 m^2/g. The material contained core-shell $Fe_XN_YS_2/Fe_XO_YS_2$ nanoparticles encapsulated by graphitic carbon. In alkaline electrolyte, it matched Pt/C for ORR ($E_1/_2$ = 0.85 V) and outperformed RuO_2 for OER (339 mV overpotential), with a ΔV of 0.72 V. A Zn-air battery delivered 188.4 mW/cm^2 peak power density and stable cycling for 240 h, compared with 150 h for the Pt/C + RuO_2 benchmark.[113]

This single proof-of-concept demonstrates the potential of plastic-derived carbons for bifunctional oxygen electrocatalysis. However, the feedstock is limited to PPS fibers, the synthesis involves multiple steps, and scalability and techno-economic viability remain unassessed. This represents a clear research gap warranting further investigation.

Table 3. A. Battery technologies: representative upcycled materials and performance

Application	Feedstock	Upcycled Material	Conversion Method	Key Performance	Stability	Ref.
LIB anode	PP centrifuge tubes	Activated PP carbon	Microwave pyrolysis + KOH activation	381 mAh/g initial; 355.1 mAh/g after 100 cycles at 0.2 A/g; 85.1% ICE	~93% retention after 100 cycles	112
LIB anode	PET	SnO_2@terephthalic acid	Molten-salt depolymerization	498 mAh/g after 500 cycles; 1657 mAh/g per SnO_2	Stable 500 cycles	15
LIB anode	PET	CoNi-MOF	Hydrolysis + solvothermal MOF	2496/1729 mAh/g initial discharge/charge; ~1200 mAh/g after 200 cycles	>99% CE after 200 cycles	16
LIB anode	Mixed plastics	Co_3O_4@C yolk-shell	Catalytic carbonization	1066 mAh/g after 100 cycles; 626 mAh/g at 1A/g after 300 cycles	Excellent cycling stability	134
LIB anode	Mixed PP/PE/PS/PVC	HCS/PCF	MgO/$Fe(acac)_3$ template carbonization	802 mAh/g after 500 cycles at 0.5 A/g	High stability	58
LIB anode	Mixed plastics	SnO_2 sphere/cube@HCS/PCF	Template carbonization + hydrothermal	0.45–0.498 Ah/g after 1000 cycles at 5 A/g	0.048-0.05% decay/cycle	129
LIB anode	PET	N-doped activated carbon	Ionothermal DES pyrolysis	276 mAh/g after 100 cycles; 53% ICE	98% retention (2^{nd}-100^{th})	115
LIB anode	HDPE/LDPE	Soft carbon	Hydrothermal sulfonation + carbonization	358 mAh/g charge; 78.6% CE	Stable cycling	119
LIB anode	PE waste	Highly crystalline graphite	Oxidative stabilization + catalytic graphitization	345 mAh/g at 0.05C; 87% ICE; 313 mAh/g after 250 cycles at 0.5 C	~100% renetion	116
LIB anode	PE/PS	Co-GNP graphitic shell	Microwave catalytic deconstruction	377–509 mAh/g after 250 cycles	~100% CE	66
LIB anode	PS foam	N-doped porous carbon	Urea doping	1101 mAh/g at 0.1 A/g	600 mAh/g after 200 cycles at 1 A/g	113

SIB anode	PET	Hard carbon	Direct pyrolysis	337–342 mAh/g	88% @100; 80% @1000	12,13
SIB anode	PC	Hard carbon	Direct pyrolysis	327 mAh/g	Stable 140 cycles	13
SIB anode	E-waste SAN	Activated carbon	CO_2 physical activation	190 mAh/g	92% @50 cycles	59
SIB anode	PE/PP/PS/PVC	Sulfur-rich carbon	Sulfur-assisted pyrolysis	662 mAh/g initial; 289 mAh/g at 10 A/g	256 mAh/g after 4000 cycles	71
SIB anode	PET	Hard carbon	Microwave vs tube pyrolysis	344 mAh/g; 70.1% ICE	97.7% @50 cycles	44
SIB anode	PS	Hybrid hard carbon	Friedel–Crafts + carbonization	279.3 mAh/g; 70.2% ICE	~85% @500 cycles	126
SIB anode	PP masks	Hard carbon	Sulfonation + carbonization	340 mAh/g	Full cell 352 Wh/kg	121
SIB anode	PET	PDC/BPDC	Molten salt + ball milling	217.8 mAh/g; 61.39% ICE	91.44% @100 cycles	68
SIB anode	PP masks	Hard carbon	Sulfonation	327.4 mAh/g; 78.4% ICE	Full cell 238 Wh/kg	122
SIB anode	PET + guanine	N-doped hard carbon	Aminolysis + microwave	452 mAh/g; 83% ICE	87.6% after 2000 cycles	131
PIB anode	PET	Hard carbon	Direct pyrolysis	305 mAh/g	_	12
PIB anode	PE waste	WPwMC	Hydrothermal with Mg	373.4 mAh/g after 200 cycles	112.1 mAh/g after 10,000 cycles at 5 A/g	69
PIB anode	PVC	Hard carbon	Direct carbonization	477 mAh/g; 58% ICE	Full cell 284 Wh/kg; 93%@1000	40
PIB anode	PS	S-doped hard carbon	In-situ vulcanization	298.1 mAh/g; 51.3% ICE	95.2% @1000; 220.2 mAh/g @5200	22
PIB anode	PS/Nylon	Turbostratic graphite	Catalytic CVD	Full cell 206 Wh/kg	Stable cycling	52
PIB anode	PVC	Soft carbon	One-step carbonization	302 mAh/g; 32.9% ICE	Stable 200	45

					cycles	
Li-S host	PVC	N,S-codoped carbon	Dehalogenation + annealing	1205 mAh/g at 0.1C	550 mAh/g after 500 cycles at 1C	125
Li-S host	PS foam	S,P-codoped carbon	Sulfonation + carbonization	1386 mAh/g	893 mAh/g at 2C; 0.049% decay over 800 cycles	120
Li-S host	Waste masks (PP)	P-SO carbon	Microwave sulfonation + pyrolysis	1313.6 mAh/g at 0.1C	38.1% retention after 400 cycles	67
Li-S host	Waste masks (PP)	S,N,O-codoped carbon	Microwave solvothermal + pyrolysis	1459.8 mAh/g at 0.1C	52.3% after 400 cycles	123
Li-S separator	PPWR	B,N-carbon/TiO_2	$CaCO_3$ activation + B,N-codoping	756 mAh/g after 200 cycles at 0.5C	0.057% decay/cycle	132
Li-S host	PPWR	N,S-codoped carbon	KOH activation + NH_3 doping	623 mAh/g after 200 cycles at 0.5C	0.089% decay/cycle	133
Li-S host	PS waste	N,S-codoped carbon	KOH/thiourea chemical activation	1079 mAh/g at 0.1C	715 mAh/g after 500 cycles	85
Zn-air cathode	PPS fiber waste	Fe,N,S-codoped carbon	Oxidation + KOH activation + NH_3 pyrolysis	188.4 mW/cm^2; 688 mAh/g Zn	240 h cycling	113

4.3 Supercapacitors

Supercapacitors are complementary to batteries: they offer high power density and long cycle life but limited energy density. Their charge storage mechanisms are either electrical double-layer formation at the electrode-electrolyte interface (EDLC) or reversible redox reactions at the electrode surface (pseudocapacitance). Carbon-based materials are ideal electrodes because of their low cost, abundance, and tunability. Plastic waste-derived carbons are attractive because feedstock chemistry and conversion route can be tuned to produce either EDLC-type or pseudocapacitive carbons with high specific surface area and heteroatom doping.

EDLC-type carbons store charge through ion adsorption at the electrode surface. Their performance is governed by specific surface area (SSA), pore size distribution, and electrical conductivity. A hierarchical porous carbon derived from PET via low-temperature carbonization and KOH activation

delivered 413 F/g at 0.5 A/g with 95% retention after 10,000 cycles.[108] The high SSA (2238 m^2/g) and mesopore volume (0.51 cm^3/g) enabled fast ion transport. A porous carbon nanosheet from PET using OMMT as template and catalyst delivered 169 F/g in aqueous electrolyte and 121 F/g in organic electrolyte, with an energy density of 30.6 Wh/kg.[33] The mesoporous structure facilitated ion diffusion and provided accessible surface area. Activated carbon from mixed polymers using K_2CO_3 activation achieved 220 F/g at 1 A/g with an energy density of 61.1 Wh/kg and a power density of 36.9 kW/kg.[111] The material retained 95% of its capacitance after 30,000 cycles, demonstrating exceptional stability. Graphene nanosheets derived from mixed PP/PE/PET via two-step pyrolysis delivered 398 F/g by CV and 273.69 F/g by GCD, with an energy density of 38 Wh/kg.[137] These examples show that conventional porous carbons from plastic waste can achieve competitive EDLC performance, with the main trade-off being the need for activation to generate high SSA, which adds cost and complexity.

Heteroatom-doped carbons enhance performance by introducing pseudocapacitance and improving wettability. Nitrogen and sulfur co-doping is particularly effective. A N,S-codoped carbon derived from PVDC via room-temperature dehalogenation achieved 427 F/g in H_2SO_4 and retained about 60% of that capacitance at 100 A/g.[42] The material also achieved a desalination capacity of 140.7 mg/g in capacitive deionization, demonstrating multifunctionality. N,S-codoped microporous carbon from polyurethane delivered 395 F/g at 1 A/g with an energy density of 24.4 Wh/kg and 95.3% retention after 4,000 cycles.[19] The N and S from the PU backbone provided pseudocapacitance without external dopants. S-doped porous carbon from PP masks via sulfonation and KOH activation delivered 365.4 F/g at 0.5 A/g with 90.4% retention after 10,000 cycles.[124] The sulfur doping enhanced conductivity and provided additional active sites. N-enriched porous carbon from polystyrene via thermal plasma achieved 482 F/g at 1 A/g with 95% retention after 5,000 cycles.[37] This is among the highest capacitance values in this dataset and was achieved in only 510 minutes of processing, demonstrating the potential of thermal plasma for rapid, scalable synthesis. A N,S-codoped carbon from PS waste using KOH and thiourea delivered 143 F/g in aqueous electrolyte but achieved a record energy density of 150 Wh/kg in nonaqueous sodium-ion electrolyte, with 99–100% retention after 10,000 cycles.[85] This demonstrates that the same carbon can serve multiple energy storage functions, improving the economic case for plastic upcycling.

Pseudocapacitive and hybrid carbons incorporate metal oxides to add faradaic charge storage. MnO_x-incorporated carbon from PVC via $Mg(OH)_2$ template carbonization and $KMnO_4$ redox deposition delivered 751.5 F/g at 1 A/g with an energy density of 121.4 Wh/kg and 83.1% retention after 5,000 cycles.[127] The MnO_x provided pseudocapacitance while the carbon scaffold ensured conductivity and stability. A PCS/MnO_2 composite from PET delivered 210.5 F/g with 90.1% retention after 5,000 cycles.[136] The MnO_2 nanoflakes were uniformly deposited on the porous carbon nanosheets, providing a synergistic effect. A PCF-MnO_2 hybrid from PS foam via MgO template and $KMnO_4$ deposition delivered 308 F/g with 93.4% retention after 10,000 cycles.[128] The carbon flakes provided a conductive network while MnO_2 contributed pseudocapacitance. An MXene-based pyro-piezoelectric

electrode from HDPE/LDPE achieved 556 F/g with an energy density of 111.11 Wh/kg and a power density of 4 kW/kg, with 93% retention after 10,000 cycles.[70] The MXene and perovskite electrolyte enabled self-charging via compressive force, bending, and heating, demonstrating a multifunctional device concept. A 3D N-doped graphene from PET via one-step thermal decomposition delivered 405 F/g at 1 A/g with an energy density of 68.1 Wh/kg and 87.7% retention after 5,000 cycles.[14] The urea used as nitrogen source also acted as a physical activator, releasing NH_3 and CO_2 during decomposition to create micropores. A graphene/mesoporous carbon from PE using basic magnesium carbonate as flame retardant and template delivered 360 F/g at 0.5 A/g with an energy density of 63.3 Wh/kg at 4 V in ionic liquid.[28] The mesoporous carbon particles prevented graphene agglomeration while the flame retardant reduced hazardous emissions during carbonization.

Device-level innovations demonstrate practical viability. An all-plastic supercapacitor using PET-derived porous carbon as both electrode and separator achieved 197.2 F/g at 0.5 A/g with 95.7% retention after 5,000 cycles.[18] The PET separator exhibited 57 MPa mechanical strength and ionic conductivity up to 2.79×10^{-2} S/cm, eliminating the need for conventional glass fiber separators. A flexible all-solid-state supercapacitor from waste polyurethane foam with CNT/CNF/PANI coating delivered 284.6 F/g and retained 97.8% of its capacitance after 1,000 cycles.[38] A wristband device powered an electronic watch. A self-healing flexible supercapacitor from PET via glycolysis and solution blending delivered 119.7 mF/cm^2 and recovered 94.3% of its capacitance after five cutting and healing cycles, and 95.1% after 1,000 bending cycles.[78] These device-level demonstrations show that plastic-derived carbons can be integrated into flexible, wearable, and self-healing energy storage systems.

Trade-offs and gaps. Higher SSA generally increases capacitance but can reduce ICE and cycling stability in battery applications; in supercapacitors, the main trade-off is between SSA and conductivity. Heteroatom doping enhances capacitance through pseudocapacitance but can lower rate capability if doping levels are too high. Metal oxide incorporation increases capacity but introduces stability concerns. The best-performing materials often require complex, multi-step synthesis routes that may hinder scalability. Key gaps include: lack of standardized testing protocols (different electrolytes, mass loadings, and cell configurations make direct comparison difficult); few studies report volumetric capacitance, which is more relevant for practical devices; and limited long-term cycling data for hybrid and pseudocapacitive materials. Future research should focus on scalable synthesis routes, standardized benchmarking, and device-level integration.

Table 3B. Supercapacitors: representative upcycled materials and performance

Feedstock	Upcycled Material	Conversion Method	Key Performance	Cycling Stability	Ref.
PET + Al cans	N-doped hierarchical porous carbon	Solvothermal MOF + carbonization	335 F/g; 20.1 Wh/kg; 225 W/kg	88.2% @10,000	130

HDPE/LDPE	MXene-based pyro-piezoelectric electrode	MXene + perovskite electrolyte	556 F/g; 111.11 Wh/kg; 4 kW/kg	93% @10,000	70
PET	Porous carbon WPPC/WPPC-A	$Ca(OH)_2$ + KOH activation	197.2 F/g at 0.5 A/g	95.7% @5,000	18
Mixed polymers	Activated carbon	K_2CO_3 activation	220 F/g at 1 A/g; 61.1 Wh/kg; 36.9 kW/kg	95% @30,000	111
Mixed PP/PE/PET	Graphene nanosheets	Two-step pyrolysis	398 F/g CV; 273.69 F/g GCD; 38 Wh/kg	_	137
PVC	N/S-doped porous carbon	RT dehalogenation + annealing	399 F/g KOH; 363 F/g H_2SO_4	>96% @1,000	41
PU	N,S-codoped microporous carbon	Pre-carbonization + KOH	395 F/g at 1 A/g; 24.4 Wh/kg	95.3% @4,000	19
LDPE	Hierarchical porous carbon spheres	Autogenic carbonization + KOH	355 F/g at 0.2 A/g; 283 F/g at 1 A/g	82.4% @5,000	20
PET	Porous carbon nanosheet	OMMT + KOH	169 F/g KOH; 121 F/g organic; 30.6 Wh/kg	95.7% @5,000	33
PET	3D N-doped graphene	One-step thermal decomposition	405 F/g at 1 A/g; 68.1 Wh/kg	87.7% @5,000	14
PET	PCS/MnO_2	MgO/Co catalyst + $KMnO_4$	210.5 F/g composite	90.1% @5,000	136
PTFE	Nanoporous carbon	Zn template carbonization	313.7 F/g at 0.5 A/g	93.1% @5,000	39
PVDC	N,S-codoped carbon	RT dehalogenation	427 F/g; CDI 140.7 mg/g	>98% first 4 CDI cycles	42
PVDF	Nanoporous graphitic carbon	Ni-catalyzed carbonization	241 F/g at 2 A/g	96.9% @5,000	49
PS foam	Hierarchical porous carbon nanosheets	MgO template + KOH	323 F/g; 44.1 Wh/kg	92.6% @10,000	106
PS foam	3D network porous carbon	Friedel–Crafts + silica template	208 F/g at 1 A/g; 22.5 Wh/kg	94.3% @5,000	29
PS	Ordered mesoporous carbon	SBA-15/Fe pyrolysis-deposition	118 F/g at 0.2 A/g	87.2% @5,000	56
EPS foam	N-doped porous carbon	Cyanuric chloride + KOH	327 F/g; CDI 34.8 mg/g	100% @10,000	30
PS	N-enriched porous carbon	Thermal plasma	482 F/g at 1 A/g	95% @5,000	37
PP masks	S-doped porous carbon	Sulfonation + KOH	365.4 F/g at 0.5 A/g	90.4% @10,000	124
Mixed plastics	Porous carbon nanosheets	OMMT + KOH	207 F/g; 30.4 Wh/kg	–	107
Flexible packaging	MWCNTs	Pyrolysis-CVD	33.5 F/g; double commercial	–	63
Polyolefins	CNTs	CB + Ni_2O_3 catalyst	~140 F/g	>98% @1,000	48
PET	Hierarchical porous carbon	Low-temp carbonization + KOH	413 F/g at 0.5 A/g; 25 Wh/kg	95% @10,000	108
Waste PU foam	CNT/CNF/PANI	Dip-coating + in-situ polymerization	372.6 F/g; 284.6 F/g all-solid	97.8% @1,000	38

PE	Graphene/mesoporous carbon	MCHP + GO	360 F/g; 63.3 Wh/kg at 4 V	93.8% @10,000	28
PVC	MnO_x-incorporated carbon	$Mg(OH)_2$ + $KMnO_4$	751.5 F/g at 1 A/g; 121.4 Wh/kg	83.1% @5,000	127
PP	Activated carbon nanosheets	Ferrocene + sulfur + KOH	349 F/g; 23 Wh/kg	99% @10,000	26
Waste masks	FMG/CaCo	Graphene + $Ca_3Co_4O_{9-\delta}$	1706.2 F/g; 208.4 Wh/kg	82.1% @1,500	100
PS	Porous carbon sheets	MgO + KOH	135 F/g; 3.4 Wh/kg	92.4% @10,000	109
PE	PE-HPC-NH_3	MCHP + NH_3	244 F/g; 43 Wh/kg at 4 V	97.1% @10,000	27
Mixed plastics	Graphene nanosheets	Two-stage MMT-catalyzed pyrolysis	38.8 F/g	–	47
PS foam	PCF-MnO_2	MgO + $KMnO_4$	308 F/g	93.4% @10,000	128
PS + sugar	Graphitic carbon	Ni butanethiolate + pyrolysis	158 F/g	90% @10,000	51
EPS/rGO	Self-standing electrode	Solution blending	11.9 mF/cm^2	99.5% @10,000	88
PS foam	3D hierarchically porous carbon	Fe_2O_3 + KOH	284.1 F/g; 19.2 Wh/kg	93.6% @5,000	110
PP	MWCNTs	CVD pyrolysis	59 F/g	–	61
Mixed plastics	Graphne/V_2O_5	Hydrothermal	139.7 F/g	82% @5,000	138
PS waste	N, S-codoped carbon	KOH/thiourea	143 F/g; 64–150 Wh/kg	99-100% @10,000	85

4.4 Energy harvesting, fuel cells, and bioenergy

Triboelectric nanogenerators (TENGs) convert mechanical energy into electricity through contact electrification and electrostatic induction. Plastic waste is attractive as a triboelectric layer because polyethylene sits near the bottom of the triboelectric series and can be paired with more tribopositive or tribonegative materials. A TENG using waste plastic bags paired with hBN achieved 68 V, 6.1μA, and 460 mW/m^2, with stable output over 10,000 cycles.[102] The output power density correlated with the product of resistivity and dielectric constant of the layered material, providing a design rule for material selection. A TENG using waste PA, PVC, and PE plastic bags coated with gold electrodes achieved 35.7 V, 5.85 μA, and 152.6 mW/m^2 for the PA-PVC pair, with the performance depending on the triboelectric series difference between the paired plastics[103]. A study using unsorted postconsumer plastic waste demonstrated that immiscibility, typically a barrier to recycling, actually enhanced triboelectric output.[91] A blend containing 60 wt% PET paired with a PET bottle film generated 130 V, 50 μA/cm^2, and 2604 μW/cm^2. The so-called rejected recyclable plastic waste fraction, which is largely landfilled, still generated over 60 V. Electrospun PVC/ZnO nanofibers from waste PVC pipes achieved 196 V, 8.1 μA, and 726.3 μW/cm^2, with 90% stability after 172,800 cycles.[43] The piezoelectric ZnO coupled with triboelectric PVC enhanced charge generation. A PET aerogel coated with polydopamine and polyethyleneimine achieved 67.7 V and 9.4 μA, with a power density of 5.47 W/m^2, and also removed over 92% of Pb(II), Hg(II), and Zn(II) from water.[105]

Microbial fuel cells (MFCs) use bacteria to oxidize organic matter and transfer electrons to an anode. A Fe-MOF/PANI composite derived from PET waste achieved 680 mW/m^2, 0.67 V open-circuit potential, and 3500 mA/m^2 limiting current density, with stable voltage over 370 hours[17]. The MOF provided high surface area for biofilm formation while PANI enhanced conductivity. A CNT-textile anode from polyester textile achieved 1098 mW/m^2 and 7.2 A/m^2, with a charge-transfer resistance of 30 Ω compared to 300 Ω for carbon cloth.[98] The open 3D structure enabled internal colonization and a tenfold larger biofilm-anode interfacial area. A CNT-sponge electrode achieved 1.99 W/m^2 and 325 W/m^3 in a continuous flow MFC, the highest volumetric power density reported for MFCs fed domestic wastewater at the time.[99] Direct borohydride fuel cells are attractive for their high theoretical voltage of 3.01 V. A N-doped graphene/Pt catalyst derived from PET waste achieved 75 mW/cm^2 at 45°C and a mass-specific power density of 15.8 W/mg$_{Pt}^{-1}$, among the highest reported.[139] The N-doped graphene support facilitated charge transfer and stabilized Pt nanoparticles.

Electrochemical synthesis using plastic-derived carbons is an emerging application. N-doped carbon from melamine formaldehyde resin waste achieved a H_2O_2 production rate of 971.6 mmolg$^{-1}_{catalyst}$ h^{-1} with over 90% Faradaic efficiency under acidic conditions.[36] In a flow cell, the catalyst maintained approximately 530 mA/cm^2 for 300 hours and achieved a production rate of 22.5 molg$^{-1}_{catalyst}$ h^{-1}, the highest among metal-free catalysts under acidic conditions. Porphyrin-like carbon defects were identified as the active sites for OOH generation. PVC functionalized with diiron carbonyl units via click chemistry was used as a film electrode for proton reduction, with a positive shift in reduction potential of over 400 mV compared to the monomeric diiron complex.[80] However, repetitive scanning caused about 80% loss of reduction current due to reductive bleaching of the active units.

Co-production of hydrogen and carbon nanomaterials from waste plastics addresses both energy and materials needs. A pilot-scale fluidized bed gasification system with Ni/Al_2O_3 catalysts achieved a hydrogen production rate of 385 mmol h^{-1} g^{-1} of catalyst and 24.3% CNT yield at 680°C.[62] The catalyst calcined under H_2 contained metallic nickel species with smaller crystallite size, which outperformed catalysts calcined under air or N_2. A microwave-initiated MAX Ti_3AlC_2 catalyzed process converted LDPE, HDPE, and PP into hydrogen with 75 to 78 vol% selectivity and carbon nanofibers with high graphitization.[140] The CNFs served as sodium-ion battery anodes with stable cycling over 2000 cycles. The MAX phase acted as both microwave susceptor and catalyst, converting to TiC and TiAl during reaction.

4.5 Sensors, Wearables, and Smart Electronics

Upcycled elastomers and recycled polyolefins enable stretchable strain sensors and stable thermistors. Upcycled thermoplastic polyester elastomer (TPEE) films from PET waste enable stretchable, self-healing strain sensors when coated layer by layer with poly(ionic liquid-co-acrylic acid) and MXene nanosheets.[95] The films elongate over 700%, heal at room temperature within 3 s, and show gauge factors of 270 at 0 to 10% strain and 2800 at 30 to 40% strain. Replacing the cationic layer with PDAC increases conductivity and retains 91% tensile strength after 100 cycles, with gauge factors of

7.4 at 40 to 60% strain and 33.5 at 80 to 100% strain.[96] These sensors detect finger, wrist, and elbow motion, and the same layer-by-layer approach works on cotton fabric. Recycled high-density polyethylene blended with virgin HDPE and carbon black provides positive temperature coefficient thermistors, but rHDPE introduces a negative temperature coefficient and weakens cycling stability.[90] Adding 0.2 wt% dicumyl peroxide eliminates the negative temperature coefficient, raises PTC intensity by 64.5% over the virgin system, and improves cyclic stability.

Conductive elastomers and ionic conductors derived from PET waste serve as soft, self-healing materials for wearable sensing. PET glycolysis with [EMIM][DCA] produces a polyurethane/poly(acrylic acid)/poly(acrylamide) dual-network ionogel with EMIES ionic liquid.[76] The ionogel reaches 4.2 MPa stress, 990% strain, and 0.09 S/cm conductivity, self-heals at 25 °C in 6 h with 100% conductivity recovery, and detects finger, wrist, elbow, and knee motion over 500 cycles at 25% strain. PET alcoholysis with polycaprolactone diol and LiTFSI yields a non-composite conductive polyurethane elastomer.[74] The optimal 10% LiTFSI sample reaches 7.05 S/cm, thermal diffusivity of 0.112 mm^2/s, stability to 260 °C, and moderate visible transmittance, making it suitable for sensors and optoelectronic components. Waste PET can also be converted in one pot using a ChCl/EG/$Zn(AC)_2$ deep eutectic solvent catalyst to form waterborne polyurethane, which is combined with P(AAM-AA) and binary ChCl/EG to produce a eutectogel.[75] This eutectogel achieves 8.87 MPa stress, 680% strain, 9.65 mS/cm ionic conductivity, and stability from -50 to 80 °C with a glass transition of -53.5 °C. It functions as a wearable strain sensor for swallowing, wrist bending, finger bending at 30°, 60°, and 90°, and knee bending over 1000 cycles at 25% strain.

Flexible energy storage devices for wearables can be fabricated from waste masks, polyurethane foams, and PET-derived polyurethanes. Waste surgical masks can be fully used in a quasi-solid-state supercapacitor: gold-sputtered outer layers support polypyrrole microcones, while the interlayer serves as separator with PVA/H_2SO_4 electrolyte.[101] The device delivers 219.1 mF/cm^2 at 1 mA/cm^2, retains 92.1% capacitance after 10,000 cycles and 88.3% after 100,000 bending cycles, and can be cut into designable shapes. Face masks coated with graphene and $Ca_3Co_4O_{9-\delta}$ oxide achieve 1706.2 F/g and 208.4 Wh/kg, maintain a stable 0.54 V output for 10 h, and retain 82.1% capacitance after 1500 cycles when encapsulated in recycled blister packs.[100] Waste polyurethane foam coated with carbon nanotubes, cellulose nanofibers, and polyaniline gives an all-solid-state supercapacitor with 284.6 F/g, 97.8% retention after 1000 cycles, and a wristband that powers an electronic watch.[38] PET glycolysis to bis(2-hydroxyethyl) terephthalate followed by self-healing polyurethane and carbon black/carbon nanotube fillers yields a conductive composite with 8.20×10^2 S/m, 94.3% capacitance after five cutting and healing cycles, and 95.1% after 1000 bending cycles.[78]

Energy harvesting and optoelectronic devices can be built from waste PVC and polystyrene. Waste PVC pipes electrospun into PVC/0.5 wt% ZnO nanofibers and paired with nylon-6 nanofibers produce a triboelectric nanogenerator with 196 V, 8.1 μA, and 726.3 $\mu W/cm^2$, retaining 90% stability after 172,800 cycles and lighting 192 green and 50 red LEDs.[43] A 3D-printed device harvests finger, hand,

and foot motion. Expanded polystyrene waste sulfonated with an imidazolium-based agent gives poly(styrene sulfonate) for PEDOT:PSS.[31] The material reaches 8.5 S/cm conductivity, 74 S/cm with dopants, an OECT mobility-capacitance product of 113.6 F/(cm·V·s), and 6.9% power conversion efficiency in a hybrid solar cell compared with 8.4% for commercial PEDOT:PSS.

Anisotropic conductive composites from discarded biaxially oriented polypropylene (BOPP) films enable directional electronics with thermal management. Discarded biaxially oriented polypropylene films alternated with conductive polypropylene random copolymer layers containing carbon nanotubes and graphene nanoplatelets, welded at 160 °C, yield a composite with in-plane conductivity of 11.4 S/m, through-thickness insulation, and anisotropy spanning nine orders of magnitude.[94] Tensile strength reaches 52.08 MPa and toughness 46.75 kJ/m^2, improvements of 224% and 360% over the isotropic control. An LED circuit lights only in the in-plane directions, and the surface temperature rises by 3.4 °C after 180 s compared with 25.1 °C for the isotropic control.

Thermal management and electromagnetic interference shielding wearables can be made from waste masks. Waste masks modified with tannic acid, electrostatically assembled with graphene nanoplatelets, and hot-pressed yield a nanocomposite with 87 W/(m·K) thermal conductivity, 88 dB electromagnetic interference shielding effectiveness (1100 dB/cm), 893 S/m electrical conductivity, and 970 N peeling force.[104] It cools LEDs and smartphones better than polyimide films or steel heat sinks, blocks signals from a Tesla coil, and shows favorable life-cycle and techno-economic assessment results.

4.6 EMI shielding, thermal management, composites, and membranes

Waste-derived polymer composites can simultaneously provide thermal management and electromagnetic interference (EMI) shielding. Pyrrhotite tailings and waste polystyrene combined with styrene-butadiene-styrene yield a block material with 1.36 W/(m·K) thermal conductivity, electrical resistivity above 10^8 Ω·m, and 33.1 dB EMI shielding effectiveness, where absorption dominates.[92] A dual-interface strategy using carbon dots and waste acrylonitrile-butadiene-styrene with pyrrhotite reaches 1.68 W/(m·K) and 43.1 dB EMI shielding, with absorption accounting for nearly all shielding and resistivity remaining above 10^{11} Ω·m.[93] Waste masks converted to polypropylene@graphene nanocomposites achieve 87 W/(m·K) thermal conductivity and 88 dB EMI shielding effectiveness (1100 dB/cm), and outperform commercial polyimide films and steel heat sinks in LED and smartphone cooling.[104] Non-recyclable rubber-rich plastic waste blended with polystyrene and carbon nanotubes forms a double-percolation network that lowers the electrical percolation threshold by 30% and improves EMI shielding, with absorption as the dominant mechanism.[89] Co-upcycling spent lithium-ion battery cathodes with polyethylene terephthalate and other plastics produces NiCoMnO/CNT composites with an effective microwave absorption bandwidth of 7.01 GHz at 2.41 mm, and life-cycle analysis shows lower global warming potential than pyrometallurgical, hydrometallurgical, or direct regeneration routes.[72]

Recycled plastics also enable conductive composites for sensing and anisotropic electronics. Recycled high-density polyethylene blended with virgin high-density polyethylene and carbon black exhibits a

positive temperature coefficient, but recycled content introduces a negative temperature coefficient and weakens cycling stability; adding 0.2 wt% dicumyl peroxide eliminates the negative effect, raises PTC intensity by 64.5% over the virgin system, and improves stability.[90] Discarded biaxially oriented polypropylene films alternated with conductive polypropylene random copolymer layers containing carbon nanotubes and graphene nanoplatelets yield in-plane conductivity of 11.4 S/m, through-thickness insulation spanning nine orders of magnitude, tensile strength of 52.08 MPa, and toughness of 46.75 kJ/m^2, with only a 3.4 °C temperature rise under electrical heating.[94] Waste polystyrene and aluminum powder composites show resistivity decreasing from 1.32×10^7 Ω·cm at 10 wt% aluminum to 1.38×10^6 Ω·cm at 40 wt%, with density increasing from 0.81 to 1.20 g/cm^3.[87] Waste polystyrene and polyvinyl chloride blends with glycolyzed PET additives reach 21.96 MPa tensile strength, 37% elongation at break, reduced burning rate to 0.5 mm/s, and enhanced permittivity and dielectric loss, making them suitable for electrical insulation and automotive components.[77]

Membranes and separators from waste plastics offer selective ion transport and electrochemical stability. Polyethylene-based anion exchange membranes with pendant ammonium chloride groups and a cross-linked matrix achieve ionic conductivities of 119.6 mS/cm in 2 N HCl and 78.8 mS/cm in 2 N HCl-0.2N CuCl, an order of magnitude higher than commercial membranes, while maintaining mechanical strength and ion selectivity.[81] Sulfonated polyvinyl chloride membranes, prepared by amination and subsequent sulfonation without destroying the porous morphology, show increased water uptake and proton conductivity that is 2.5 to 4 times higher than Nafion 115 at similar conditions, with performance maintained even at 45% relative humidity.[83] Recycled respirator mask filter layers modified with fuming sulfuric acid become hydrophilic separators for aqueous zinc-ion batteries, reducing overpotential from 80 mV to 24 mV, retaining 93.5% capacity after 200 cycles, and extending the anodic potential window to 4.75 V in lithium-ion cells.[84]

Conductive textile and sponge electrodes enable wearable energy storage and microbial fuel cells. Textiles coated with single-walled carbon nanotubes via a simple dipping and drying process reach 125 S/cm conductivity, less than 1 Ω/sq sheet resistance, and 0.48 F/cm^2 areal capacitance, with capacitance increasing 24-fold after MnO_2 deposition and negligible degradation over 35,000 cycles.[97] Carbon nanotube-textile anodes for microbial fuel cells provide a 10-fold larger analyte-biofilm-anode interfacial area than carbon cloth, reduce charge-transfer resistance from 300 Ω to 30 Ω, increase maximum current density by 157%, and improve energy recovery by 141%.[98] Carbon nanotube-sponge electrodes offer a tunable, uniform macroporous structure with pores up to 1 mm, lower internal resistance, and mechanical flexibility; they achieve 1.24 W/m^2 areal power density and 182 W/m^3 volumetric power density in microbial fuel cells fed domestic wastewater, the highest values reported at the time.[99]

5. Challenges and Outlook

5.1 Technology Readiness Level and Climate Performance: An Integrated Assessment

To evaluate the validity of a waste plastic chemical upcycling method, an integrated assessment of both technology readiness level and climate performance must be considered. Technology readiness is insufficient on its own to evaluate the effectiveness of a recycling technique. Conventional incineration and combustion techniques exhibit high maturity, but significantly hinder the environment, resulting in low circularity and high carbon burden and loss of embedded carbon.[141]

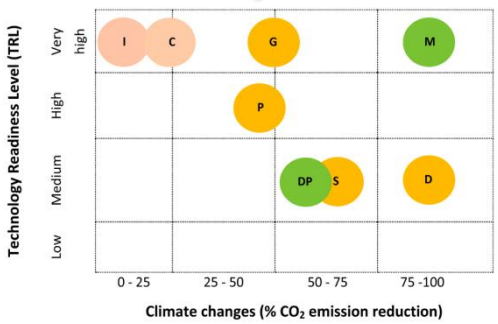


Figure 10. Technology Readiness Level versus CO_2 emission reduction potential for plastic recycling pathways. Reproduced from ref [141]. Abbreviation: I–Incineration, C–Combustion, G–Gasification, M–Mechanical recycling, P–Pyrolysis, DP–Dissolution/precipitation, S–Solvolysis, D–Depolymerization

Figure 10 places the main recycling pathways on a two-axis map of technology readiness and carbon dioxide emission reduction potential.[141] Mechanical recycling occupies the high readiness and strong climate performance region, but its applicability is limited by feedstock purity, mixed polymer streams, contamination, and the inability to produce conductive carbons directly. Incineration and combustion also have high readiness, yet their circularity is poor because they destroy the carbon backbone and release the embedded energy and carbon as emissions. Thermochemical routes such as gasification and pyrolysis show moderate climate performance and higher maturity. They can process mixed and contaminated plastics, and they can yield carbon nanomaterials, syngas, and fuels. Their climate benefit is nevertheless moderate because high temperatures, byproducts, and incomplete carbon recovery can offset the value of the products. Dissolution and precipitation have medium readiness and moderate climate performance. They purify polymers and preserve molecular structure, but they do not by themselves close the carbon loop into conductive materials.

Chemical recycling through solvolysis and depolymerization occupies the white space of low readiness and high potential climate benefit.[15,16,73,75,76] Its advantage is selective cleavage of ester, amide, and carbonate linkages under milder conditions, which preserves monomers and functional groups for repolymerization, MOF synthesis, polymer electrolytes, and carbon precursors. Its weakness is that scale up is unproven, feedstock tolerance is narrow, and solvent, catalyst, and purification costs can erase the climate gain. An integrated assessment therefore needs three axes: technology readiness,

climate performance, and life-cycle plus techno-economic viability.[72,73,104] A route with high readiness but low carbon dioxide reduction should not be scaled without redesign. A route with high carbon dioxide reduction but low readiness needs targeted research on yield, selectivity, and process integration. The most realistic near-term strategy combines mature mechanical and thermochemical steps with selective chemical recycling for clean condensation polymers. The long-term opportunity is to move solvolysis and depolymerization from lab scale to pilot scale while measuring energy demand, carbon efficiency, material quality, and cost from the start.

5.2 Pathways to Scale-up Solvolysis and Depolymerization

Solvolysis and depolymerization are attractive because they can recover monomers and oligomers from condensation polymers such as PET, PC, PU, PA, and PES.[15,16,73–75,79,131] Their scale up depends on four linked pathways: feedstock pretreatment and tolerance, catalyst development and process intensification, economic viability and government support, and infrastructure and integration.

5.2.1 Feedstock Pretreatment and Tolerance

Real waste streams contain mixed polymers, dyes, fillers, inks, adhesives, metals, and multilayer structures.[31,58,67,89,107] Solvolysis works best on clean, single polymer feedstocks, but real waste is rarely clean. Pretreatment must therefore combine sorting, size reduction, washing, decontamination, and selective separation. Polyolefins lack cleavable polar bonds and are poor candidates for solvolysis, so feedstock selection should target condensation polymers.[15,16,73,75,76] Mixed streams can be handled by sequential depolymerization or selective solvents, but each added step raises cost and energy use.[73,75,76] Tolerance to impurities is equally important. Catalysts and solvents must resist dyes, additives, and residual metals. For example, dyes in polystyrene cups interfered with sulfonation and reduced the degree of substitution,[31] while HCl released from PVC can poison catalysts and corrode equipment unless neutralized.[58] If pretreatment is too strict, the process loses its economic advantage. If it is too loose, monomer yield and purity fall. The practical goal is not perfect purity but consistent quality that downstream polymerization, MOF synthesis, or carbonization can accept.[16,17,130,131]

5.2.2 Catalyst Development and Process Intensification

Current depolymerization systems use Zn acetate, organocatalysts, ionic liquids, deep eutectic solvents, molten salts, and metal salts.[15,74–76,78] Many give high monomer yields with model feedstocks, but few have been demonstrated with real waste at scale. Future catalysts must be selective, recoverable, low cost, and tolerant to impurities. Heterogeneous catalysts and continuous flow reactors are promising because they simplify catalyst recovery and reduce solvent use, though most demonstrations remain at lab scale.[62,64] Process intensification through microwave heating, reactive extrusion, and one pot conversion can lower temperature, time, and energy demand.[67,75,76,118,123,131] One pot routes that use the depolymerization product directly without monomer purification can improve economics, but they trade purity for simplicity.[75,76] The best pathway will likely couple selective depolymerization with downstream polymerization, MOF synthesis, or carbonization so that oligomers and coproducts are used rather than discarded.[16,17,130,131]

5.2.3 Economic Viability and Government Support

Solvolysis and depolymerization must compete with virgin monomers and with mechanical recycling. They become viable when feedstock is cheap, solvent and catalyst are recovered, and products have high value. Techno-economic analysis should include capital cost, operating cost, catalyst lifetime, solvent losses, energy input, and product purity.[72,73,104] Life-cycle assessment should compare the route against incineration, mechanical recycling, and virgin production.[72,73,104] Policy support is essential because virgin resin prices rarely include environmental externalities. Carbon pricing, extended producer responsibility, subsidies for pilot and demonstration plants, green procurement, and standards for recycled content can all improve the business case. Without such support, promising chemical recycling routes may remain lab curiosities. With it, they can attract investment and reach commercial scale.

5.2.4 Infrastructure and Integration

Scaling up requires more than a reactor. It requires collection, sorting, pretreatment, solvent handling, catalyst recovery, and product purification. Existing PET recycling plants, chemical parks, and battery recycling facilities can provide infrastructure and feedstock.[72,73,130] Modular units can serve low-volume waste streams, while centralized plants can handle mixed urban waste. Integration with downstream manufacturing is equally important. Depolymerized monomers can feed polyurethane, polyester, polymer electrolyte, ionogel, and MOF production.[16,17,74–76,78,130,131] They can also serve as precursors for conductive carbons and composites. Renewable energy and closed-loop design can further reduce emissions. Plastics should be designed for depolymerization, and additives that poison catalysts should be avoided.[31,58] Scaling up will not be linear. It requires codevelopment of feedstock logistics, catalyst systems, process control, policy, and end-use markets. The white space of solvolysis and depolymerization is therefore not only a technical challenge but also an economic, environmental, and institutional one.

6. Conclusion

The review demonstrates that waste plastics can be effectively upcycled into high-performance conductive materials, but commercialization requires addressing specific technical and economic barriers. Concrete findings emerge from the benchmarking analysis. Plastic-derived hard carbons, for example from PET and PC, reach reversible capacities of roughly 300 to 450 mAh/g, marking them competitive anodes for sodium-ion and potassium-ion batteries. Heteroatom-doped porous carbons, including N,S-codoped carbons from PU and dehalogenated PVDC, reach specific capacitances of about 395 to 427 F/g in supercapacitors. Beyond storage, hierarchical carbons and composites provide electromagnetic interference shielding up to 88 dB and enable stretchable strain sensors with gauge factors up to 2800.

However, several critical gaps currently hinder industrial adoption. First, the field lacks standardized testing protocols for electrode fabrication and performance reporting, preventing reliable cross-study

comparisons. Second, the scalability of high-performing materials remains a major challenge, as most require complex multi-step syntheses such as template etching or multi-stage chemical vapor deposition that are difficult to translate to continuous-flow operation. Third, techno-economic and life-cycle validation is severely limited; while selective climate benefits exist, advanced chemical recycling remains at a low technology readiness level with unproven economic viability.

Addressing these gaps requires coordinated efforts to move beyond laboratory proof of concept toward pilot- and demonstration-scale systems. Such efforts would bring plastic upcycling closer to industrial adoption, turning a source of environmental pollution into a valuable, circular resource for next-generation energy and electronic technologies.

References

(1) Dokl, M.; Copot, A.; Krajnc, D.; Fan, Y. V.; Vujanović, A.; Aviso, K. B.; Tan, R. R.; Kravanja, Z.; Čuček, L. Global Projections of Plastic Use, End-of-Life Fate and Potential Changes in Consumption, Reduction, Recycling and Replacement with Bioplastics to 2050. *Sustainable Production and Consumption* **2024**, *51*, 498–518. https://doi.org/10.1016/j.spc.2024.09.025

(2) Wechselberger, C.; Lang, T.; Popadić, S.; Lipp, A.-M. Environmental Impacts of Plastic Degradation: Toxic Byproducts, Environmental Risks, and Eco-Friendly Alternatives. *Microplastics* **2026**, *5* (1), 40. https://doi.org/10.3390/microplastics5010040

(3) Houssini, K.; Li, J.; Tan, Q. Complexities of the Global Plastics Supply Chain Revealed in a Trade-Linked Material Flow Analysis. *Commun Earth Environ* **2025**, *6* (1), 257. https://doi.org/10.1038/s43247-025-02169-5

(4) *Global primary plastic waste generation by polymer*. Our World in Data. https://ourworldindata.org/grapher/plastic-waste-polymer (accessed 2026-10-30)

(5) Tan, A. F. J.; Yu, S.; Wang, C.; Yeoh, G. H.; Teoh, W. Y.; Yip, A. C. K. Reimagining Plastics Waste as Energy Solutions: Challenges and Opportunities. *npj Mater. Sustain.* **2024**, *2* (1), 2. https://doi.org/10.1038/s44296-024-00007-x

(6) Namjoufar, M.; Wei, Y.; Maloney, K. J.-R.; Laghaei, M.; Patadiya, J.; Hadigheh, S. A.; Naebe, M.; Zabihi, O. Overcoming Technical Barriers in Mechanical Recycling of Plastic Waste: The Role of Engineered Additives. *Journal of Environmental Chemical Engineering* **2026**, *14* (2), 121559. https://doi.org/10.1016/j.jece.2026.121559

(7) Leal Filho, W.; Barbir, J.; Carpio-Vallejo, E.; Dobri, A.; Voronova, V. Decarbonising the Plastic Industry: A Review of Carbon Emissions in the Lifecycle of Plastics Production. *Science of The Total Environment* **2025**, *999*, 180337. https://doi.org/10.1016/j.scitotenv.2025.180337

(8) Luo, H.; Tyrrell, H.; Bai, J.; Ibrahim Muazu, R.; Long, X. Fundamental, Technical and Environmental Overviews of Plastic Chemical Recycling. *Green Chem.* **2024**, *26* (23), 11444–11467. https://doi.org/10.1039/D4GC03127J

(9) Vinci, G.; Gobbi, L.; Porcaro, D.; Pinzi, S.; Carmona-Cabello, M.; Ruggeri, M. Environmental Evaluation of Chemical Plastic Waste Recycling: A Life Cycle Assessment Approach. *Resources* **2024**, *13* (12), 176. https://doi.org/10.3390/resources13120176

(10) *Global battery markets are growing strongly – and so are the supply risks*. IEA. https://www.iea.org/commentaries/global-battery-markets-are-growing-strongly-and-so-are-the-supply-risks (accessed 2026-10-30)

(11) Parr, D. *Supercapacitors for Data Centers Set to Become US$950 Million Market*. IDTechEx. https://www.idtechex.com/en/research-article/supercapacitors-for-data-centers-set-to-become-us-950-million-market/35121 (accessed 2026-10-30)

(12) Nagmani; Puravankara, S. Utilization of PET Derived Hard Carbon as a Battery-Type, Higher Plateau Capacity Anode for Sodium-Ion and Potassium-Ion Batteries. *Journal of Electroanalytical Chemistry* **2023**, *946*, 117731. https://doi.org/10.1016/j.jelechem.2023.117731

(13) Chen, D.; Luo, K.; Yang, Z.; Zhong, Y.; Wu, Z.; Song, Y.; Chen, G.; Wang, G.; Zhong, B.; Guo, X. Direct Conversion of Ester Bond-Rich Waste Plastics into Hard Carbon for High-Performance Sodium Storage. *Carbon* **2021**, *173*, 253–261. https://doi.org/10.1016/j.carbon.2020.11.004

(14) Elessawy, N. A.; El Nady, J.; Wazeer, W.; Kashyout, A. B. Development of High-Performance Supercapacitor Based on a Novel Controllable Green Synthesis for 3D Nitrogen Doped Graphene. *Sci Rep* **2019**, *9* (1), 1129. https://doi.org/10.1038/s41598-018-37369-x

(15) Kamali, A. R.; Li, S. Molten Salt-Assisted Valorization of Waste PET Plastics into Nanostructured SnO2@terephthalic Acid with Excellent Li-Ion Storage Performance. *Applied Energy* **2023**, *334*, 120692. https://doi.org/10.1016/j.apenergy.2023.120692

(16) Wang, Y.; Wang, H.; Li, S.; Sun, S. Waste PET Plastic-Derived CoNi-Based Metal–Organic Framework as an Anode for Lithium-Ion Batteries. *ACS Omega* **2022**, *7* (39), 35180–35190. https://doi.org/10.1021/acsomega.2c04264

(17) Kaur, R.; Singh, S.; Chhabra, V. A.; Marwaha, A.; Kim, K.-H.; Tripathi, S. K. A Sustainable Approach towards Utilization of Plastic Waste for an Efficient Electrode in Microbial Fuel Cell Applications. *Journal of Hazardous Materials* **2021**, *417*, 125992. https://doi.org/10.1016/j.jhazmat.2021.125992

(18) Chen, S.; Hu, Y. H. All-Plastic Supercapacitors from Poly(Ethylene Terephthalate) Waste. *Energy Fuels* **2025**, *39* (37), 18128–18137. https://doi.org/10.1021/acs.energyfuels.5c03370

(19) Xiang, S.; Yang, X.; Lin, X.; Chang, C.; Et., A. Nitrogen and Sulfur Co-Doped Polyurethane-Based Porous Carbon Materials as Supercapacitors Exhibit Excellent Electrochemical Performance. *Journal of Solid State Electrochemistry* **2017**. https://doi.org/10.1007/s10008-017-3505-7

(20) Zhang, H.; Zhou, X.-L.; Shao, L.-M.; Lü, F.; He, P.-J. Hierarchical Porous Carbon Spheres from Low-Density Polyethylene for High-Performance Supercapacitors. *ACS Sustainable Chem. Eng.* **2019**, *7* (4), 3801–3810. https://doi.org/10.1021/acssuschemeng.8b04539

(21) Kitchamsetti, N.; Mhin, S.; Han, H.; de Barros, A. L. F. From Environmental Burden to Energy Resource: Waste Plastic-Derived Carbons for Sustainable Batteries and Supercapacitors. *Polymers* **2026**, *18* (8), 983. https://doi.org/10.3390/polym18080983

(22) Chen, X.; Cheng, X.-B.; Liu, Z. High Sulfur-Doped Hard Carbon Anode from Polystyrene with Enhanced Capacity and Stability for Potassium-Ion Storage. *Journal of Energy Chemistry* **2022**, *68*, 688–698. https://doi.org/10.1016/j.jechem.2021.12.007

(23) Gong, J.; Liu, J.; Jiang, Z.; Wen, X.; Chen, X.; Mijowska, E.; Wang, Y.; Tang, T. Effect of the Added Amount of Organically-Modified Montmorillonite on the Catalytic Carbonization of Polypropylene into Cup-Stacked Carbon Nanotubes. *Chemical Engineering Journal* **2013**, *225*, 798–808. https://doi.org/10.1016/j.cej.2013.03.112

(24) Zhang, J.; Yan, B.; Wan, S.; Kong, Q. Converting Polyethylene Waste into Large Scale One-Dimensional Fe_3O_4 @C Composites by a Facile One-Pot Process. *Ind. Eng. Chem. Res.* **2013**, *52* (16), 5708–5712. https://doi.org/10.1021/ie4004392

(25) Pol, V. G.; Thiyagarajan, P. Remediating Plastic Waste into Carbon Nanotubes. *J. Environ. Monit.* **2010**, *12* (2), 455–459. https://doi.org/10.1039/B914648B

(26) Liu, X.; Ma, C.; Wen, Y.; Chen, X.; Zhao, X.; Tang, T.; Holze, R.; Mijowska, E. Highly Efficient Conversion of Waste Plastic into Thin Carbon Nanosheets for Superior Capacitive Energy Storage. *Carbon* **2021**, *171*, 819–828. https://doi.org/10.1016/j.carbon.2020.09.057

(27) Lian, Y.; Ni, M.; Huang, Z.; Chen, R.; Zhou, L.; Utetiwabo, W.; Yang, W. Polyethylene Waste Carbons with a Mesoporous Network towards Highly Efficient Supercapacitors. *Chemical Engineering Journal* **2019**, *366*, 313–320. https://doi.org/10.1016/j.cej.2019.02.063

(28) Lian, Y.-M.; Utetiwabo, W.; Zhou, Y.; Huang, Z.-H.; Zhou, L.; Faheem, M.; Chen, R.-J.; Yang, W. From Upcycled Waste Polyethylene Plastic to Graphene/Mesoporous Carbon for High-Voltage Supercapacitors. *Journal of Colloid and Interface Science* **2019**, *557*, 55–64. https://doi.org/10.1016/j.jcis.2019.09.003

(29) Zhang, Y.; Shen, Z.; Yu, Y.; Liu, L.; Wang, G.; Chen, A. Porous Carbon Derived from Waste Polystyrene Foam for Supercapacitor. *J Mater Sci* **2018**, *53* (17), 12115–12122. https://doi.org/10.1007/s10853-018-2513-z

(30) Deka, N.; Barman, J.; Kasthuri, S.; Nutalapati, V.; Dutta, G. K. Transforming Waste Polystyrene Foam into N-Doped Porous Carbon for Capacitive Energy Storage and Deionization Applications. *Applied Surface Science* **2020**, *511*, 145576. https://doi.org/10.1016/j.apsusc.2020.145576

(31) Lo, C.-Y.; Koutsoukos, K. P.; Nguyen, D. M.; Wu, Y.; Angel Trujillo, D. A.; Miller, T.; Shrestha, T.; Mackey, E.; Damani, V. S.; Kanbur, U.; Opila, R.; Martin, D. C.; Kaphan, D.; Kayser, L. V. Imidazolium-Based Sulfonating Agent to Control the Degree of Sulfonation of Aromatic Polymers and Enable Plastics-to-Electronics Upgrading. *JACS Au* **2024**, *4* (7), 2596–2605. https://doi.org/10.1021/jacsau.4c00355

(32) Qi, X.-Y.; Yan, D.; Jiang, Z.; Cao, Y.-K.; Yu, Z.-Z.; Yavari, F.; Koratkar, N. Enhanced Electrical Conductivity in Polystyrene Nanocomposites at Ultra-Low Graphene Content. *ACS Appl. Mater. Interfaces* **2011**, *3* (8), 3130–3133. https://doi.org/10.1021/am200628c

(33) Wen, Y.; Kierzek, K.; Min, J.; Chen, X.; Gong, J.; Niu, R.; Wen, X.; Azadmanjiri, J.; Mijowska, E.; Tang, T. Porous Carbon Nanosheet with High Surface Area Derived from Waste Poly(Ethylene Terephthalate) for Supercapacitor Applications. *J of Applied Polymer Sci* **2020**, *137* (5), 48338. https://doi.org/10.1002/app.48338

(34) Kamali, A. R.; Yang, J.; Sun, Q. Molten Salt Conversion of Polyethylene Terephthalate Waste into Graphene Nanostructures with High Surface Area and Ultra-High Electrical Conductivity. *Applied Surface Science* **2019**, *476*, 539–551. https://doi.org/10.1016/j.apsusc.2019.01.119

(35) Kogolev, D.; Semyonov, O.; Metalnikova, N.; Fatkullin, M.; Rodriguez, R. D.; Slepicka, P.; Yamauchi, Y.; Guselnikova, O.; Boukherroub, R.; Postnikov, P. S. Waste PET Upcycling to Conductive Carbon-Based Composite through Laser-Assisted Carbonization of UiO-66. *J. Mater. Chem. A* **2023**, *11* (3), 1108–1115. https://doi.org/10.1039/D2TA08127J

(36) Wen, Y.; Fang, Y.; Huang, B.; Zhang, T.; Cai, C.; Niu, B.; Wang, H.; Guo, Q.; Ding, S.; Yao, G.; Qian, X.; Zhao, Y. Scalable Carbonization of Waste Plastics for Producing Nitrogen-Doped Carbon for Efficient Hydrogen Peroxide Electrosynthesis. *Journal of Energy Chemistry* **2025**, *108*, 181–189. https://doi.org/10.1016/j.jechem.2025.04.029

(37) Sahoo, R. K.; Kumar Chitumalla, R.; Das, A.; Mohapatra, M.; Moon Yun, J.; Jang, J.; Ho Kim, K.; Singh, S. K. Scalable Processing Method Using Waste Polystyrene to Produce Nitrogen-Enriched Porous Carbon for Boosting Supercapacitor Performance. *Materials Letters* **2021**, *300*, 130135. https://doi.org/10.1016/j.matlet.2021.130135

(38) Wang, Q.; Xia, T.; Wu, W.; Zhao, J.; Xue, X.; Ao, C.; Zhang, J.; Deng, X.; Zhang, X.; Zhang, W.; Lu, C. Flexible, All-Solid-State Supercapacitors Derived from Waste Polyurethane Foams. *Chemical Engineering Journal* **2022**, *431*, 133228. https://doi.org/10.1016/j.cej.2021.133228

(39) Chen, X. Y.; Cheng, L. X.; Deng, X.; Zhang, L.; Zhang, Z. J. Generalized Conversion of Halogen-Containing Plastic Waste into Nanoporous Carbon by a Template Carbonization Method. *Ind. Eng. Chem. Res.* **2014**, *53* (17), 6990–6997. https://doi.org/10.1021/ie500685s

(40) Nagmani; Tyagi, A.; Verma, P.; Puravankara, S. Effect of Pore Morphology on the Enhanced Potassium Storage in Hard Carbon Derived from Polyvinyl Chloride for K-Ion Batteries. *Electrochimica Acta* **2023**, *464*, 142903. https://doi.org/10.1016/j.electacta.2023.142903

(41) Chang, Y.; Pang, Y.; Dang, Q.; Kumar, A.; Zhang, G.; Chang, Z.; Sun, X. Converting Polyvinyl Chloride Plastic Wastes to Carbonaceous Materials via Room-Temperature Dehalogenation for High-Performance Supercapacitor. *ACS Appl. Energy Mater.* **2018**, acsaem.8b01252. https://doi.org/10.1021/acsaem.8b01252

(42) Chang, Y.; Zhang, G.; Han, B.; Li, H.; Hu, C.; Pang, Y.; Chang, Z.; Sun, X. Polymer Dehalogenation-Enabled Fast Fabrication of N,S-Codoped Carbon Materials for Superior

Supercapacitor and Deionization Applications. *ACS Appl. Mater. Interfaces* **2017**, *9* (35), 29753–29759. https://doi.org/10.1021/acsami.7b08181

(43) Yavari, S.; Sembay, M.; Bushanov, Y.; Bakenov, Z.; Shafiee, M.; Kalimuldina, G. Recycling Polyvinyl Chloride (PVC) Pipe Wastes into PVC/ZnO Nanofiber-Based Triboelectric Nanogenerators. *ENERGY & ENVIRONMENTAL MATERIALS* **2025**, *8* (3), e12884. https://doi.org/10.1002/eem2.12884

(44) Zhang, P.; Shu, Y.; Wang, Y.; Ye, J.; Yang, L. Simple and Efficient Synthesis Methods for Fabricating Anode Materials of Sodium-Ion Batteries and Their Sodium-Ion Storage Mechanism Study. *J. Mater. Chem. A* **2023**, *11* (6), 2920–2932. https://doi.org/10.1039/D2TA09051A

(45) He, X.; Zhong, L.; Qiu, X.; Wen, F.; Sun, S.; Zu, X.; Zhang, W. Sustainable Polyvinyl Chloride-Derived Soft Carbon Anodes for Potassium-Ion Storage: Electrochemical Behaviors and Mechanism. *ChemSusChem* **2023**, *16* (19), e202300646. https://doi.org/10.1002/cssc.202300646

(46) Gong, J.; Liu, J.; Wen, X.; Jiang, Z.; Chen, X.; Mijowska, E.; Tang, T. Upcycling Waste Polypropylene into Graphene Flakes on Organically Modified Montmorillonite. *Ind. Eng. Chem. Res.* **2014**, *53* (11), 4173–4181. https://doi.org/10.1021/ie4043246

(47) Karakoti, M.; Pandey, S.; Jangra, R.; Dhapola, P. S.; Singh, P. K.; Mahendia, S.; Abbas, A.; Sahoo, N. G. Waste Plastics Derived Graphene Nanosheets for Supercapacitor Application. *Materials and Manufacturing Processes* **2021**, *36* (2), 171–177. https://doi.org/10.1080/10426914.2020.1832680

(48) Wen, X.; Chen, X.; Tian, N.; Gong, J.; Liu, J.; Rümmeli, M. H.; Chu, P. K.; Mijiwska, E.; Tang, T. Nanosized Carbon Black Combined with $Ni_2 O_3$ as "Universal" Catalysts for Synergistically Catalyzing Carbonization of Polyolefin Wastes to Synthesize Carbon Nanotubes and Application for Supercapacitors. *Environ. Sci. Technol.* **2014**, *48* (7), 4048–4055. https://doi.org/10.1021/es404646e

(49) Cheng, L. X.; Zhu, Y. Q.; Chen, X. Y.; Zhang, Z. J. Polyvinylidene Fluoride-Based Carbon Supercapacitors: Notable Capacitive Improvement of Nanoporous Carbon by the Redox Additive Electrolyte of 4-(4-Nitrophenylazo)-1-Naphthol. *Ind. Eng. Chem. Res.* **2015**, *54* (41), 9948–9955. https://doi.org/10.1021/acs.iecr.5b02490

(50) Liu, X.; Xu, D.; Ding, H.; Widenmeyer, M.; Xie, W.; Mellin, M.; Qu, F.; Chen, G.; Zhang, Y. S.; Zhang, Z.; Rashid, A.; Molina-Luna, L.; Hofmann, J. P.; Riedel, R.; Brett, D. J. L.; Weidenkaff, A. Multi-Scale Designed Co Mn3–O4 Spinels: Smart Pre-Catalysts towards High-Efficiency Pyrolysis-Catalysis Recycling of Waste Plastics. *Applied Catalysis B: Environmental* **2023**, *324*, 122271. https://doi.org/10.1016/j.apcatb.2022.122271

(51) Urgunde, A. B.; Bahuguna, G.; Dhamija, A.; Das, P. P.; Gupta, R. Ni Ink-Catalyzed Conversion of a Waste Polystyrene–Sugar Composite to Graphitic Carbon for Electric Double-Layer Supercapacitors. *ACS Appl. Electron. Mater.* **2020**, *2* (10), 3178–3186. https://doi.org/10.1021/acsaelm.0c00542

(52) Kim, H. S.; Hyun, J. C.; Choi, Y.; Ha, S.; Kang, D. H.; Heo, Y. H.; Kwak, J. H.; Yoon, J.; Lee, J. B.; Kim, J.-Y.; Jin, H.-J.; Lee, J.; Lim, H.; Yun, Y. S. A New Perspective for Potassium Intercalation Chemistry in Graphitic Carbon Materials. *Energy Storage Materials* **2024**, *70*, 103514. https://doi.org/10.1016/j.ensm.2024.103514

(53) Zhang, J.; Du, J.; Qian, Y.; Xiong, S. Synthesis, Characterization and Properties of Carbon Nanotubes Microspheres from Pyrolysis of Polypropylene and Maleated Polypropylene. *Materials Research Bulletin* **2010**, *45* (1), 15–20. https://doi.org/10.1016/j.materresbull.2009.09.007

(54) Pol, V. G. Upcycling: Converting Waste Plastics into Paramagnetic, Conducting, Solid, Pure Carbon Microspheres. *Environ. Sci. Technol.* **2010**, *44* (12), 4753–4759. https://doi.org/10.1021/es100243u

(55) Fonseca, W. S.; Meng, X.; Deng, D. Trash to Treasure: Transforming Waste Polystyrene Cups into Negative Electrode Materials for Sodium Ion Batteries. *ACS Sustainable Chem. Eng.* **2015**, *3* (9), 2153–2159. https://doi.org/10.1021/acssuschemeng.5b00403

(56) Liang, K.; Liu, L.; Wang, W.; Yu, Y.; Wang, Y.; Zhang, L.; Ma, C.; Chen, A. Conversion of Waste Plastic into Ordered Mesoporous Carbon for Electrochemical Applications. *J. Mater. Res.* **2019**, *34* (6), 941–949. https://doi.org/10.1557/jmr.2018.493

(57) Ma, J.; Liu, J.; Song, J.; Tang, T. Pressurized Carbonization of Mixed Plastics into Porous Carbon Sheets on Magnesium Oxide. *RSC Adv.* **2018**, *8* (5), 2469–2476. https://doi.org/10.1039/C7RA12733B

(58) Min, J.; Wen, X.; Tang, T.; Chen, X.; Huo, K.; Gong, J.; Azadmanjiri, J.; He, C.; Mijowska, E. A General Approach towards Carbonization of Plastic Waste into a Well-Designed 3D Porous Carbon Framework for Super Lithium-Ion Batteries. *Chem. Commun.* **2020**, *56* (64), 9142–9145. https://doi.org/10.1039/D0CC03236K

(59) Kumar, U.; Goonetilleke, D.; Gaikwad, V.; Pramudita, J. C.; Joshi, R. K.; Sharma, N.; Sahajwalla, V. Activated Carbon from E-Waste Plastics as a Promising Anode for Sodium-Ion Batteries. *ACS Sustainable Chem. Eng.* **2019**, *7* (12), 10310–10322. https://doi.org/10.1021/acssuschemeng.9b00135

(60) Mishra, N.; Das, G.; Ansaldo, A.; Genovese, A.; Malerba, M.; Povia, M.; Ricci, D.; Di Fabrizio, E.; Di Zitti, E.; Sharon, M.; Sharon, M. Pyrolysis of Waste Polypropylene for the Synthesis of Carbon Nanotubes. *Journal of Analytical and Applied Pyrolysis* **2012**, *94*, 91–98. https://doi.org/10.1016/j.jaap.2011.11.012

(61) Mishra, N.; Shinde, S.; Vishwakarma, R.; Kadam, S.; Sharon, M.; Sharon, M. MWCNTs Synthesized from Waste Polypropylene Plastics and Its Application in Super-Capacitors; Mumbai, India, 2013; pp 228–236. https://doi.org/10.1063/1.4810063

(62) Yang, R.-X.; Chuang, K.-H.; Wey, M.-Y. Effects of Nickel Species on Ni/Al_2O_3 Catalysts in Carbon Nanotube and Hydrogen Production by Waste Plastic Gasification: Bench- and Pilot-Scale Tests. *Energy Fuels* **2015**, *29* (12), 8178–8187. https://doi.org/10.1021/acs.energyfuels.5b01866

(63) Abbas, A.; Yi, Y. M.; Saleem, F.; Jin, Z.; Veksha, A.; Yan, Q.; Lisak, G.; Lim, T. M. Multiwall Carbon Nanotubes Derived from Plastic Packaging Waste as a High-performance Electrode Material for Supercapacitors. *Int J Energy Res* **2021**, *45* (13), 19611–19622. https://doi.org/10.1002/er.6967

(64) Nam, E.; Park, G.; Nam, J. Y.; Park, S.; Jo, Y.; Kim, J.; Park, B. G.; Baek, K.; Kang, S. J.; Ra, H. W.; Park, Y.; Seo, M. W.; Lee, K. J.; An, K. Upcycling of Plastic Waste into Carbon Nanotubes as

Efficient Battery Additives. *Green Chem.* **2023**, *25* (20), 8007–8018. https://doi.org/10.1039/D3GC02100A

(65) Zhang, Y.; Li, W.; Hu, J.; Yue, M. Trash to Treasure: Transforming Wasted Polystyrene Foam to Conductive Fibers by Polymer Pyrolysis Deposition on Glass Fibers. *Materials Chemistry and Physics* **2023**, *309*, 128380. https://doi.org/10.1016/j.matchemphys.2023.128380

(66) Palanisamy, M.; Perumal, R.; Zhang, D.; Wang, H.; Maximova, O.; Rokhinson, L.; Pol, V. G. Graphene Triggered Catalytic Attack on Plastic Waste Produces Graphitic Shell Encapsulation on Cobalt Nanoparticles for Ferromagnetism and Stable Li^+ Ion Storage. *J. Mater. Chem. A* **2024**, *12* (30), 19081–19093. https://doi.org/10.1039/D4TA01354A

(67) Yuwen, C.; Liu, B.; Rong, Q.; Zhang, L.; Guo, S. Porous Carbon Materials Derived from Discarded COVID-19 Masks via Microwave Solvothermal Method for Lithium-sulfur Batteries. *Science of The Total Environment* **2022**, *817*, 152995. https://doi.org/10.1016/j.scitotenv.2022.152995

(68) Ren, S.; Kamali, A. R. Upcycling Waste Polyethylene Terephthalate for Enhanced Na-Ion Storage. *Journal of Energy Storage* **2025**, *118*, 116127. https://doi.org/10.1016/j.est.2025.116127

(69) Kong, T.; Qian, Y.; Li, Y.; Lin, N.; Qian, Y. Plastic-Derived Sandwich-like Porous Carbon Nanosheet-Supported Hexagonal Carbon Micro-Flakes for K-Ion Storage. *Chem. Commun.* **2023**, *59* (28), 4169–4172. https://doi.org/10.1039/D3CC00473B

(70) Padha, B.; Verma, S.; Prerna; Ahmed, A.; Patole, S. P.; Arya, S. Plastic Turned into MXene–Based Pyro-Piezoelectric Hybrid Nanogenerator-Driven Self-Powered Wearable Symmetric Supercapacitor. *Applied Energy* **2024**, *356*, 122402. https://doi.org/10.1016/j.apenergy.2023.122402

(71) Tang, Y.; Cen, Z.; Ma, Q.; Zheng, B.; Cai, Z.; Liu, S.; Wu, D. A Versatile Sulfur-Assisted Pyrolysis Strategy for High-Atom-Economy Upcycling of Waste Plastics into High-Value Carbon Materials. *Advanced Science* **2023**, *10* (15), 2206924. https://doi.org/10.1002/advs.202206924

(72) Qiu, B.; Hou, Y.; Shi, Z.; Du, P.; Xu, N.; Xie, H.; Liu, K.; Chen, J.; Li, B.; Han, Q.; Wang, D.; Lee, L. Y. S.; Liu, M.; Fu, D.; Yin, H. Co-Upcycling Spent Lithium-Ion Batteries and Plastics into Microwave Absorbing Materials with Ni-Co Catalyst Control. *Nat Commun* **2026**, *17* (1), 2822. https://doi.org/10.1038/s41467-026-69501-1

(73) Zhang, T.; Shen, K.; Zhang, Y.; Tang, W.; Dai, W.; Zhang, W. Cathode and Plastic Corecycling from Spent Batteries via Paired Electrolysis. *ACS Sustainable Chem. Eng.* **2025**, *13* (43), 18633–18641. https://doi.org/10.1021/acssuschemeng.5c06970

(74) Guo, R. Preparation and Properties of High Electrical Conductivity Elastomer from Alcoholysis Product of Waste Plastic. *Essential Chem* **2024**, *1* (1), 1–10. https://doi.org/10.1080/28378083.2024.2362676

(75) Hao, P.; Cheng, X.; Lu, X.; Zhou, Q.; Yan, D.; Xin, J.; Xu, J.; Li, Y. Waste Plastics to Prepare Eutectogel: Wearable, Highly Deformable, Transparent Flexible Ionic Conductors. *Chemical Engineering Journal* **2024**, *493*, 152871. https://doi.org/10.1016/j.cej.2024.152871

(76) Hao, P.; Zhang, R.; Xu, K.; Lu, X.; Zhou, Q.; Xin, J.; Xu, J.; Li, Y. Valorization of Waste Plastics to Prepare Tough, Stretchable and Highly Conductive Ionicgels. *Chemical Engineering Journal* **2024**, *481*, 148605. https://doi.org/10.1016/j.cej.2024.148605

(77) Shafik, E. S. Sustainable Valorization of Waste Polystyrene and PVC Blends for High-Performance Applications. *Sci Rep* **2026**, *16* (1), 14277. https://doi.org/10.1038/s41598-026-49599-5

(78) Wang, Y.; Park, B.; Vu, V.-P.; Lee, S.-H. Self-Healing Conducting Composite Electrodes Derived from Chemical Recycling of PET Plastic Wastes for Flexible Supercapacitors. *Polymer Engineering & Science* **2025**, *65* (4), 1854–1867. https://doi.org/10.1002/pen.27117

(79) Tan, M. Y.; Goh, L.; Safanama, D.; Loh, W. W.; Ding, N.; Chien, S. W.; Goh, S. S.; Thitsartarn, W.; Lim, J. Y. C.; Fam, D. W. H. Upcycling Waste Poly(Ethylene Terephthalate) into Polymer Electrolytes. *J. Mater. Chem. A* **2022**, *10* (46), 24468–24474. https://doi.org/10.1039/D2TA06692K

(80) Wang, L.; Xiao, Z.; Ru, X.; Liu, X. Enable PVC Plastic for a Novel Role: Its Functionalisation with Diiron Models of the Sub-Unit of [FeFe]–Hydrogenase, Assembly of Film Electrodes, and Electrochemical Investigations. *RSC Adv.* **2011**, *1* (7), 1211. https://doi.org/10.1039/c1ra00343g

(81) Zhang, M.; Kim, H. K.; Chalkova, E.; Mark, F.; Lvov, S. N.; Chung, T. C. M. New Polyethylene Based Anion Exchange Membranes (PE–AEMs) with High Ionic Conductivity. *Macromolecules* **2011**, *44* (15), 5937–5946. https://doi.org/10.1021/ma200836d

(82) Tang, X.; Din, C.; Yu, S.; Liu, Y.; Luo, H.; Zhang, D.; Chen, S. Synthesis of Dielectric Polystyrene via One-Step Nitration Reaction for Large-Scale Energy Storage. *Chemical Engineering Journal* **2022**, *446*, 137281. https://doi.org/10.1016/j.cej.2022.137281

(83) Allan, J. T. S.; Prest, L. E.; Easton, E. B. The Sulfonation of Polyvinyl Chloride: Synthesis and Characterization for Proton Conducting Membrane Applications. *Journal of Membrane Science* **2015**, *489*, 175–182. https://doi.org/10.1016/j.memsci.2015.03.093

(84) Kim, S.; Yang, X.; Yang, K.; Guo, H.; Cho, M.; Kim, Y. J.; Lee, Y. Recycling Respirator Masks to a High-Value Product: From COVID-19 Prevention to Highly Efficient Battery Separator. *Chemical Engineering Journal* **2022**, *430*, 132723. https://doi.org/10.1016/j.cej.2021.132723

(85) Archana, S.; Sharafudeen, P. C.; Elumalai, P. N, S Codoping and Mesoporous-Induced Capacitive Storage Enhancement in Supercapacitor and Improved Li–S Battery Performances of Polystyrene Waste-Derived Carbon Electrode. *Energy Tech* **2023**, *11* (3), 2201125. https://doi.org/10.1002/ente.202201125

(86) Chang, T.-E.; Kisliuk, A.; Rhodes, S. M.; Brittain, W. J.; Sokolov, A. P. Conductivity and Mechanical Properties of Well-Dispersed Single-Wall Carbon Nanotube/Polystyrene Composite. *Polymer* **2006**, *47* (22), 7740–7746. https://doi.org/10.1016/j.polymer.2006.09.013

(87) Ighalo, J. O.; Adeniyi, A. G. Utilization of Recycled Polystyrene and Aluminum Wastes in the Development of Conductive Plastic Composites: Evaluation of Electrical Properties. In *Handbook of*

Environmental Materials Management; Hussain, C. M., Ed.; Springer International Publishing: Cham, 2020; pp 1–9. https://doi.org/10.1007/978-3-319-58538-3_228-1

(88) Vijaya, S.; Kennedy, L. J. From Waste to Energy Storage: Post-Consumer Waste Expanded Polystyrene/rGO Composite as a High Performance Self-Standing Electrode for Coin Cell Supercapacitors. *RSC Adv.* **2024**, *14* (1), 689–699. https://doi.org/10.1039/D3RA07071A

(89) Ahmadian Hoseini, A. H.; Erfanian, E.; Kamkar, M.; Sundararaj, U.; Liu, J.; Arjmand, M. Waste to Value-Added Product: Developing Electrically Conductive Nanocomposites Using a Non-Recyclable Plastic Waste Containing Vulcanized Rubber. *Polymers* **2021**, *13* (15), 2427. https://doi.org/10.3390/polym13152427

(90) Hu, H.; Ding, X.; Li, G.; Jiang, D.; Jin, Y.; Bai, S.; Wang, H.; Shi, X.; Shi, Q.; Zhang, Y.; Li, Q. Preparation and Performance of Modified Positive Temperature Coefficient Conductive Polymer Composites From Recycled High-Density Polyethylene. *Journal of Applied Polymer Science* **2025**, *142* (45), e57760. https://doi.org/10.1002/app.57760

(91) Slobodian, P.; Riha, P.; Hausnerova, B. Unsorted Postconsumer Plastic Waste in Energy Conversion Using Piezoelectric, Triboelectric, and Pyroelectric Generation Mechanisms. *ACS Sustainable Chem. Eng.* **2025**, *13* (7), 2683–2693. https://doi.org/10.1021/acssuschemeng.4c06984

(92) Wang, Z.; Su, J.; Wang, J.; Feng, Y.; Xu, Q.; Wang, H.; Jiang, H. Unification of Thermal Conductivity, Electrical Insulation, and Electromagnetic Shielding: A Bulk Thermal Conductive Polymer from Solid Waste. *Chemical Engineering Journal* **2024**, *498*, 155065. https://doi.org/10.1016/j.cej.2024.155065

(93) Wang, Z.; Wang, J.; Wang, H.; Jiang, H.; Wang, C.; Zhang, Y.; Hou, H.; Zhang, L. Dual Interface Strategies Using Carbon Dots for Fabricating Thermally Conductive Polymers by Pyrrhotite and Waste Plastics. *Advanced Industrial and Engineering Polymer Research* **2026**, *9* (1), 49–62. https://doi.org/10.1016/j.aiepr.2025.09.006

(94) Jiang, Q.; Wu, Q.; Nie, M. Sustainable Fabrication of Anisotropic Conductive Composites from Discarded Biaxially Oriented Polypropylene Films. *Advanced Sustainable Systems* **2025**, *9* (9), e00501. https://doi.org/10.1002/adsu.202500501

(95) Chang, C.-W.; Chang, C.-T.; Ciou, J.-H.; Kuo, K.-C.; Wu, C.-T.; Lin, J.; Lo, T.-Y.; Chen, Y.; Lin, H.-W.; Tseng, Y.-H.; Li, M.-L.; Lin, C.-T.; Chen, J.-T. Layer-by-Layer Techniques Incorporating Upcycled TPEE: From Waste to Conductive, Multi-Responsive, Self-Healable, and Highly-Stretchable Electronics. *J. Mater. Chem. A* **2025**, *13* (25), 19850–19863. https://doi.org/10.1039/D5TA01392E

(96) Chang, C.-T.; Chang, C.-W.; Ciou, J.-H.; Kuo, K.-C.; Lin, J.; Wu, C.-T.; Li, M.-L.; Tseng, Y.-H.; Lin, Y.-L.; Lin, C.-T.; Chen, J.-T. Transforming Plastic Waste into Strain Sensors: Multifunctional Upcycled TPEE Elastomers with MXene Multilayer Assemblies. *Advanced Materials Technologies* **2025**, *10* (17), e00652. https://doi.org/10.1002/admt.202500652

(97) Hu, L.; Pasta, M.; La Mantia, F.; Cui, L.; Jeong, S.; Deshazer, H. D.; Choi, J. W.; Han, S. M.; Cui, Y. Stretchable, Porous, and Conductive Energy Textiles. *Nano Lett.* **2010**, *10* (2), 708–714. https://doi.org/10.1021/nl903949m

(98) Xie, X.; Hu, L.; Pasta, M.; Wells, G. F.; Kong, D.; Criddle, C. S.; Cui, Y. Three-Dimensional Carbon Nanotube−Textile Anode for High-Performance Microbial Fuel Cells. *Nano Lett.* **2011**, *11* (1), 291–296. https://doi.org/10.1021/nl103905t

(99) Xie, X.; Ye, M.; Hu, L.; Liu, N.; McDonough, J. R.; Chen, W.; Alshareef, H. N.; Criddle, C. S.; Cui, Y. Carbon Nanotube-Coated Macroporous Sponge for Microbial Fuel Cell Electrodes. *Energy Environ. Sci.* **2012**, *5* (1), 5265–5270. https://doi.org/10.1039/C1EE02122B

(100) Mendoza, R.; Oliva, J.; Padmasree, K. P.; Oliva, A. I.; Mtz-Enriquez, A. I.; Zakhidov, A. Highly Efficient Textile Supercapacitors Made with Face Masks Waste and Thermoelectric Ca3Co4O9-δ Oxide. *Journal of Energy Storage* **2022**, *46*, 103818. https://doi.org/10.1016/j.est.2021.103818

(101) Zuo, W.; Zang, L.; Liu, Q.; Qiu, J.; Lan, M.; Yang, C. A Quasi-Solid-State Supercapacitor Based on Waste Surgical Masks with High Flexibility and Designable Shape. *Colloids and Surfaces A: Physicochemical and Engineering Aspects* **2022**, *634*, 128020. https://doi.org/10.1016/j.colsurfa.2021.128020

(102) Das, B.; Paul, R.; Karmakar, R.; Meikap, A. K.; Kumar, A.; Krishnamurthy, S.; Ghosh, R. A Triboelectric Nanogenerator Based on Waste Plastic and Layered Materials via Modulation of the Electrical and Dielectric Properties. *ACS Appl. Energy Mater.* **2024**, *7* (16), 7025–7036. https://doi.org/10.1021/acsaem.4c01205

(103) Feng, X.; Li, Q.; Wang, K. Waste Plastic Triboelectric Nanogenerators Using Recycled Plastic Bags for Power Generation. *ACS Appl. Mater. Interfaces* **2021**, *13* (1), 400–410. https://doi.org/10.1021/acsami.0c16489

(104) Zhang, X.; Luo, W.; Chen, Y.; Guo, Q.; Luo, J.; Burey, P.; Gao, Y.; Lu, Y.; Gao, Q.; Li, J.; Li, J.; Song, P. Highly Thermal Conductive and Electromagnetic Shielding Polymer Nanocomposites from Waste Masks. *Nano-Micro Lett.* **2025**, *17* (1), 263. https://doi.org/10.1007/s40820-025-01796-z

(105) Roy, S.; Maji, P. K.; Goh, K.-L. Sustainable Design of Flexible 3D Aerogel from Waste PET Bottle for Wastewater Treatment to Energy Harvesting Device. *Chemical Engineering Journal* **2021**, *413*, 127409. https://doi.org/10.1016/j.cej.2020.127409

(106) Ma, C.; Liu, X.; Min, J.; Li, J.; Gong, J.; Wen, X.; Chen, X.; Tang, T.; Mijowska, E. Sustainable Recycling of Waste Polystyrene into Hierarchical Porous Carbon Nanosheets with Potential Applications in Supercapacitors. *Nanotechnology* **2020**, *31* (3), 035402. https://doi.org/10.1088/1361-6528/ab475f

(107) Wen, Y.; Kierzek, K.; Chen, X.; Gong, J.; Liu, J.; Niu, R.; Mijowska, E.; Tang, T. Mass Production of Hierarchically Porous Carbon Nanosheets by Carbonizing “Real-World” Mixed Waste Plastics toward Excellent-Performance Supercapacitors. *Waste Management* **2019**, *87*, 691–700. https://doi.org/10.1016/j.wasman.2019.03.006

(108) Liu, X.; Wen, Y.; Chen, X.; Tang, T.; Mijowska, E. Co-Etching Effect to Convert Waste Polyethylene Terephthalate into Hierarchical Porous Carbon toward Excellent Capacitive Energy Storage. *Science of The Total Environment* **2020**, *723*, 138055. https://doi.org/10.1016/j.scitotenv.2020.138055

(109) Wen, Y.; Wen, X.; Wenelska, K.; Chen, X.; Mijowska, E. Novel Strategy for Preparation of Highly Porous Carbon Sheets Derived from Polystyrene for Supercapacitors. *Diamond and Related Materials* **2019**, *95*, 5–13. https://doi.org/10.1016/j.diamond.2019.03.015

(110) Ma, C.; Min, J.; Gong, J.; Liu, X.; Mu, X.; Chen, X.; Tang, T. Transforming Polystyrene Waste into 3D Hierarchically Porous Carbon for High-Performance Supercapacitors. *Chemosphere* **2020**, *253*, 126755.

(111) Dědek, I.; Bartusek, S.; Dvořáček, J. J.; Nečas, J.; Petruš, J.; Jakubec, P.; Kupka, V.; Otyepka, M. Maximizing the Electrochemical Performance of Supercapacitor Electrodes from Plastic Waste. *Journal of Energy Storage* **2023**, *72*, 108660. https://doi.org/10.1016/j.est.2023.108660

(112) Mohd Abdah, M. A. A.; Mohammad Azlan, F. N.; Wong, W. P.; Mustafa, M. N.; Walvekar, R.; Khalid, M. Microwave-Assisted Upcycling of Plastic Waste to High-Performance Carbon Anode for Lithium-Ion Batteries. *Chemosphere* **2024**, *349*, 140973. https://doi.org/10.1016/j.chemosphere.2023.140973

(113) Wang, M.; Du, X.; Zhang, M.; Su, K.; Li, Z. From S-Rich Polyphenylene Sulfide to Honeycomb-like Porous Carbon with Ultrahigh Specific Surface Area as Bifunctional Electrocatalysts for Rechargeable Zn-Air Batteries. *Carbon* **2022**, *198*, 264–274. https://doi.org/10.1016/j.carbon.2022.07.042

(114) Huang, J.; Lin, Y.; Ji, M.; Cong, G.; Liu, H.; Yu, J.; Yang, B.; Li, C.; Zhu, C.; Xu, J. Nitrogen-Doped Porous Carbon Derived from Foam Polystyrene as an Anode Material for Lithium-Ion Batteries. *Applied Surface Science* **2020**, *504*, 144398. https://doi.org/10.1016/j.apsusc.2019.144398

(115) Ehi-Eromosele, C. O.; Onwucha, C. N.; Ajayi, S. O.; Melinte, G.; Hansen, A.-L.; Indris, S.; Ehrenberg, H. Ionothermal Synthesis of Activated Carbon from Waste PET Bottles as Anode Materials for Lithium-Ion Batteries. *RSC Adv.* **2022**, *12* (53), 34670–34684. https://doi.org/10.1039/D2RA06786B

(116) Kim, K.-J.; Pham, V. H.; Gao, Y.; Huynh, N. T.; Lee, Y.-Y.; Wang, C.; Matranga, C. Synthesizing Highly Crystalline Graphite Powder from Bulk Polyethylene Waste for Lithium-Ion Battery Anodes. *ACS Sustainable Resour. Manage.* **2025**, *2* (1), 146–156. https://doi.org/10.1021/acssusresmgt.4c00398

(117) Villagómez-Salas, S.; Manikandan, P.; Acuña Guzmán, S. F.; Pol, V. G. Amorphous Carbon Chips Li-Ion Battery Anodes Produced through Polyethylene Waste Upcycling. *ACS Omega* **2018**, *3* (12), 17520–17527. https://doi.org/10.1021/acsomega.8b02290

(118) Kim, P. J.; Fontecha, H. D.; Kim, K.; Pol, V. G. Toward High-Performance Lithium–Sulfur Batteries: Upcycling of LDPE Plastic into Sulfonated Carbon Scaffold via Microwave-Promoted

Sulfonation. *ACS Appl. Mater. Interfaces* **2018**, *10* (17), 14827–14834. https://doi.org/10.1021/acsami.8b03959

(119) Hong, S.; Ku, J.; Park, S.; Park, J.; Yu, Y.-S.; Kim, C. Recycling of Polyethylene via Hydrothermal Carbonization for the Li-Ion Battery Anode. *Carbon Lett.* **2024**, *34* (5), 1529–1536. https://doi.org/10.1007/s42823-024-00721-5

(120) Zhao, T.; Tan, X.; Song, L.; Guo, L.; Liu, Y.; Kang, X.; Meng, X.; Wang, H.; Chu, W. Up-Scalable Conversion of White-Waste Polystyrene Foams to Sulfur, Phosphorus-Codoped Porous Carbon for High-Performance Lithium–Sulfur Batteries. *ACS Appl. Energy Mater.* **2020**, *3* (9), 9369–9378. https://doi.org/10.1021/acsaem.0c01730

(121) Lee, G.; Eui Lee, M.; Kim, S.-S.; Joh, H.-I.; Lee, S. Efficient Upcycling of Polypropylene-Based Waste Disposable Masks into Hard Carbons for Anodes in Sodium Ion Batteries. *Journal of Industrial and Engineering Chemistry* **2022**, *105*, 268–277. https://doi.org/10.1016/j.jiec.2021.09.026

(122) Zhang, S.; Sun, N.; Jiang, M.; Soomro, R. A.; Xu, B. Trash to Treasure: Sulfonation-Assisted Transformation of Waste Masks into High-Performance Carbon Anode for Sodium-Ion Batteries. *Carbon* **2023**, *209*, 118034. https://doi.org/10.1016/j.carbon.2023.118034

(123) Yuwen, C.; Liu, B.; Rong, Q.; Zhang, L.; Guo, S. Self-Activated Pyrolytic Synthesis of S, N and O Co-Doped Porous Carbon Derived from Discarded COVID-19 Masks for Lithium Sulfur Batteries. *Renewable Energy* **2022**, *192*, 58–66. https://doi.org/10.1016/j.renene.2022.04.103

(124) Hu, X.; Lin, Z. Transforming Waste Polypropylene Face Masks into S-Doped Porous Carbon as the Cathode Electrode for Supercapacitors. *Ionics* **2021**, *27* (5), 2169–2179. https://doi.org/10.1007/s11581-021-03949-7

(125) Hu, C.; Chang, Y.; Chen, R.; Yang, J.; Xie, T.; Chang, Z.; Zhang, G.; Liu, W.; Sun, X. Polyvinylchloride-Derived N, S Co-Doped Carbon as an Efficient Sulfur Host for High-Performance Li–S Batteries. *RSC Adv.* **2018**, *8* (66), 37811–37816. https://doi.org/10.1039/C8RA07885H

(126) Qiu, Y.; Jiang, G.; Su, Y.; Zhang, X.; Du, Y.; Xu, X.; Ye, Q.; Zhang, J.; Ban, M.; Xu, F.; Wang, H. Hybrid Hard Carbon Framework Derived from Polystyrene Bearing Distinct Molecular Crosslinking for Enhanced Sodium Storage. *Carbon Energy* **2024**, *6* (7), e479. https://doi.org/10.1002/cey2.479

(127) Cheng, L. X.; Zhang, L.; Chen, X. Y.; Zhang, Z. J. Efficient Conversion of Waste Polyvinyl Chloride into Nanoporous Carbon Incorporated with MnOx Exhibiting Superior Electrochemical Performance for Supercapacitor Application. *Electrochimica Acta* **2015**, *176*, 197–206. https://doi.org/10.1016/j.electacta.2015.07.007

(128) Min, J.; Zhang, S.; Li, J.; Klingeler, R.; Wen, X.; Chen, X.; Zhao, X.; Tang, T.; Mijowska, E. From Polystyrene Waste to Porous Carbon Flake and Potential Application in Supercapacitor. *Waste Management* **2019**, *85*, 333–340.

(129) Min, J.; Xu, X.; Koh, J. J.; Gong, J.; Chen, X.; Azadmanjiri, J.; Zhang, F.; Liu, S.; He, C. Diverse-Shaped Tin Dioxide Nanoparticles within a Plastic Waste-Derived Three-Dimensional Porous

Carbon Framework for Super Stable Lithium-Ion Storage. *Science of The Total Environment* **2022**, *815*, 152900. https://doi.org/10.1016/j.scitotenv.2021.152900

(130) Xu, X.; Li, J.; Dymerska, A.; Koh, J. J.; Min, J.; Liu, S.; Azadmanjiri, J.; Mijowska, E. MIL-53(Al) Assisted in Upcycling Plastic Bottle Waste into Nitrogen-Doped Hierarchical Porous Carbon for High-Performance Supercapacitors. *Chemosphere* **2023**, *340*, 139865. https://doi.org/10.1016/j.chemosphere.2023.139865

(131) Zhang, P.; Shu, Y.; Zhong, B.; Yang, L.; Guo, X. Optimizing Sodium Storage Mechanisms and Electrochemical Performance of High Nitrogen-Doped Hard Carbon Anode Materials Derived from Waste Plastics for Sodium-Ion Batteries. *Chemical Engineering Journal* **2024**, *498*, 155231. https://doi.org/10.1016/j.cej.2024.155231

(132) Gim, H.; Park, J. H.; Choi, W. Y.; Yang, J.; Kim, D.; Lee, K.-H.; Lee, J. W. Plastic Waste Residue-Derived Boron and Nitrogen Co-Doped Porous Hybrid Carbon for a Modified Separator of a Lithium Sulfur Battery. *Electrochimica Acta* **2021**, *380*, 138243. https://doi.org/10.1016/j.electacta.2021.138243

(133) Kim, H.; Yang, J.; Gim, H.; Hwang, B.; Byeon, A.; Lee, K.-H.; Lee, J. W. Coupled Effect of TiO2-x and N Defects in Pyrolytic Waste Plastics-Derived Carbon on Anchoring Polysulfides in the Electrode of Li-S Batteries. *Electrochimica Acta* **2022**, *408*, 139924. https://doi.org/10.1016/j.electacta.2022.139924

(134) Li, J.; Dou, F.; Gong, J.; Gao, Y.; Hua, Y.; Sielicki, K.; Zhang, D.; Mijowska, E.; Chen, X. Recycling of Plastic Wastes for the Mass Production of Yolk–Shell-Nanostructured Co_3O_4 @C for Lithium-Ion Batteries. *ACS Appl. Nano Mater.* **2023**, *6* (2), 1171–1180. https://doi.org/10.1021/acsanm.2c04757

(135) Xiang, S.; Yang, X.; Lin, X.; Chang, C.; Que, H.; Li, M. Nitrogen and Sulfur Co-Doped Polyurethane-Based Porous Carbon Materials as Supercapacitors Exhibit Excellent Electrochemical Performance. *J Solid State Electrochem* **2017**, *21* (5), 1457–1465. https://doi.org/10.1007/s10008-017-3505-7

(136) Mu, X.; Li, Y.; Liu, X.; Ma, C.; Jiang, H.; Zhu, J.; Chen, X.; Tang, T.; Mijowska, E. Controllable Carbonization of Plastic Waste into Three-Dimensional Porous Carbon Nanosheets by Combined Catalyst for High Performance Capacitor. *Nanomaterials* **2020**, *10* (6), 1097. https://doi.org/10.3390/nano10061097

(137) Pandey, S.; Karakoti, M.; Surana, K.; Dhapola, P. S.; SanthiBhushan, B.; Ganguly, S.; Singh, P. K.; Abbas, A.; Srivastava, A.; Sahoo, N. G. Graphene Nanosheets Derived from Plastic Waste for the Application of DSSCs and Supercapacitors. *Sci Rep* **2021**, *11* (1), 3916. https://doi.org/10.1038/s41598-021-83483-8

(138) Sahoo, N.; Tatrari, G.; Tewari, C.; Karakoti, M.; Bohra, B. S.; Danadapat, A. Vanadium Pentaoxide-Doped Waste Plastic-Derived Graphene Nanocomposite for Supercapacitors: A

Comparative Electrochemical Study of Low and High Metal Oxide Doping. *RSC Adv.* **2022**, *12* (9), 5118–5134. https://doi.org/10.1039/D1RA07458J

(139) Elessawy, N. A.; Backović, G.; Hirunthanawat, J.; Martins, M.; Rakočević, L.; Gouda, M. H.; Toghan, A.; Youssef, M. E.; Šljukić, B.; Santos, D. M. F. From PET Bottles Waste to N-Doped Graphene as Sustainable Electrocatalyst Support for Direct Liquid Fuel Cells. *Catalysts* **2023**, *13* (3), 525. https://doi.org/10.3390/catal13030525

(140) Cao, Q.; Dai, H.-C.; He, J.-H.; Wang, C.-L.; Zhou, C.; Cheng, X.-F.; Lu, J.-M. Microwave-Initiated MAX Ti3AlC2-Catalyzed Upcycling of Polyolefin Plastic Wastes: Selective Conversion to Hydrogen and Carbon Nanofibers for Sodium-Ion Battery. *Applied Catalysis B: Environmental* **2022**, *318*, 121828. https://doi.org/10.1016/j.apcatb.2022.121828

(141) Heleno, L.; Vasco, J. C.; Oliveira, N. S.; Gaspar, M.; Silveira, A. Technology Readiness and Environmental Performance of Plastic Recycling Pathways: An Integrated Systematic Review. *Environmental Technology & Innovation* **2026**, *43*, 105091. https://doi.org/10.1016/j.eti.2026.105091